

University of Puerto Rico  
Rio Piedras Campus  
College of Natural Sciences  
Chemistry Department

# **NICOTINIC ACETYLCHOLINE RECEPTOR SOLUBILIZATION USING LIPID ANALOG DETERGENTS: A KEY ASPECT TOWARDS RECEPTOR CRYSTALLIZATION AND FUNCTIONAL CHARACTERIZATION**

**By**

**Luis F. Padilla Morales**

A thesis dissertation submitted in fulfillment of the requirements for the degree of Doctor of Philosophy (Ph.D.), Chemistry Department, University of Puerto Rico, Rio Piedras Campus.

December 2018

**Thesis Committee:**

---

**José A. Lasalde Dominicci, Ph.D.**  
Professor, Biology Department  
University of Puerto Rico, Rio Piedras Campus

---

**Orestes Quesada, Ph.D.**  
Professor, Physical Sciences Department  
University of Puerto Rico, Rio Piedras Campus

---

**Carlos I. González, Ph.D.**  
Professor, Biology Department  
University of Puerto Rico, Rio Piedras Campus

---

**José A. Prieto, Ph.D.**  
Professor, Chemistry Department  
University of Puerto Rico, Rio Piedras Campus

---

**Suranganie Dharmawardhane, Ph.D.**  
Professor, Department of Biochemistry  
University of Puerto Rico, Medical Sciences Campus

*This thesis is dedicated to mentors and my family, especially my parents, wife, and daughters.  
To my family for their unconditional love, support, and understanding; and to my mentors for guiding me through this exciting journey.*

## Autobiography

I was born in the rural town of Naranjito, Puerto Rico. I was a curious child, who was always eager to learn and from a very young age became interested in science. I completed a Bachelor's Degree in Chemistry from the University of Puerto Rico, Rio Piedras Campus (UPR-RP). During my undergraduate studies, as part of the MARC Program, I had my first experience in research. I worked on the synthesis of natural compounds with anticancer activity under the guidance of Dr. Nestor Carballeira at the Chemistry Department. I also had the opportunity of participating in a summer research program at the laboratory of Dr. Gregory Reinhart from the Molecular Biophysics Department at Texas A&M University. These exciting experiences made me realize how passionate I was about research and motivated me to pursue a Ph.D. in Chemistry/Biochemistry; being the first member of my family to aspire a science-based doctorate.

In 2007 I began my Ph.D. studies at the Chemistry Department, UPR-RP, soon after I joined the Dr. Jose A. Lasalde's Laboratory. My thesis project had the objective of isolating the nAChR using lipid analog detergents and studying its stability and functionality in a lipidic matrix. The ultimate goal was to perform nAChR crystallization trials. During my doctoral studies, I became proficient in affinity chromatography, electrophysiological assays such as Planar Lipid Bilayer and two electrode voltage clamping. Moreover, I learned confocal imaging and X-Ray diffraction of protein crystals techniques.

During this time, I also was able to visit several national laboratories (SSRL-SLAC Menlo Park, CA; NSLS Brookhaven, NY and the APS-ANL Lemont, IL) as well as research institutes (MIT and SCRIPPS) to perform X-Ray diffraction experiments, through my own rapid access proposal GUP-33562 and get training in novel technologies such as lipidic cubic phase crystallization. Also, I have been able to share my research work through over twenty poster presentations and contribute to the scientific community with four research papers.

## Acknowledgments

- I want to give special thanks to my thesis committee members for taking time out of their busy agendas to assist my mentor in guiding me through this journey. They have trained me and provided me with skills that will allow me to succeed in my upcoming endeavors. Especially, I want to thank Dr. Reginal Morales, who loved science and dedicated his life to promoting the careers of young scientists; he was a role model for everyone who knew him and gave me the best example of dedication and commitment.
- Thanks to my thesis advisors José A. Lasalde-Dominicci and Orestes Quesada. They have always been accessible and willing to give me advice. They encouraged me to challenge myself, ask the right questions, and never doubt my potential. They are a role model and example of excellence.
- I want to thank all my friends at the Chemistry Department: Juan Carlos Aponte, Kenneth Rivero, Edward Aviles, Ismael Alicea, Raquel Otano, Alexandra Cruz for sharing this experience with me and for being there when I needed it.
- Thanks to all the members of the Lasalde Laboratory, the undergraduate and graduate students, post-doctoral fellows, and laboratory personnel. All of them contributed to my development as a scientist. I am grateful for having them around when I needed advice.



- Thanks to my family for always being there. To my parents for always encouraging me to attain my goal. To my wife for her unconditional love, patience, and understanding. I could not have done it without her!
- I also want to acknowledge the financial support I have received from: the MBRS-RISE Program and its personnel, the “Beca Torneo de Golf” fellowship, and the Chemistry Department Teaching Assistant program.
- Finally, I want to express my gratitude to the staff at the Chemistry Department at the University of Puerto Rico, Rio Piedras Campus: Wilma Santiago, Dr. Ingrid Montes, Dr. Nestor Carballeira, Dr. Jose A. Prieto. The staff at the Molecular Research and Science Building: Dr. Abel Baerga, Dr. Vallance Washington, Dr. Eduardo Nicolao, and Dr. Carlos Gonzalez. I appreciate your friendship, your help and particularly your commitment to all the graduate students.

## Table of contents

<b>Section</b>	<b>Page</b>
<b>Dedication</b> .....	2
<b>Autobiography</b> .....	3
<b>Acknowledgements</b> .....	4
<b>Table of contents</b> .....	6
<b>List of abbreviations</b> .....	8
<b>Abstract</b> .....	10
<b>Chapter 1. Introduction</b> .....	12
1. Background and Overview.....	12
2. Medical Relevance and Significance.....	13
3. Function and Binding Advances.....	14
4. Advances in the nAChR Structure Initiative.....	17
5. The Need for Better Solubilization Strategies and Appropriate Crystallization Conditions.....	37
6. The Role of Lipids in the Solubilization of Membrane Proteins .....	40
7. Outlining Our Contribution.....	43
Introduction References.....	44
<b>Chapter 2. Thesis Aims</b> .....	57
Thesis Aims References.....	60
<b>Chapter 3. Materials and Methods</b> .....	61
1. Detergent Purification of the nAChR from the <i>Torpedo Californica</i> .....	61
2. Characterization of Detergent Purified nAChR.....	74
Materials and Methods References.....	98
<b>Chapter 4. Results</b> .....	99
1. Affinity Purification Using Lipid Analog Detergents.....	99
2. Soluble Stability and Ion Channel Functionality of Detergent Purified nAChR....	102
3. Macroscopic Ion Channel Functional Assessment of Detergent Solubilized and Affinity Purified nAChR Using Lipid and Non-lipid Analog Detergents.....	112
4. Mobility Assessment of Detergent Purified nAChR in LCP Using Lipid Analog Detergents.....	120
5. LCP Stability Assessment of Detergent Purified nAChR Using Lipid Analog Detergents.....	133
6. Vapor Diffusion Crystallization of Detergent Purified nAChR Using Lipid Analog Detergents.....	141
7. Lipidic Cubic Phase Crystallization of Detergent Purified nAChR Using Lipid Analog Detergents.....	145

8. Lipidic Cubic Phase Crystallization of Detergent Purified nAChR Using Lipid Analog Detergents Applying Electric Potential.....	149
Results References.....	153
<b>Chapter 5. Discussion</b> .....	155
1. Affinity Purification of the nAChR from <i>T. Californica</i> Membranes.....	155
2. Soluble Stability and Ion Channel Functionality of Detergent Purified nAChR...	156
3. Macroscopic Ion Channel Functional Assessment of Detergent Solubilized and Affinity Purified nAChR Using Lipid and Non-lipid Analog Detergents.....	158
4. Mobility Assessment of Detergent Purified nAChR in LCP Using Lipid Analog Detergents.....	163
5. LCP Stability Assessment of Detergent Purified nAChR Using Lipid Analog Detergents.....	167
6. Vapor Diffusion Crystallization of Detergent Purified nAChR Using Lipid Analog Detergents.....	172
7. Lipidic Cubic Phase Crystallization of Detergent Purified nAChR Using Lipid Analog Detergents.....	175
8. Lipidic Cubic Phase Crystallization of Detergent Purified nAChR Using Lipid Analog Detergents Applying Electric Potential.....	179
Discussion References.....	185
<b>Chapter 6. Conclusions and Future Perspectives</b> .....	192
Conclusions and Future Perspectives References.....	196

## List of Abbreviations

ACh: Acetylcholine

AChBP: Acetylcholine Binding Protein

APS: Advanced Photon Source

A-SEC: analytical-size exclusion chromatography

CDC: Center for Disease Control

CH: cholesterol

CMC: critical micelle concentration

Cys-Loop: cysteine-loop

DDM: dodecyl-b-D-maltoside

ECD: extracellular domain

EDTA: ethylenediamine tetra-acetic acid

EM: electron microscopy

ELIC: ligand-gated ion channel from *Erwinia chrysanthemi*

FFR: fractional fluorescence recovery

FRAP: Fluorescent Recovery After Photo-Bleaching

GABA<sub>A</sub>:  $\gamma$ -aminobutyric

GLIC: gloeobacter ligand-gated ion channel

GluCl: chloride permeable glutamate receptor

GLyR: glycine receptor

GPCR: G-protein couple Receptor

HLB: hydrophilic-lipophilic balance

LCP: lipidic cubic phase

LFC: lysofoscholine

LGIC: ligand-gated ion channel

LSP: Lipidic Sponge Phase

MOPS: 3-N-Morpholino propanesulfonic acid

nAChR: nicotinic acetylcholine

nAChR-DC: nAChR-detergent complex

NaCl: Sodium Chloride

NaN<sub>3</sub>: Sodium Azide

PA: phosphatidic acid

PC: phosphatidylcholine

PE: phosphatidylethanolamine

PLB: planar lipid bilayer

POPC: 1-palmitoyl-2-oleoyl-sn-glycero-3 phosphocholine

POPS: 1-palmitoyl-2-oleoyl-sn-glycero-3-phosphoserine

ROI: region of interest

TEVC: two electrode voltage clamp experiments

TM: transmembrane

α-BTx: α-Bungarotoxin

β<sub>2</sub>AR: Beta-2 Adrenergic Receptor

5-HT<sub>3</sub>: serotonin 5-hydroxytryptamine

## Abstract

The nicotinic acetylcholine receptor (nAChR) is a ligand-gated ion channel (LGIC) composed of five subunits (2 $\alpha$ , 1 $\beta$ , 1 $\gamma$ , and 1 $\delta$ ) in a pentameric arrangement. The nAChR is a crucial component of the cholinergic pathway and manages the synaptic transmission between the brain and muscle. During the past five decades, the nAChR from *T. californica* has been extensively studied and used as a representative model for crystallization trials. There have been several accomplishments in the nAChR crystallization efforts, particularly using Cryo-EM and molecular engineering coupled with hanging drop crystallography. However, a high-resolution crystal structure of the native nAChR has not yet been developed, in part due to the poor understanding of the lipid-protein-detergent interactions occurring within the receptor. Lipidic matrixes as crystallization environments for membrane proteins have been used to improve the yield of membrane protein's crystal structures. Nevertheless, little is known about the effect of the isolation methodologies (i.e., detergents, buffers, and endogenous lipid composition) towards the LCP. Our laboratory designed a lipid-based characterization approach and examined the stability, functionality, and mobility of the *T. californica* nAChR. Size exclusion chromatography was used to assay soluble stability, two electron voltage clamp (TEVC) to study ion channel functionality, and fluorescence recovery after photobleaching (FRAP) to assess nAChR mobility on the LCP. The evaluation of these criteria is essential to determine the appropriate conditions to conduct nAChR crystallization. Our studies showed it is possible to extract *T. californica* nAChR by employing lipid analog detergents and provided valuable

insights for the preparation of functionally active nAChR–detergent complexes. We demonstrated that phospholipid-analog detergents with 16 carbon chains sustain nAChR function and stability.

## CHAPTER 1. Introduction

### 1. Background and Overview

The nicotinic acetylcholine receptor (nAChR) is a transmembrane protein, a type of integral membrane protein with gateway characteristics for selective or non-selective substances. Each of the nAChR is composed of five transmembrane subunits, with a stoichiometry of  $\alpha_2\beta\gamma\delta$ , in a pentameric spatial arrangement that creates an inner ion channel in the center. The nAChRs subunits are composed of four transmembrane segments M1, M2, M3, and M4; with M2 subunits being the inner segments, followed by the M1s and M3s while the M4s compose the outer segments [1]. Molecular modeling coupled with kinetic studies concluded that the M2 regions mainly compose the ion channel and that the M1, M3 and M4 segments are exposed to the membranous environment [1, 2, 3]. During the cloning boom in the mid-1980s, four significant characteristics were revealed among the structurally homologous M1-M4 subunits of the nAChR: 1) a conserved NH<sub>2</sub>-Terminal domain of ~200 amino acids, 2) three conserved transmembrane (TM) domains, 3) a fourth TM domain with relatively short and variable carboxyl terminal sequence, and 4) a cytoplasmic loop of variable size and amino acid sequence [4]. Also, a cysteine-loop (Cys-Loop), characterized by two cysteines that are essential for agonist binding, in the first extracellular domain (ECD) is a common feature in this type of receptors. The subunits were later classified as  $\alpha$  or non- $\alpha$  based on the presence of the Cys-loop [5, 6].

Based on subunit composition, the nAChRs can be subdivided into two major subtypes: the muscle and the neuronal nAChR. Muscle nAChR follows the stoichiometry 2:1:1:1 and two different constructs have been derived from  $\alpha_1$ ,  $\beta_1$ ,  $\delta$ , and  $\gamma$  or  $\alpha_1$ ,  $\beta_1$ ,  $\delta$ , and  $\epsilon$ . Neuronal nAChRs are either homopentamers or heteropentamers, composed mainly by  $\alpha$  and  $\beta$  subunits [7]. nAChRs have been identified as a model for ligand-gated ion channels which



include the neuronal nAChR ( $\alpha 4\beta 2$ ), muscular nAChR (nAChR-*Torpedo californica*), the glycine receptor (GLyR),  $\gamma$ -aminobutyric (GABA<sub>A</sub>) receptor, serotonin 5-hydroxytryptamine (5-HT<sub>3</sub>) receptor and chloride permeable glutamate receptor (GluCl) [1, 2, 3].

## **2. Medical Relevance and Significance**

The mechanism of a ligand-gated ion channel (LGIC) can be described as a gating mechanism initiated by the binding of a precursor molecule that promotes the conformational changes necessary to generate the ion pore, allowing ion flux at a specific time. This type of mechanism is key for the regulation of important biological processes such as the transmission of nerve impulses within the muscular and nervous systems. Consequently, the nAChR has been identified as a prime target to treat diseases associated with impaired neurological functions such as Alzheimer's, Parkinson's, Epilepsy, Dementia and Turret's. Moreover, recent studies have demonstrated the nAChR plays an important role in inflammation and cancer. The reduced production of proinflammatory cytokines evidences the role of the nAChR in inflammation upon activation of the macrophage  $\alpha 7$ -nAChR [8]. In the cancer research field, recent studies suggest that nAChR associated pathways could promote cancer by influencing metabolism and tumorigenesis to promote tumor growth and metastasis [9]. The high incidence and mortality associated with cancer and neurological and inflammatory diseases highlight the importance of studying nAChRs.

Per the United States Center for Disease Control (CDC), breast, prostate, and lung cancer are the most common forms of cancer in the United States among all races; and several studies suggest that the nAChR might be playing an important role in cancer development [9, 10]. In 2015, the World Health Organization estimated that 47.47 million people suffer from dementia associated with neurological diseases such as Alzheimer's. These numbers are substantially higher than the 2009 World Alzheimer Report, and statistical modeling predicts there will be a substantial increment in the number of cases in the future. Dementia cases

around the world are expected to double every 5.9 years. By 2030, a total of 75.63 million people are expected to suffer from this type of dementia [11, 12]. Understanding the structure and function of the nAChR will impact the development of novel therapeutic approaches against the previously mentioned diseases. However, there is still a major gap in knowledge in the structural features of the nAChR; a detailed three-dimensional (3D) structure of the nAChR is not available. Knowledge of the nAChR receptor structure can be used to postulate binding characteristics that could evolve into binding modeling and the subsequent development of nAChR-targeted therapeutics for neurological and immunological malignancies and cancer.

### **3. Function and Binding Advances**

Functional assays and site-directed mutagenesis have been used to determine the binding characteristics of the nAChR. Between the 1950's and the 70's, binding and kinetics studies contributed to the characterization of the nAChR binding site, from which a significant amount of information emerged. The characterization of the nAChR binding site allowed for a better understanding of how acetylcholine binds to the receptor and how binding translated to channel activation and subsequent engagement of the gating mechanism. These findings were also integral for the generation of postulates about the mechanism of desensitization of the nAChR [13, 14, 15, 16]. Nevertheless, it has been challenging to visualize how the electrophysiological data could be translated into a descriptive mechanism of action without the nAChR 3D structure. In the 1980's, advanced cloning technologies and access to High Power X-Ray diffracting technologies increased interest in elucidating the nAChR 3D Structure. These efforts resulted in the determination of the first 3D structure of the nAChR from a *Torpedo californica* Electric Ray. However, a significant part of the intracellular domain could not be determined as a result of poor resolution. The Acetylcholine Binding Protein (AChBP) structure was also determined; this structure resembles the pentameric arrangement

and the binding characteristics of the nAChR [17, 18]. The combination of the 3D structures of the nAChR and AChBP, and all the data available from decades of mutagenesis and kinetic studies allowed the postulation of comprehensive mechanisms of binding and channel gating. Before such 3D structures were available, mutagenesis data suggested that residues with an important role in the gating mechanism are located in the extracellular domain of the nAChR. Moreover, it was suggested that the binding and gating mechanism was the result of complex but distinctive steps involving conformational changes in the protein. However, we now recognize that the binding and gating mechanism works as a continuous equestrian where several changes are highly coordinated and occur simultaneously, rather than as independent sequential steps [19, 20].

In general, when a ligand binds to the nAChR between the  $\alpha$ -subunit and the adjacent subunit, it produces a conformational change that can be interpreted as a torsion induced force in the  $\beta$ -barrel. This force engages the transmembrane domain M2 to rotate creating a hydrophilic environment suitable for ion passage [4]. A Cys-Cys pair is essential, such as Cys191 and Cys192 in the nAChR from *Torpedo californica* to the binding mechanism. The Cys-Cys pair is located within a loop (C-loop) in the binding pocket of the  $\alpha$ -subunit. This loop, which acts as an interlocking gate between the  $\alpha$  subunit and the adjacent subunit, is the major contributor to the binding force of the nAChR [21, 22]. Nevertheless, aromatic residues Tyr93, Trp149, Tyr190, and Tyr198 positioned in the  $\alpha$  subunit of the nAChR from *Torpedo* also contribute to ligand binding. The position of these residues has been shown to dictate the magnitude of ligand affinity; whereas residues such as Leu112, Trp53, and Met114, located relatively outside of the binding pocket, have shown to dictate ligand binding selectivity. Based on a comprehensive analysis of available protein structures and the strong interactions that have been reported between the ligand and the residues mentioned above, it has been proposed that once the ligand binds, it gets buried within the receptor's subunits.

The bulkiness of certain residues within the binding site creates some type of barrier that seems to cover the ligand once it binds [4].

After a ligand binds to the nAChR, a cascade of conformational changes is activated which is almost instantaneously (microseconds) translated into channel opening; suggesting that the nAChR has been evolutionally engineered to respond rapidly, and clearly explains why these domains of the nAChR are highly conserved [4, 21, 22]. Computational simulation of the nAChR has been thoroughly analyzed to determine its channeling mechanism. The resulting models have suggested a great rearrangement of hydrogens bonds (H-bonds) within the surroundings of the binding site; Asp 85 in nAChR or analog residues Arg33 and Phe29 in AChBP along with several water molecules and polar residues in adjacent main chains are proposed to move as result of ligand binding [23, 24]. The C-loop has been suggested to move towards the inner core of the receptor pore, supporting the theory that once bound, the ligand gets buried within the nAChR creating a capping effect. Moreover, this movement creates a torsion force to the  $\beta$ -barrel loops. As a result, the extracellular surface of the nAChR pentamer opens and pulls M2 towards M1 and M3 creating a channel pore. Depending on the ligand and particular residues involved, the amount of torsion towards M2 can vary to modulate conductivity or selectivity of ions [24, 25, 26, 27, 28]. Nevertheless, the models discussed so far has been developed using the AChBP 3D structure and the partial 3D structure for nAChR that was determined using Cryo-electron microscopy (EM). Knowing the identity and location of each nAChR domain is essential to fully understand its mechanism of action and how ligands interact with the protein [1, 4]. Mechanistic models and predictions can only be as good as its foundations, which in turn relies on the structures used. Obtaining an unaltered nAChR structure is crucial for the development of treatments for Alzheimer's, Epilepsy, cancer, and other neurodegenerative, cardiovascular, and inflammatory diseases in which the nAChR is suggested to play a crucial role.

#### **4. Advances in the nAChR Structure Initiative**

Until today, a complete and unaltered structure of the nAChR is not available. All the structures that have emerged in the last decade have contributed significantly towards our current knowledge of the nAChR. However, all known structures have been altered to achieve a stable crystallization or truncated due to poor resolution data. Available models and structure analysis studies, including the secondary analysis of protein analogs, conclude the nAChR is a complex molecule that is very sensitive to mutations/alterations and interactions along the protein body [29]. There are three major milestones to reach the goal of having a high-resolution 3D structure for the nAChR: 1) there is no cellular model that will produce high amounts of nAChR in a native manner, without significant alteration; 2) the protein is highly complex, thus efficient solubilization has been very challenging; and 3) the crystallization process requires a stable protein to be organized into a reticle over a significant period of time, and this requires the protein to be isolated in a media that will support protein stability. A native structure of the nAChR will be integral for the development of accurate, comprehensive models of regulation and to fully understand the complexity of receptor assembly and its mechanism of action.

##### **4.1. Contributions of AChBP to the nAChR Structure Initiative**

For over a decade the AChBP and the Cryo-EM nAChR structure have made the significant contributions to the nAChR structure initiative. Thousands of scientific publications have used the AChBP and the Cryo-EM nAChR structural information to support their findings. In addition, two prokaryotic LGIC homologs (gloeobacter ligand-gated ion channel (GLIC) and ligand-gated ion channel from *Erwinia chrysanthemi* (ELIC)), GABA<sub>A</sub> receptor, 5-HT<sub>3</sub> receptor, human  $\alpha$ 3 glycine receptor, zebrafish  $\alpha$ 1 glycine receptor, two  $\alpha$ 7 nAChR/AChBP ECDs chimeras,  $\alpha$ 1 ECD structure,  $\alpha$ 2 ECD structure,  $\alpha$ 9 ECD structure, GluCl, and the  $\alpha$ 4 $\beta$ 2 structure among others, have emerged to supplement the structural data available [30 – 40].

All of the structures mentioned above have proven to be significantly similar to the native nAChR from *Torpedo californica*, thus appropriate for modeling. In 2005, the first quasi-high resolution crystal structure of the nAChR emerged. The protein was isolated from *Torpedo marmorata*, and the electron density map was generated using Cryo-EM technology. This structure reveals significant information regarding the functional and pharmacological characteristics of the nAChR [1]. Unfortunately, even though this structure represented a significant advance, it lacks the desired resolution to achieve accurate drug design. Moreover, because of a resolution limitation, the protein was truncated, leaving out the structure of a significant section of the intracellular domain.

AChBP structures have been available for over 15 years. The AChBP shares approximately 24% sequence identity with the nAChRs and has a similar pentameric arrangement [41]. The AChBP structure and the diversity of other structures available for proteins that share similarities with nAChR have provided detailed information on agonists and antagonist binding as well. However, the limitation of using the AChBP structure as a model for studying nAChR structure and function is that AChBP is not an ion channel and it lacks the essential structural features for transmitting the ligand-binding signal through the protein body [41]. The major contribution provided by the AChBP structure was the high-resolution images of the Cys-Loop on the binding site. The AChBP structures have been necessary for the determination of the gating role of the Cys-Loop. It has been proposed that the Cys-Loop might have a unique connection with the transmembrane domains, a feature that could explain the selectivity between subunit associations when pentamers are assembled [42].

#### **4.2. Contributions of ELIC to the nAChR Structure Initiative**

In 2008 and 2009, two structures of LGIC were obtained using X-ray diffraction technologies and the structures were diffracted at high resolution (ELIC 3.3Å and GLIC 2.9Å). Elucidating the structures of these nAChR homologs was a breakthrough because for the

first time, a ligand-gated ion channel was crystallized with high resolution and the structure included the transmembrane domain. Even though the ELIC structure shares only 16% sequence identity with the nAChR, it has a similar pentameric special arrangement with similar function. On artificial bilayers, the ELIC channel could create membrane depolarization through cation-selective currents; and, although it seems to be unable to discriminate between monovalent cations ( $\text{Na}^+$ ,  $\text{K}^+$ ,  $\text{Cs}^+$ ), this behavior appears to be similar to the nAChR's action [43]. The overall dimensions of the ELIC channel ( $95\text{\AA} \times 110\text{\AA}$ ) closely resemble the nAChR, but the cytoplasmic region is absent in ELIC. In addition, ELIC is very similar to its eukaryotic counterparts and to AChBP, except for an N-terminal  $\alpha$ -helix that is abundant in eukaryotic proteins and missing in bacterial pLGICs. Nevertheless, the Cys-loop that connects  $\beta_6$  and  $\beta_7$  in ELIC is similar in spatial arrangement to the Cys-loop on the nAChR; although it does not share the contiguous disulfide-bridged cysteine residues that are strictly conserved among eukaryotic pentameric LGICs [33]. There are four helices in ELIC named  $\alpha_1$ – $\alpha_4$  that resemble the previously described transmembrane regions M1–M4 of the nAChR. Soaking the crystals in different ion solutions ( $\text{Rb}^+$ ,  $\text{Cs}^+$ , and  $\text{Tl}^+$ ), allows for the determination of ordered binding of ions in the extracellular binding domain. This experiment alongside with an electrostatic potential analysis within the ion permeation path of ELIC provided information, for the first time, about possible interactions and selectivity of ions through the ion pore [33]. The excess of acidic residues in the ELIC protein creates a highly negative potential across the ion channel, which provides an attractive environment for cations. Even though residues are not highly conserved, especially along the center and the peripheral areas of the ion pore, the hydrophobic residues in the center and the charged residues in the periphery of the ELIC channel are well organized and seem to share very similar roles within the ion transport mechanism to their counterparts in the nAChR [33]. Periphery charged residues had been identified to be highly involved in ion selectivity, discriminating in favor of cations, although not as specific as it has been shown for  $\text{K}^+$

Channels [43]. The significant contributions of the ELIC structure can be associated with the development of a model for channeling capability and to postulate how the ions are likely to flow through the ion channels of LGICs.

#### **4.3. Contributions of GLIC to the nAChR Structure Initiative**

The GLIC is a LGIC with the same pentameric arrangement as the nAChR. Most LGIC channels are known to undergo desensitization as a result of prolonged exposure to the agonist. This complicates the structural investigations of the transient open conformation of LGICs. However, GLIC is activated by protons and does not suffer from desensitization, even under its maximal electrophysiological response at pH = 4.5 [45]. In general, the overall architecture of GLIC resembles that of ELIC, the AChBPs, the nAChR from Torpedo and the recently discovered AChR- $\alpha 4\beta 2$  (**Figure 1 A-C**).

The subunits (5) that composed the nAChRs are arranged in a tube/barrel like manner around a central symmetry axis; this mainly constitutes the ion permeation pathway; very similar to the  $\beta$ -barrel arrangement observed in the nAChR. In eukaryotic LGICs such as the nAChR, the interface between ECDs holds the neurotransmitter-binding pocket or binding site as discussed before. GLIC equivalent regions show structural similarity despite a low sequence identity, notably in the capping  $\beta 9$ – $\beta 10$  loop [32]. The TM domain of each subunit consists of four helices (M1 to M4). M2 helices form the pore's wall are bordered by rings of homologous residues, as previously observed in the Torpedo nAChRs [46, 47]. The GLIC structure shows that the M1 helices are kinked at Pro205 and form a second circle of helices with M3 interacting with M2; whereas, M4 helices are peripheral. Well defined electron densities (of high resolution and definition) are observed in the grooves between M4 and both M1 and M3 of GLIC, close to hydrophobic residues that have been identified in the Torpedo nAChR. The electron densities were attributed to lipids that might grip the M4 into its position [32]. The GLIC ion channel consists of an extracellular hydrophilic section with more than 12Å wide opening, linked to a funnel-shaped transmembrane pore [32]. The M2 domains of GLIC



are located within the ion pore, tilted with respect to the pore axis. While the outer hydrophobic side chains in M2 seem to be oriented towards the helix interfaces, the inner polar side chains are geared towards the ion channel pore [32]. Detergent molecules were found in the GLIC crystal structure, six detergent molecules (dodecyl- $\beta$ -D-maltoside, DDM) obstruct the ion pore, with a ratio of one detergent per monomer and one detergent sitting on the five-fold axis, the sugar moiety being much less ordered than the aliphatic chains. Even though DDM has been shown to interact with the hydrophobic rings, and seems to shield their side chains from the solvent (with the polar heads pointing up, towards the extracellular hydrophilic section), experiments with heavy atoms substitution show that the presence of the detergent did not affect the GLIC opened conformation. However, the identity of channel-associated detergents has been revealed to affect current fluxes in the eukaryote LGIC nAChR when inserted into a non-natural lipid bilayer [48, 49]. The GLIC structure has made a great contribution towards the nAChR structure initiative by presenting an open structure of a eukaryote LGIC homolog. Such structure allowed high-resolution appreciation of the pore structure injunction with the mostly hydrophilic extracellular section. Finally, the GLIC structure provided information about detergent/receptor interactions and the possible role of detergents/lipids with a crystal.

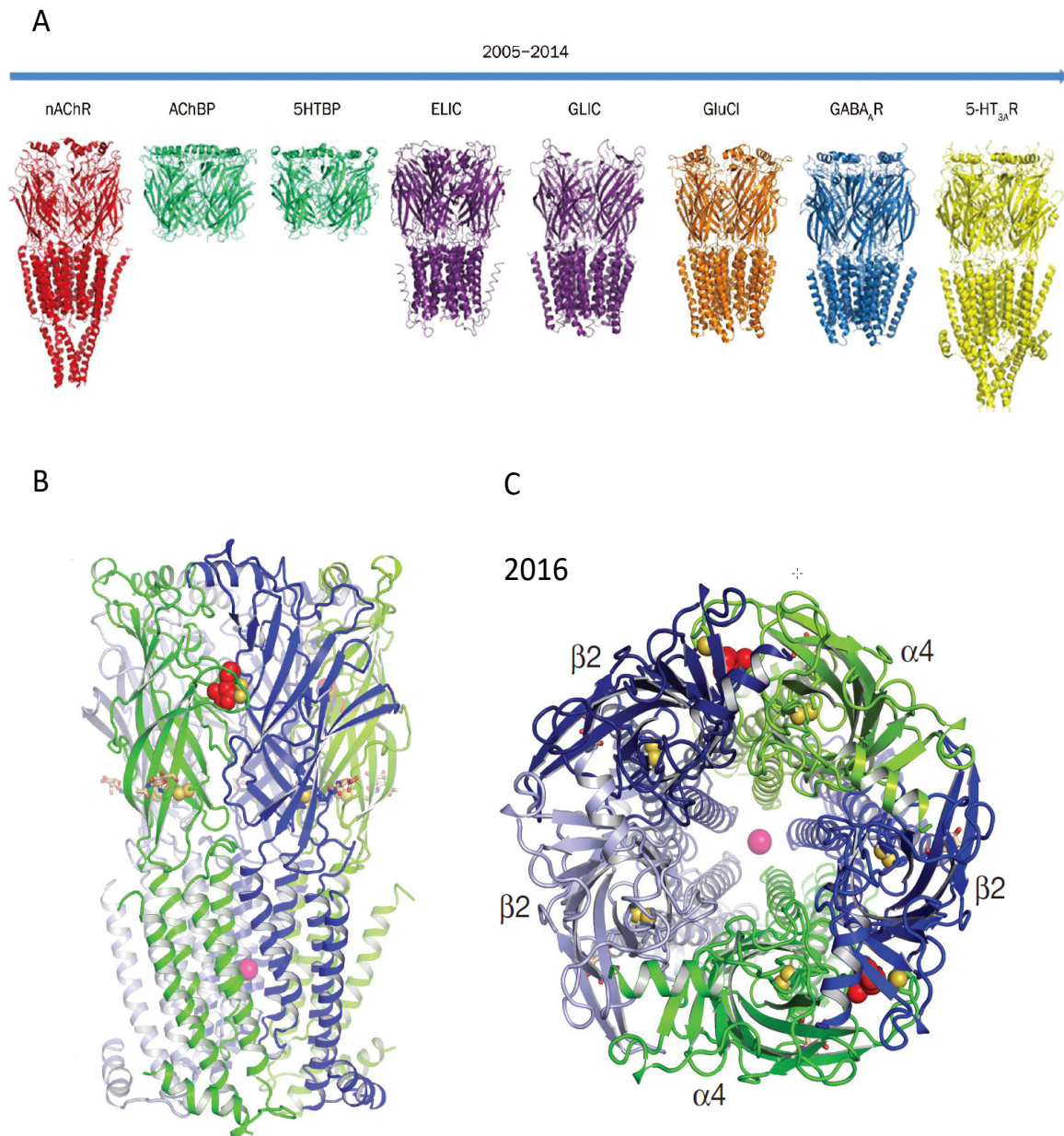


**Figure 1:** A) Published LGIC structures from 2005 to 2014 [29], and recently discovered nAChR- $\alpha$ 4 $\beta$ 2 structure B) lateral view C) top view [40].

#### **4.4. Contributions of GABA<sub>A</sub> Receptor to the nAChR Structure Initiative**

The GABA<sub>A</sub> receptor is the principal mediator of rapid inhibitory synaptic transmission in the human brain and a part of the Cys-Loop family, like the nAChRs [37]. Upon binding to the neurotransmitter GABA<sub>A</sub>, which is released at inhibitory synapses, the GABA<sub>A</sub> chloride channels open and depress neuronal excitability in the adult central nervous system [50]. Low GABA<sub>A</sub> signaling triggers hyperactive neurological disorders such as insomnia, anxiety, and epilepsy [37]. The crystal structure of the GABA<sub>A</sub> was determined at the high 3 Å resolution and provided very significant information about LGICs. The GABA<sub>A</sub> structure presents the pentameric arrangement typical of the Cys-Loop family. However, crystallization of the GABA<sub>A</sub> receptor required truncation between transmembrane helices M3 and M4 and substitution of Gly308 and Asn421 by a linker sequence SQPARAA to increase stabilization [51]. The GABA<sub>A</sub> construct used for crystallization was tested for functionality and showed currents in patch-clamped HEK293T cells expressing said vector (called GABA<sub>A</sub>R-b3cryst). Moreover, currents from this GABA<sub>A</sub>R-b3cryst were inhibited by the channel blockers fipronil and picrotoxin even after stimulation with agonists histamine or propofol [37]. The structure obtained using the GABA<sub>A</sub>R-b3cryst shows a cylinder of 110Å in height, with a diameter of 60Å to 80Å, extended across the plasma membrane and protruding approximately 65 Å into the extracellular environment [37]. The pentamer arrangement has a toroidal (doughnut-like) profile characteristic of the LGICs, surrounded by 15 (3 per subunit) N-linked glycans. Each ECD comprises an amino-terminal  $\alpha$ -helix ( $\alpha$ 1) followed by ten  $\beta$ -strands folded into a curled  $\beta$ -sandwich, another feature of LGICs [37]. Four additional helices (M1–M4) from each subunit come together to create the pentameric transmembrane domain, with M2 segments lining a pore towards the intracellular side of the membrane forming the ion channel. The structure also shows a group of positively charged residues (charged ring) in the extracellular section or vestibule that hosts putative ion binding in each inter-subunit interface; similar features were observed in the ELIC and GLIC structures [37]. The positively charged ring in the

vestibule corresponds to the proposed ion selectivity filter in the Cys-Loop receptors [52]. Per the GABA<sub>A</sub> structure, chloride ions are attracted and bound to residues around the vestibule, creating several chloride-binding sites that might be important for LGIC stabilization; these sites were identified as anion binding sites in the GLIC structure. The same type of charged ring might be present and could play a role in nAChR stabilization [32, 37].

Within the transmembrane domain, there are two large non-overlapping pockets near the residues located at the edge of the vestibule, these pockets have been identified as binding sites for the intravenous anesthetics etomidate and propofol. In contrast, the propofol putative binding site in GLIC is structurally different [37]. These structural differences explain the opposite responses after propofol binding to each receptor; propofol potentiates and activates GABA<sub>A</sub> but inhibits GLIC [53, 54]. The GABA<sub>A</sub> structure shows that the side chains Arg26 and Asp17 form a salt-bridge network extending to Asp24 and Lys13. Such residues appear to be necessary for receptor stabilization. Within GABA<sub>A</sub>  $\alpha$ 2 helices, the intersubunit interface is stabilized by a system of hydrogen bonds and salt bridges surrounding Arg86; these features are specific to the GABA<sub>A</sub> and Glycine Receptors but have not been identified on the nAChR [37].

The neurotransmitter-binding pocket of GABA<sub>A</sub> is located between ECDs and comprises the  $\beta$ 4 strand and adjacent residues (Asp95 – Leu99), part of the  $\beta$ 7– $\beta$ 8 loop (Glu155 – Tyr159) and the  $\beta$ 9– $\beta$ 10 loop (Phe200 – Tyr205). Even though the binding characteristics of the GABA<sub>A</sub> receptor differ from the nAChR, the closure mechanism and stabilization are indeed similar [37]. The closure process is stabilized by salt bridges between the side chains of Arg207, Glu153, and Glu155; these residues are essential in GABA<sub>A</sub> ligand binding and channel inactivation. Similar interactions have been shown to be crucial for ligand binding and activation of the nAChR [55, 56, 57, 58].

The ECD and transmembrane domain interface has two significant contributors of interaction: an array of polar contacts linking the outer portion of the M2–M3 loop with the  $\beta$ 6–

$\beta 7$  (Cys-loop), and van der Waals contacts between residues in the inner part of the M2–M3 loop near the pore, the  $\beta 1$ – $\beta 2$  loop and the  $\beta 6$ – $\beta 7$  loop [37]. Therefore, the ECD–transmembrane domain interface is structurally tightly coupled, with a solvent-inaccessible surface area of  $689 \text{ \AA}^2$ , which translates into an area  $100 \text{ \AA}^2$  larger than observed in ELIC, yet comparable to those found in GluCl $\alpha$ , GLIC, and the nAChR structure solved by electron microscopy [37].

In the GABA<sub>A</sub> structure the pore is too narrow to allow for the passage of chlorine ions. Thus the structure is determined to be in a closed state. Interestingly, the geometry shown by the GABA<sub>A</sub> structure differs from the previously discussed closed-state structures of ELIC and Torpedo nAChR [1, 33]. On the other hand, the GABA<sub>A</sub> pore-lining is well aligned with protonation of charged residues in the open nAChR [59, 60]. The GABA<sub>A</sub> receptor structure highlights the interactions associated with the pore structural support and identifies the salt bridges and hydrogen interactions that connect the LGIC ECDs with the transmembrane domains. The most important contributions of the GABA<sub>A</sub> crystal structure to the nAChR structure initiative are that: 1) the GABA<sub>A</sub> receptor structure allows for ligand binding modeling and 2) confirms an interesting feature shared among the LGICs, the presence of putative ion binding sites that support receptor stability.

#### **4.5. Contributions of 5-HT<sub>3</sub> Receptor to the nAChR Structure Initiative**

The 5-HT<sub>3</sub> receptor is a neurotransmitter that mediates transmission through the nervous system upon serotonin binding [38]. The serotonin-gated 5-HT<sub>3</sub> receptor, which belongs to a family of pentameric LGICs termed Cys-Loop receptors, is the target of potent drugs that alleviate chemotherapy-induced and post-operative nausea and vomiting and may enable personalized therapies for irritable bowel syndrome and various psychiatric disorders [61, 62, 63]. The 5-HT<sub>3</sub> receptor and the nAChR belong to the Cys-Loop family, and both are cation-selective ion channels that promote excitatory signals through the nervous system. The importance of the Cys-Loop family relies on the critical role played by its members in the

regulation of brain functions; they are known to be involved in numerous pathologies [38]. Therefore, Cys-Loop receptors are targets of many psychoactive and therapeutic compounds including nicotine, alcohol, benzodiazepines, barbiturates, steroids and local and general anesthetics [38].

Even though LGICs have been extensively studied, due to the absence of high-resolution crystal structures our knowledge on their structure and mechanism of action is limited to speculations [38]. In addition, the intracellular domain of LGICs is exclusive for multicellular organisms and the structures available for the related prokaryotic ELIC and GLIC lack such a domain. In vertebrates, the intracellular domain is composed of 50 to 70 residues and accounts for gating kinetics and trafficking and clustering within the synapse region [38]. The 5-HT<sub>3</sub> structure, obtained from a mammalian source, provided significant information that could more accurately support the proposed mechanism of action for LGIC family members at a higher evolutionary level, such as the nAChR. However, once again receptor complexity limited the potential of achieving high-resolution data; consecutively, the 5-HT<sub>3</sub> receptor was cleaved by approximately 60 residues to yield 7Å resolution data. The 5-HT<sub>3</sub> receptor was later co-crystallized with a crystallant chaperone, a single chain antibody that not only helped with stabilization but provided better hydrophilic/hydrophobic ratio to increase the chances of reticle formation. Both strategies combined resulted in a 3.5Å resolution structure [38]. The 5-HT<sub>3</sub> structure is composed of cylindrical extracellular and membrane domains that have similar architecture to ELIC, GLIC, nAChR, and GluCl [38]. Unlike GLIC and ELIC, the intracellular domain of the 5-HT<sub>3</sub> receptor has a conical/bullet-like shape and comprises an additional portion proximal to the membrane, the post-M3 loops, and the MX helices. The intracellular helices of the 5-HT<sub>3</sub> receptor are twisted, forming a tight bundle at the receptor's inner tip. The ion channel vestibule is approximately 20 Å wide, being narrower than those found in homologous structures [38]. The first residues available for interaction in the vestibule are Asp105 and Lys108 from loop β4-β5, and it has been suggested that position 105 is critical

for smooth channel conductance [64]. This information is consistent with previous postulates that proposed vestibule charged residues in  $\alpha 1$ -nAChR and GABA<sub>A</sub> structures potentially influenced receptor conductance [65, 66]. The pore is approximately 40Å long and delineated by the M2 helices, similar to the arrangement found in the nAChR structure from EM. In the extracellular part of the M2, a conglomerate of hydrophobic residues that constitute the funnel has been identified; this region is believed to contain the main channel gate. However, because of the complexity of the hydrophobic arrangement, it is not simple to determine the receptor pore state [38]. The pore conformation of the 5-HT<sub>3</sub> receptor has been compared with that presented in GLIC and CluCl opened channel structures. A fair comparison with the Torpedo nAChR will require all contributing factors. Unfortunately the available pore structure lacks one helix turn [67, 68].

The intracellular region of the 5-HT<sub>3</sub> receptor is essential for trafficking and gating, but it also plays an important role in regulating channel conductance [69, 70]. Within the intracellular region, the 5-HT<sub>3</sub> structure shows 20 residues that form a loop and a short MX helix that clamps MA-M4 and 25 residues forming the MA helix as a continuation of M4 [38]. However, poor resolution data renders the modeling of this segment somewhat unreliable, suggesting that the intracellular region of the 5-HT<sub>3</sub> receptor might be an area of high flexibility, capable of adopting numerous conformations [38]. Similar findings can be observed for homologous residues 410–440 in the nAChR; these residues have been found to be responsible for different gating kinetics of nAChR receptors containing either  $\gamma$  or  $\epsilon$  subunits [71]. Nevertheless, it is essential to keep in mind that 62 residues had to be removed to improve receptor stabilization [38] and that also the amino acid stretch that was removed most likely influences structure conformation and could contribute to receptor flexibility. This missing segment could provide interaction sites for proteins modulating activity, assembly, trafficking and clustering [70 - 72].

Inherently the structure provided does not offer an exit pathway for ions, mainly as a result of a narrow 17Å long zone with a minimum diameter of 4.2Å located next to the post-M3 Loop and the MX helix, at the bottom of the funnel [38]. The structure is suggested to contain lateral portals to release the ions; however, significant conformational changes need to occur for the lateral release of ions [38]. More likely, the narrow pore could be a consequence of the manipulations required to achieve the structure (trypsin digestion for example); detergent solubilization could also influence the resulting structure. The flexibility of the post-M3 loop and the MX helix could contribute to a global twist of the receptor thus widening the funnel for ion passage. This postulate will remain the only speculation as long as there is no 5-HT<sub>3</sub> receptor native structure available for analysis. Finally, the most significant contribution of the 5-HT<sub>3</sub> receptor structure relies on the intracellular structure, a domain that is not available in the *Torpedo* nAChR structure currently available. The 5-HT<sub>3</sub> receptor structure allows for the understanding of putative lateral ion release mechanism and the comprehension of the clustering mechanism and intracellular influences that might regulate receptor conductance.

#### **4.6. Contributions of GlyR to the nAChR Structure Initiative**

The GlyRs are LGICs in a metameric arrangement that mediates fast inhibitory synaptic transmission within the nervous system (spinal cord and brainstem) [73, 74]. The GlyRs also belong to the Cys-Loop family [39] and can exist as homopentamers with only  $\alpha$ -subunits or as heteropentamers with both  $\alpha$ - and  $\beta$ -subunits [75]. Upon glycine binding (neurotransmitter) to the extracellular domain, the receptor undergoes a series of conformational changes that allow the TM domain to selectively open, allowing the passage of anions [39]. Even though there are at least a handful of LGIC structures available, no structural information is available to help us understand the mechanism of inactivation by competitive antagonists. The GlyR was crystallized in complex with the antagonist strychnine, an alkaloid from a poisonous plant that causes muscle spasms, convulsion, and death. Strychnine effects are the result of its binding to the GlyR and the subsequent impact on synaptic transmission [76, 77]. To achieve



protein stabilization and obtain high quality diffracting crystals, 76 residues, between the M3 helix and the M4 helix, were replaced with an Ala-Gly-Thr tripeptide and four residues from the C-terminal were deleted. After this significant alteration, the altered GlyR protein was challenged for binding capacity and conductance. Results showed the binding capability to strychnine and glycine dependent conductance [39]. The GlyR structure was resolved at a 3 Å resolution with strychnine bound to the ECD. Similar to other LGICs, the GlyR structure shows similar spatial arrangement, fivefold symmetry and the funnel shape structure in the center. Unlike the GABA<sub>A</sub> receptor, the glycans in the GlyR are solvent exposed and do not interact with other residues [39].

The strychnine binding pocket is formed by two loops and Phe63 and Phe159 from the hydrophobic base of the binding pocket. Residues Tyr202, Thr204, and Phe207, have been shown to be necessary for strychnine binding; most interactions within the strychnine binding pocket are hydrophobic in nature except for a hydrogen bond involving Phe159. This spatial arrangement of the strychnine binding pocket supports previous data from GlyR mutagenesis studies [7, 79].

LGIC agonist-bound structures have shown significant differences when compared to strychnine-bound GlyR. The orthosteric binding site is more extensive and the loop C adopts an open conformation in the strychnine-bound state, this is reminiscent of antagonist-bound AChBP structures [39]. In contrast, the orthosteric site is smaller, and loop C adopts a closed conformation that caps the binding site in the agonist-bound state of GluCl and GABA<sub>A</sub> receptor. This is indicative of an antithetical behavior as a result of agonist/antagonist binding in relation to other LGICs. The pore is lined by the M2, and there are several constrictions along the channel length, down to the narrowest 1.4Å segment, caused by the side chain of Leu261 in the mid-point of the channel. Consequently, the ion channel of strychnine-bound GlyR is consistent with a closed channel, because the narrowest segment is 1.4Å and the radius of a dehydrated chloride ion is 1.8Å [39].

Within the pore region of the GlyR, several residues have been identified to possess critical roles. For example, Leu261 is considered to act as a shut gate within the channel; and Pro250, located in the cytoplasmic end of M2, has been shown to have a significant impact in ion selectivity. Other mutations along the M2 domain have been associated with spontaneous channel activity (V260M, T265I, Q266H, and S267N) [80]. Molecular simulations of GluCl, based on the GlyR structure, predicted that the unbinding of agonist and the opening of the orthosteric site lead to repositioning of the  $\beta 1$ – $\beta 2$  loop and inward displacement of the M2–M3 loop towards the pore, which is then coupled to the untilting of the M2 helix and the closing of the pore. This gating mechanism was subsequently validated by the apo-GluCl structure where the pore is closed [39]. The GlyR structure has provided important structural information to create models that could explain the closed states of LGICs, including the nAChR. However, there is still not enough structural information about the intracellular domain of LGICs, mostly due to protein truncation necessary for crystallization. Moreover, binding characteristics have shown to be unique in nature, where the effects of allosteric binding could influence each LGIC very differently from one another.

#### **4.7. Contributions of GluCl to the nAChR Structure Initiative**

The structures of GluCl in an apo state shows a solvent-accessible pathway from the outermost region of the extracellular domain [36]. The GluCl structure was achieved by binding the receptor to a lipid, 1-palmitoyl-2-oleoyl-sn-glycero-3 phosphocholine (POPC). This is the first LGIC crystal structure that has shown the great influence that the lipid environment can have in receptor conformation. The POPC-GluCl structure showed a solvent-accessible pathway from the outermost region of the extracellular domain, through the vase-shaped extracellular vestibule, to the transmembrane ion channel pore [36]. The pore is lined by the M2 helices, with Pro243 and Leu254, homologs to Pro250 and Leu261 in GlyR, occupying key sites at the cytoplasmic and middle portion of the ion channel. Moreover, the POPC-GluCl structure showed lipid molecules bound between subunits, close to the extracellular segment

of the transmembrane domain and with their head groups wedged between the M1 and M3 helices. The POPC-GluCl receptor pore is straight, but wider than in the apo state and has a constriction at Leu 254, the inner gating residue, yielding a pore with a radius of 2.4Å [36]. The arrangement of POPC in the structure was defined by densities located between M1 and M3. The GluCl structure generated with molecular modeling, suggests that the POPC head groups are accommodated towards the center of the pore and the lipid molecules overlap with the binding site of ivermectin, an antihelmintics drug used to kill parasites through paralysis [81, 82]. The structure model was challenged in the presence of several lipids and ivermectin; 1-palmitoyl-2-oleoyl-sn-glycero-3-phosphoserine (POPS) competes for ivermectin binding with an inhibition constant ( $K_i$ ) of 167 mM. Even though POPS bound relatively strong to GluCl, a POPS-GluCl crystal structure could not be generated because the protein crystals did not provide well diffracting data. However, even though POPC binds weakly to GluCl, relative to POPS, the POPC-GluCl protein crystal provided high-resolution data [36]. This indicates that the type of lipid within the receptor membranous environment could contribute to receptor stabilization or could influence receptor conformation. Furthermore, when comparing the apo and POPC-bound states, the transmembrane domain undergoes a rotation about an axis approximately parallel to the pore, which in turn gives rise to a 3Å displacement from the pore axis in the membrane's plane [36]. These movements lead to an expansion of the ion channel pore while the M2 helices remain oriented parallel to the pore axis. In addition, the ivermectin- and POPC-bound state comparison shows a large movement of the extracellular and transmembrane domains, with the M2 helix undergoing a tilt by 8.7° and a translational movement of 6Å [36]. Therefore, the binding of POPC is considered to promote the movement of key residues towards the neurotransmitter binding site, strengthening the binding potential; thus, POPC/POPS potentiates glutamate binding [36]. The GluCl structures provided a great advantage in understanding how the lipidic environment can influence

receptor stability and binding characteristics. The data derived from these structures highlights the importance of the lipidic environment during the crystallization process.

#### **4.8. Contributions of $\alpha 4\beta 2$ Receptor to the nAChR Structure Initiative**

Recent efforts in the nAChR structure initiative have been directed towards the determination of the human  $\alpha 4\beta 2$  nAChR structure [40]. Until today the elucidation of the  $\alpha 4\beta 2$  nAChR structure is considered one of the most significant advance in the field of transmembrane protein crystallization. The structure has provided significant information that has contributed greatly towards the understanding of the nAChR function and regulation. Mostly encountered within the nervous system, the  $\alpha 4\beta 2$  receptor mediates signal transmission within the brain cells and spinal cord [83-85]. Unfortunately, to achieve a high-quality diffracting crystal, most of the intracellular domain was removed [40]. Despite the removal of the intracellular domain, the receptor remains active, showing conductance and binding characteristics comparable to a full  $\alpha 4\beta 2$  receptor ( $\alpha 4\beta 2$  WT) [40] (See **Figure 2**).

The  $\alpha 4\beta 2$  receptor was co-crystallized with nicotine and a cholesterol analog; once again confirming the importance of receptor stability associated with potent ligand binding and transmembrane domain support by lipids. The  $\alpha 4\beta 2$  receptor resembles a cylinder formed from five subunits in a pseudo-symmetrical arrangement relative to the channel axis. The crystal structure reveals a subunit ordering of  $\alpha-\beta-\beta-\alpha-\beta$  around the pentameric ring consistent with functional studies and with the spatial arrangement that characterizes LGICs [85, 86]. The Cys-Loop receptor superfamily is characterized by a conserved disulfide bond linking the  $\beta 6$  and  $\beta 7$  strands in the extracellular domain (**Figure 3**). However, in the  $\alpha 4\beta 2$  receptor a second disulfide bond is formed between adjacent cysteines at the tip of loop C in the  $\alpha 4$  subunits. This feature is unique to nicotinic receptor  $\alpha$  subunits and is absent in all other Cys-Loop receptors [87]. An electron density was observed related to nicotine within  $\alpha\beta$  interfaces in the receptor ECD and for a single N-acetylglucosamine residue linked to a conserved asparagine in the Cys-Loop of each subunit, whereas the binding sites are believed

to be located within adjacent subunits in the EDC [40]. Residues Tyr100, Trp57, Trp156, Leu121, Try197, Val111 and Phe119 are the critical players in nicotine binding in the  $\alpha 4\beta 2$  receptor [40]. Together these residues form a hydrophobic jacket where Trp156 forms a cation- $\pi$  interaction between the indole ring and the pyrrolidine nitrogen; additionally, a hydrogen bond that is formed between the nicotine electropositive pyrrolidine nitrogen and the backbone carbonyl oxygen of W156 contributes to nicotine binding [40, 88].

The receptor begins at a large extracellular vestibule and narrows down into a funnel-like transmembrane channel supported by M2  $\alpha$  helices [89]. When considering the structures available for comparison, the  $\alpha 4\beta 2$  and GABA<sub>A</sub> receptor structures represent distinct desensitized states, where simulation shows a closed pore after ligand binding, as described in **Figure 4** along the pore there is a segment where the largest portion of the pore is  $\sim 2.8$  Å, this is comparable to GABA<sub>A</sub> and GlyR closed states. The structural data has shown to be consistent for both electrophysiological studies of the nAChR and GABA<sub>A</sub> receptors [90-92]. The  $\alpha 4\beta 2$  receptor has contributed significantly to the initiative of fully comprehending the regulation, binding and mechanism of action of the nAChR. Finally, the  $\alpha 4\beta 2$  receptor structure shows the nicotine binding characteristics and has contributed to information regarding the conformational changes that underlie a desensitization state through the Cys-Loop family [40, 93].

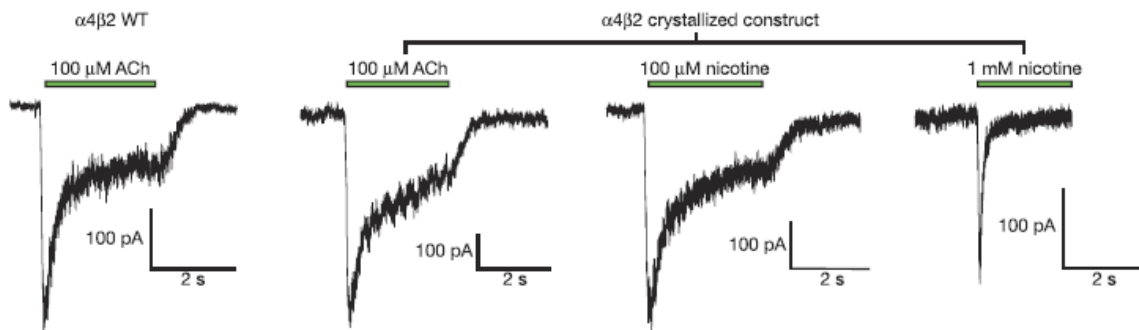


**Figure 2:** Patch-clamp current recordings of the  $\alpha 4\beta 2$  WT receptor and crystallized  $\alpha 4\beta 2$  receptor; under the induction of acetylcholine (ACh) and nicotine [40]. The  $\alpha 4\beta 2$  seems to retain functionality after removal of intracellular domain segments, when comparing currents, the  $\alpha 4\beta 2$  construct seems to have higher current amplitude when exposed to  $100 \mu\text{M}$  ACh. In addition, a slight difference was observed in the closing kinetics, nevertheless the  $\alpha 4\beta 2$  construct seems to represent a functional  $\alpha 4\beta 2$  in comparison with the wild type.

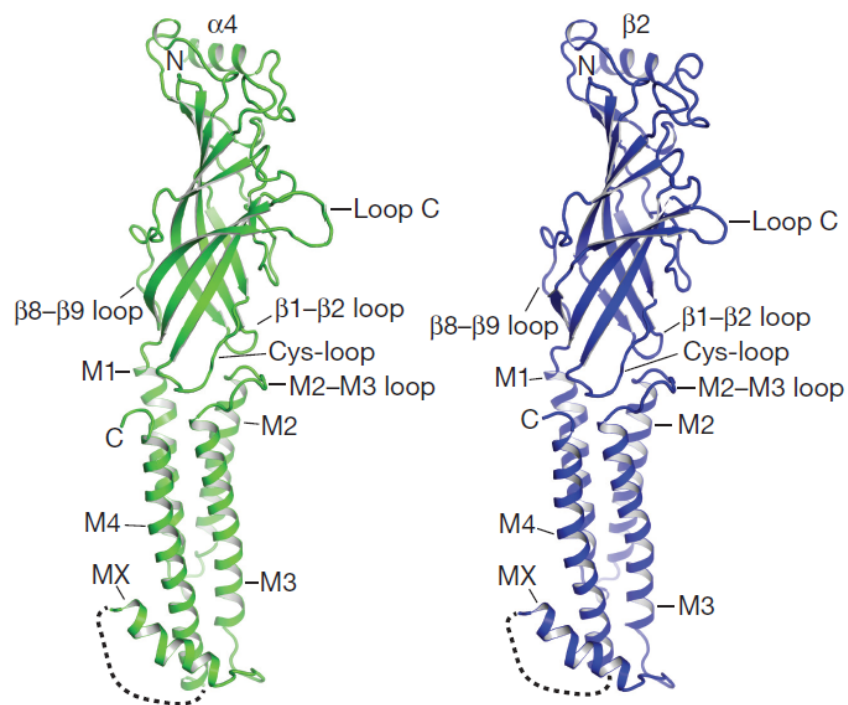


**Figure 3:** This is a view parallel to the plasma membrane from each independent subunit. This structure clearly shows the conserved segments that characterize the nAChR – Ligand Gated Ion channels; such as the four transmembrane segments M1 – M4, the Cys-Loop, the Loop C as well as the MX Loop, which is not present in other structures. The Beta arrangement in the extracellular loop is also characteristic of the nAChR.

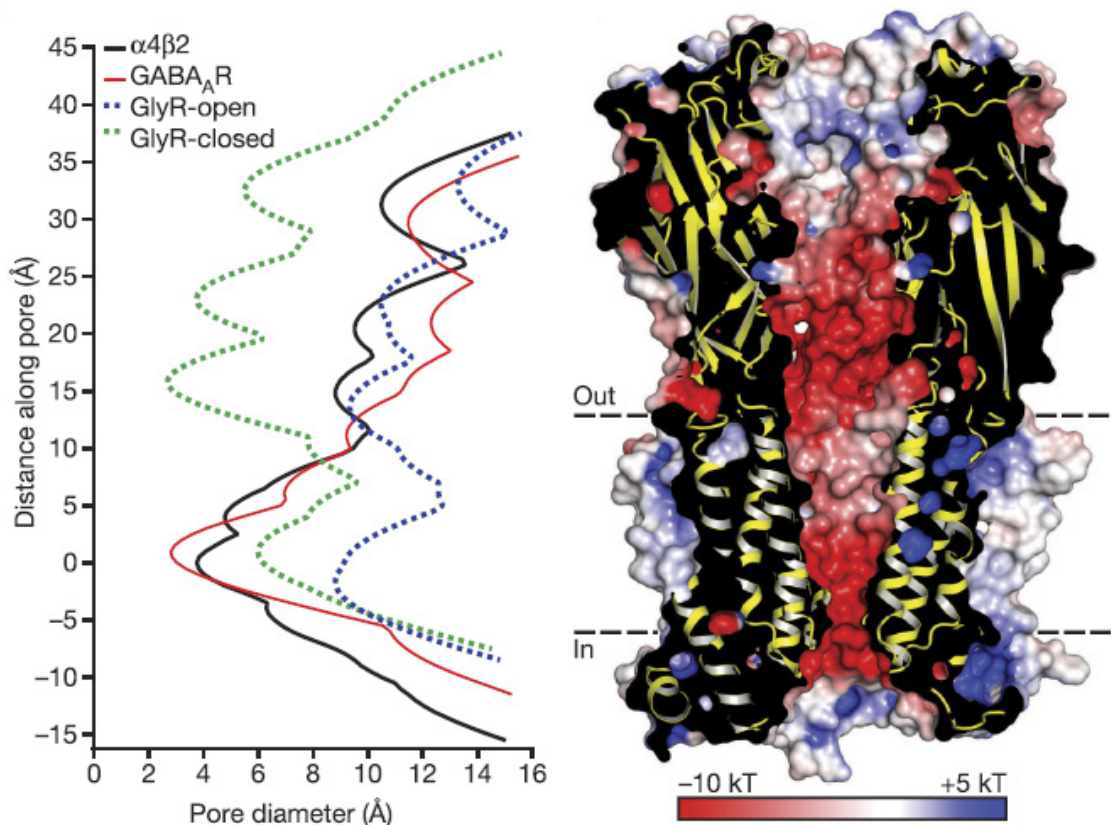


**Figure 4:** This is a  $\alpha 4\beta 2$  diameter mapping of the of the ion permeation pathway. The figure compares the GlyR,  $\text{GABA}_A \text{R}$ , and  $\alpha 4\beta 2$ . A comparison between the closed state of the  $\text{GABA}_A \text{R}$  and the  $\alpha 4\beta 2$  actual structure is shown. In addition, the colored electrostatic potential mapping allows the visualization of the highly negatively charged residues concentrated towards the center; a feature that allows ion permeation.



## **5. The Need for Better Solubilization Strategies and Appropriate Crystallization Conditions**

Through the years, crystallization of transmembrane proteins has relied on detergent solubilization and traditional hanging/sitting drop crystallization technologies on achieving protein crystals with high quality arrangement and diffracting properties. Detergents have served as tools to isolate, solubilize, and manipulate membrane proteins in order to comprehend their biochemical and physical properties [94]. However, even though a detergent might seem to be appropriate to crystallize a protein, it is essential to consider the behavior of such detergent within the crystallization environment. Henceforth, detergent selection and experiment conditions will have a great impact on whether a technique can be successfully applied to a specific membrane protein [94-97]. Having a clear understanding of detergent behavior, structure of micelles and protein-detergent complexes is thus crucial [94]. Detergent molecules have unique features: they are surface-active molecules that self-associate under the appropriate conditions, and bind to hydrophobic surfaces, particularly in a concentration-dependent manner [95-97]. The amphipathic character of detergents is evident: detergents are composed of a polar (or charged) head group and a hydrophobic tail, similar to naturally occurring lipids [94]. Most detergents can be sub-divided in three groups, depending on the type of head group: ionic (cationic or anionic), nonionic, or zwitterionic; although there are polymer-like detergents that are used as strong surfactants as well. Even though lipids and detergents have very similar characteristics, there are significant differences between them such as the concentration required for self-association and the type of multimolecular structures formed upon association [94].

The main problem during membrane protein isolation is working with mixed surfactant systems. Thus, understanding how detergents and lipids impact the physical nature of a protein-detergent-lipid complex is integral for successful isolation [95-97]. Detergent properties need to be carefully considered before membrane protein isolation [94]. The

detergents molecules can be classified as compounds called surfactants, which are surface active agents that reduce interfacial surface tension in mixtures, this is possible because of their chemical properties. Detergents use their amphiphilic properties to create a quasi-miscible environment allowing for the solvation of liquids. Under specific conditions, detergents agglomerate into spherical or ellipsoid micelles that are water-soluble [99-101]. Micelles are detergent macrostructures that occur when surface-active compounds form non-covalent clusters in solution; a process that is driven by the hydrophobic effect [99]. This type of spherical macrostructures is highly influenced by the detergent structural features, such as the net charge in the head group, head group size and the total amphiphilic effect known as hydrophilic-lipophilic balance (HLB). The HLB have been previously defined in the literature [102]; the HLB number can range from 0 to 40; an HLB number <10 is indicative of a detergent that has low water solubility, while an HLB number between 10 and 20 is indicative of a detergent that is highly soluble in water [102]. Furthermore, for single-chain detergents, HLB can be determined by the following equation (Eq 1) [105, 106]:

$$\text{Eq 1: HLB} = \Sigma H - \Sigma L + 7$$

In Eq 1 (H) is the contribution from the hydrophilic group, and (L) is the contribution from the lipophilic group as previously described in the literature [105, 106]. HLB values could be useful to select detergents for membrane protein extraction and purification, although the combination of a comprehensive analysis of the lipid content within the protein environment and the detergent structures, aggregation factor/number, and critical micelle concentration (CMC) could work as well [107, 108].

Detergent performance is highly dependable in the characteristics of the head groups. Ionic detergents are effective at extracting proteins from the membrane; nevertheless, such detergents are harsh and tend to drive the denaturing mechanism because they efficiently disrupt both inter- and intra-molecular protein-protein interactions [94]. On the other hand, nonionic detergents are mild and nondenaturing because they disrupt protein-lipid and lipid-

lipid interactions, rather than protein-protein interactions. Zwitterionic detergents are neutral (considering the net electrical charge) like the nonionic detergents, nevertheless it can disrupt protein-protein interactions like the ionic detergents; therefore, they are considered intermediate in their mildness. Several successful NMR-based structural studies of membrane proteins have been carried out in zwitterionic detergent solutions, a technique that completely relies on long-term protein stability in solution [111, 112].

The hydrophobic tail allows the detergent molecule to access into the lipid bilayer during the solubilization of membrane proteins. Furthermore, the detergent's hydrophobic tail sustains the hydrophobic portions of membrane proteins once they have been solubilized, thus preventing protein aggregation. Any alterations within the acyl chain have a direct effect on the detergent's physical properties, alternating the aggregation number, micelle CMC and even the sensitivity to electrolytes [94, 107, 108].

The length of the hydrophobic chain has shown influence in the protein functionality and stability as well. Short chain nonionic detergents, between 7 to 10 carbons in the acyl chain, are typically more deactivating than a longer chain, 12 carbons in the acyl chain or higher [109, 110]. As expected the hydrophobic chain length decreases the water solubility of the detergent monomer; thus causes close packing of detergent monomers within micelles. Branching and unsaturation of the hydrophobic chain also affect packing by inducing loose packing of detergent monomers in micelles [94, 107, 110].

There are no shortcuts when it comes to selecting the appropriate detergent for the isolation of a membrane protein. A rigorous analysis is required to achieve successful isolation of a stable/functional membrane protein [94,107,108]. Therefore, it is essential to conduct functional assays and use analytical methods to study detergent-purified membrane protein aggregation before using such protein for crystallization trials, structural NMR experiments, or Cryo-EM. The best approach towards a successful membrane protein isolation is the use of

a lipid-detergent holistic analysis, were the lipid environment and the structural characteristics of the membrane protein are considered before the purification process.

## **6. The Role of Lipids in the Solubilization of Membrane Proteins**

Transmembrane protein structures have shown that the identity or location of associated lipids could influence protein conformation or function [32, 36, 40 and 98]. Membrane proteins in their native environment are surrounded by a lipid bilayer. Consequently, the composition of the lipid bilayer must support the optimal functioning of membrane proteins [113]. Many elements and/or properties of the lipidic environment such as hydrophobic effects, hydrogen bonding or charge interactions, and lipid shape, as well as holistic influences like lipid fluidity and membrane tension, can influence the function of membrane proteins (See **Figure 5**).

There are two different levels of interaction between protein and lipids, provided by co-factor lipids and annular lipids [113]. The co-factor lipids are usually bound between the transmembrane domains or in direct contact with the protein and the lipid bilayer; these type of lipids are responsible for molecular regulations of transmembrane proteins and in some cases, are essential for protein functionality. Co-factor lipids usually have quasi-specific binding sites and can modulate protein conformation and kinetics [36, 40, 98, 100, 101, 113]. Furthermore, solvent lipids, better known as boundary/annular lipids, form an annular shell of lipids around the protein. Annular lipids do not interact directly with the protein body; however, they can indirectly impact membrane protein functionality by influencing the adjacent environment to modulate membrane fluidity and tension [113]. Even though co-factor lipids are more likely to appear in a crystalline protein arrangement, because of their strong protein-binding capabilities, annular lipids have also been identified in the crystal structures of several membrane proteins [114, 115]. Usually, the head groups of co-factor lipids are responsible for the strong binding; interactions are based in strong ion bridges or hydrogen bonds formed between the head groups of co-factor lipids and amino acid residues at headgroup-specific

sites. In occasions, headgroup-specific sites have been shown to be essential for protein function [116-118].

As is the case for most membrane proteins, LGICs are influenced by the lipidic environment. The GluCl receptor is an example of a LGIC where differences in co-factor lipid head groups significantly change receptor functionality and conformation [36]. The conformation and function of the nAChR have also been shown to be influenced by the lipidic environment [119, 120, 130, 131]. Agonist-induced conformational transitions of the Torpedo nAChR have been shown to be highly dependent on the surrounding lipid environment [121,122,123]. The nAChR exists predominantly in a resting (non-conducting) state. Agonist binding promotes a transient open (conducting) state and the continued presence of agonist results in a desensitized (nonconducting) state [124, 125]. When purified, Torpedo nAChRs are reconstituted into a synthetic lipid bilayer, comprised of either phosphatidylcholine (PC) or phosphatidylethanolamine (PE), the two most abundant phospholipids present in native Torpedo membranes. Under such conditions, a desensitized state is most common. However, insertion of cholesterol (CH) and phosphatidic acid (PA) to PC membranes (PC/PA/CH) completely restores nAChR functionality [126, 127]. Membranes containing PA or CH alone can stabilize differing proportions of nAChRs in the resting state; clearly, the presence of both lipids is required for full receptor functionality [126 - 128]. Cholesterol has been shown to influence the function and membrane distribution of the nAChR as well as other GPCRs; levels of approximately 35 mol percentage composition have been reported to promote maximal nAChR functionality. The existence of cholesterol recognition motifs in the transmembrane regions of the  $\beta$ 2AR and the nAChR further support cholesterol's role in the structure and function of the nAChR and related receptors [120-131]. Therefore, the lipid environment has been established as an essential modulator of membrane protein functionality. However, the development of descriptive models of nAChR-lipid interactions has been impaired by the lack of a detailed characterization of the nAChR conformation [120,132,133].

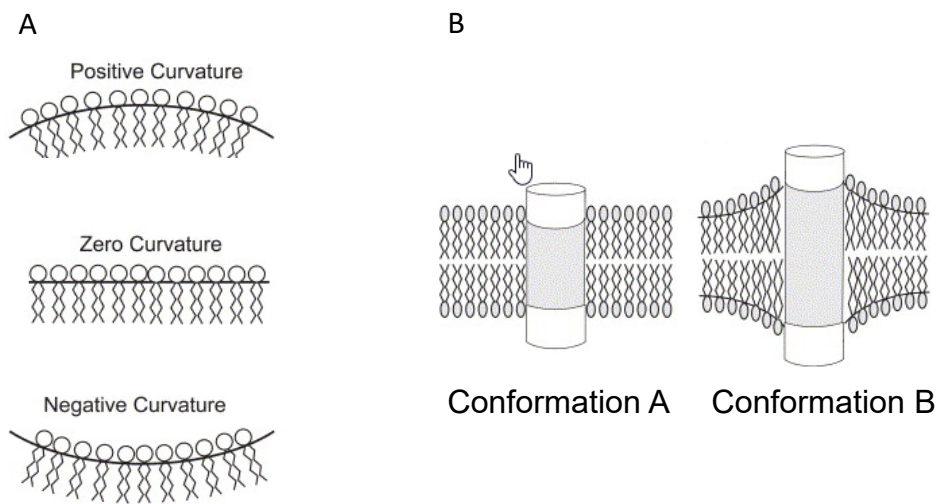


**Figure 5:** Lipid bilayer curvature can be influenced by the lipid structure. Depending on the lipid content the bilayer membrane can adopt a positive, negative or neutral curvature (A); this arrangement can influence protein conformation (B). In addition, a protein conformational change, as a result of a ligand/signal stimuli, can also induce the transformation of the lipid arrangement (B) (113). Thus, it is important to consider the lipid content and identity during crystallization characterizations.

## 7. Outlining our Contribution

Our research group has identified a class of detergents that show to be efficient in the isolation of a stable and fully functional nAChR from *Torpedo Californica* [134]. Such efforts have provided guidance regarding the basic molecular features required for the successful isolation of nAChR from the *Torpedo Californica* electroplax organ. Moving forward, we have performed a comprehensive analysis of nAChR purification using lipid analog detergents that sustain receptor functionality and stability [135, 136]. Planar Lipid Bilayer Electrophysiology was used to determine the functionality of the detergent-purified nAChR from *Torpedo Californica*; the unitary data were analyzed to compare lipid analog detergents in order to determine the best candidate for purification [135]. Analytical size exclusion chromatography was used to determine protein aggregation. Results provided a clear comparison of detergents, allowing us to identify those that promote receptor stability in solution [135]. After considering the functional and aggregation data, we performed traditional hanging drop and sitting drop crystallography, using novel lipidic cubic phase (LCP) crystallography as part of the lipid based approach [136].

Receptor mobility is essential for a successful crystallization within the LCP matrix and detergents have been shown to impact the integrity of the LCP [137, 138]. Thus, we analyzed the mobility of the detergent-purified nAChR on LCP [136, 139]. We have also examined how detergent-purified nAChR behaves in the LCP matrix over a 30-day period. Our results provided appropriate conditions for the isolation of a native nAChR from *Torpedo Californica* that would support receptor stability and functionality for LCP crystallization. Therefore, our findings will positively impact the nAChR structure initiative, bringing us one step closer to a high-resolution nAChR structure.

## Introduction References

1. Unwin N. "Refined structure of the nicotinic acetylcholine receptor at 4Å resolution". *J Mol Biol* vol. 346, 4 (2005): 967-89.
2. Brannigan G et al. "Embedded cholesterol in the nicotinic acetylcholine receptor". *PNAS* vol. 105, 38 (2008): 14418–14423.
3. Eiselé J. et al. "Chimaeric nicotinic-serotonergic receptor combines distinct ligand binding and channel specificities". *Nature* vol. 366, 6454 (1993): 479-483.
4. Albuquerque E. et al. "Mammalian Nicotinic Acetylcholine Receptors: From Structure to Function" *Physiol Rev* vol. 89, 1 (2009): 73–120.
5. Karlin A. et al. "Functional domains of the nicotinic acetylcholine receptor". *Ann NY Acad Sci* vol. 463 (1986): 53–69.
6. Lukas R.J. et al. "International Union of Pharmacology. XX. Current status of the nomenclature for nicotinic acetylcholine receptors and their subunits" *Pharmacol Rev* vol. 51 (1999): 397–401.
7. Hogg R.C. "Nicotinic acetylcholine receptors: from structure to brain function" *Rev Physiol Biochem Pharmacol* vol. 147 (2003): 1–46.
8. Báez-Pagán C.A. "Activation of the Macrophage  $\alpha 7$  Nicotinic Acetylcholine Receptor and Control of Inflammation" *Journal of Neuroimmune Pharmacology* vol. 10, 3 2015; 468–476.
9. Grando S.A. et al. "Connections of nicotine to cancer. *Nature Reviews Cancer* vol. 14 (2014): 419–429.
10. U.S. Cancer Statistics Working Group. United States Cancer Statistics: 1999–2013 Incidence and Mortality Web-based Report. Atlanta: U.S. Department of Health and



- Human Services, Centers for Disease Control and Prevention and National Cancer Institute; 2016. Available at: [www.cdc.gov/uscs](http://www.cdc.gov/uscs) 11/17/2018 6:43pm.
11. Alzheimer's Disease International. Policy Brief for G8 Heads of Government. The Global Impact of Dementia 2013-2050. London: Alzheimer's Disease International; 2013. [http://www.who.int/mental\\_health/neurology/dementia/en/](http://www.who.int/mental_health/neurology/dementia/en/) 11/17/2018 6:43pm.
  12. This thematic briefing of the World Health Organization is available on the WHO website ([http://www.who.int/mental\\_health/neurology/dementia/en/](http://www.who.int/mental_health/neurology/dementia/en/)) 11/17/2018 6:43pm.
  13. Katz B. et al. "A study of the "desensitization" produced by acetylcholine at the motor endplate" *J Physiol* vol. 138 (1957): 63–80.
  14. Takeuchi N. et al. "Effects of calcium on the conductance change of the end-plate membrane during the action of transmitter" *J Physiol* vol. 167 (1963): 141–155.
  15. Simpson J. A. et al. "The Release of Neural Transmitter Substances". *J Neurol Neurosurg Psychiatry* vol 32, 6 (1969): 638
  16. Albuquerque E.X. "The density of acetylcholine receptors and their sensitivity in the postsynaptic membrane of muscle endplates" *Proc Natl Acad Sci USA* vol. 71 (1974): 2818–2822.
  17. Kistler J. et al. "Crystalline arrays of membrane-bound acetylcholine receptor" *Proc Natl Acad Sci USA* vol. 78 (1981): 3678–3682.
  18. Noda M. et al. "Primary structure of  $\alpha$ -subunit precursor of Torpedo californica acetylcholine receptor deduced from cDNA sequence" *Nature* vol. 299 (1982): 793–797.
  19. Changeux J.P. et al. "The functional architecture of the acetylcholine nicotinic receptor explored by affinity labelling and site-directed mutagenesis" *Q Rev Biophys* vol. 25 (1992): 395–432.

20. Corringer P.J. et al. "Critical elements determining diversity in agonist binding and desensitization of neuronal nicotinic acetylcholine receptors" *J Neurosci* vol. 18 (1998): 648–657.
21. Celie P.H. et al. "Nicotine and carbamylcholine binding to nicotinic acetylcholine receptors as studied in AChBP crystal structures" *Neuron* vol. 41 (2004): 907–914.
22. Karlin A. et al. "Functional domains of the nicotinic acetylcholine receptor" *Ann NY Acad Sci* vol. 463 (1986): 53–69.
23. Bourne Y et al. "Crystal structure of a Cbtx-AChBP complex reveals essential interactions between snake  $\alpha$ -neurotoxins and nicotinic receptors" *EMBO J* vol. 24 (2005): 1512–1522.
24. Gao F. et al. "Agonist-mediated conformational changes in acetylcholine-binding protein revealed by simulation and intrinsic tryptophan fluorescence. *J Biol Chem* vol. 280 (2005): 8443–8451.
25. Hansen S.B. et al. "Structures of *Aplysia* AChBP complexes with nicotinic agonists and antagonists reveal distinctive binding interfaces and conformations" *EMBO J* vol. 24 (2005): 3635–3646.
26. Kuryatov A. "Mutation causing autosomal dominant nocturnal frontal lobe epilepsy alters  $\text{Ca}^{2+}$  permeability, conductance, gating of human  $\alpha 4\beta 2$  nicotinic acetylcholine receptors" *J Neurosci* vol. 17 (1997): 9035–9047.
27. Lester H.A. et al. "Hypersensitive knockin mouse strains identify receptors and pathways for nicotine action" *Curr Opin Drug Discov Dev* vol. 6 (2003): 633–639.
28. Lee W.Y. et al. "Principal pathway coupling agonist binding to channel gating in nicotinic receptors" *Nature* vol. 438 (2005): 243–247.
29. Zhong-Shan W. et al. "Ion channels gated by acetylcholine and serotonin: structures, biology, and drug discovery" *Acta Pharmacologica Sinica* vol. 36 (2015): 895-907

30. Dellisanti C.D. et al. "Crystal structure of the extracellular domain of nAChR alpha1 bound to alpha-bungarotoxin at 1.94 Å resolution" *Nat Neurosci* vol. 10,8 (2007): 953–962.
31. Zouridakis M. et al. "Crystal structures of free and antagonist-bound states of human  $\alpha 9$  nicotinic receptor extracellular domain" *Nat Struct Mol Biol* vol. 21, 11 (2014): 976–980.
32. Bocquet N. et al. "X-ray structure of a pentameric ligand-gated ion channel in an apparently open conformation" *Nature* vol. 457, 7225 (2009): 111–114.
33. Hilf R.J. et al. "X-ray structure of a prokaryotic pentameric ligand-gated ion channel" *Nature* vol. 452, 7185 (2008): 375–379.
34. Li S.X. et al. "Ligand-binding domain of an  $\alpha 7$ -nicotinic receptor chimera and its complex with agonist" *Nat Neurosci* vol. 14, 10 (2011): 1253–1259.
35. Nemezc A. "Creating an  $\alpha 7$  nicotinic acetylcholine recognition domain from the acetylcholine-binding protein: Crystallographic and ligand selectivity analyses" *J Biol Chem* vol. 286, 49 (2011): 42555–42565.
36. Althoff T. "X-ray structures of GluCl in apo states reveal a gating mechanism of Cys-loop receptors" *Nature* vol. 512, 7514 (2014): 333–337.
37. Miller P.S. et al. "Crystal structure of a human GABA<sub>A</sub> receptor" *Nature* vol. 512, 7514 (2014): 270–275.
38. Hassaine G. et al. "X-ray structure of the mouse serotonin 5-HT<sub>3</sub> receptor" *Nature* vol. 512, 7514 (2014): 276–281.
39. Huang X. "Crystal structure of human glycine receptor- $\alpha 3$  bound to antagonist strychnine" *Nature* vol. 526, 7572 (2015): 277–280.
40. Morales-Perez C.L. et al. "X-ray structure of the human  $\alpha 4\beta 2$  nicotinic receptor" *Nature* vol. 538 (2016): 411–415.

41. Rucktooa P. et al. "Insight in nAChR subtype selectivity from AChBP crystal structures" *Biochem Pharmacol* vol. 78 (2009): 777–787.
42. Wells G.B. et al. "Structural answers and persistent questions about how nicotinic receptors work" *Front Biosci* vol.13 (2008): 5479–5510.
43. Adams D.J. et al. "The permeability of endplate channels to monovalent and divalent metal cations" *J. Gen. Physiol.* Vol. 75 (1980): 493–510.
44. Zhou Y. et al. "Chemistry of ion coordination and hydration revealed by a K1 channel–Fab complex at 2.0Å resolution" *Nature* vol. 414 (2001): 43–48.
45. Bocquet, N. et al. "A prokaryotic proton-gated ion channel from the nicotinic acetylcholine receptor family" *Nature* vol. 445 (2007): 116–119.
46. Imoto, K. et al. "Rings of negatively charged amino acids determine the acetylcholine receptor channel conductance" *Nature* vol. 335 (1988): 645–648.
47. Giraudat J. "Structure of the high-affinity binding site for noncompetitive blockers of the acetylcholine receptor: Serine-262 of the delta subunit is labeled by [3H]chlorpromazine" *Proc. Natl Acad. Sci. USA* vol. 83 (1986): 2719–2723.
48. Padilla-Morales L.F. et al. "Effects of Lipid-Analog Detergent Solubilization on the Functionality and Lipidic Cubic Phase Mobility of the Torpedo californica Nicotinic Acetylcholine Receptor" *J Membrane Biol* vol. 243 (2011): 47–58.
49. Asmar-Rovira G.A. et al. "Biophysical and Ion Channel Functional Characterization of the Torpedo californica Nicotinic Acetylcholine Receptor in Varying Detergent–Lipid Environments" *J Membrane Biol* vol. 223, 1 (2008): 13–26.
50. Rabow L.E. et al. "From ion currents to genomic analysis: recent advances in GABA<sub>A</sub> receptor research. *Synapse* vol. 21 (1995): 189–274.
51. Jansen M. et al. "Modular design of Cys-loop ligand-gated ion channels: functional 5-HT<sub>3</sub> and GABA r1 receptors lacking the large cytoplasmic M3-M4 loop" *J Gen Physiol* vol. 131 (2008): 137–146.

52. Hansen S. B. et al. "An ion selectivity filter in the extracellular domain of Cys-loop receptors reveals determinants for ion conductance" *J Biol Chem* vol. 283 (2008): 36066–36070.
53. Yip G. M. et al. "A propofol binding site on mammalian GABA<sub>A</sub> receptors identified by photolabeling" *Nature Chem Biol* vol. 9 (2013): 715–720.
54. Nury H. et al. "X-ray structures of general anaesthetics bound to a pentameric ligand-gated ion channel" *Nature* vol. 469 (2011): 428–431.
55. Brejc K. et al. "Crystal structure of an ACh-binding protein reveals the ligand-binding domain of nicotinic receptors" *Nature* vol. 411 (2001): 269–276.
56. Newell J. G. et al. "Mutation of glutamate 155 of the GABA<sub>A</sub> receptor  $\beta$ 2 subunit produces a spontaneously open channel: a trigger for channel activation" *J Neurosci* vol. 24 (2004): 11226–11235.
57. Wagner D. A. et al. "Anarginine involved in GABA binding and unbinding but not gating of the GABA<sub>A</sub> receptor" *J Neurosci* vol. 24 (2004): 2733–2741.
58. Mukhtasimova N. et al. "Initial coupling of binding to gating mediated by conserved residues in the muscle nicotinic receptor" *J Gen Physiol* vol. 126 (2005): 23–39.
59. Xu M. et al. "Identification of channel-lining residues in the M2 membrane-spanning segment of the GABA<sub>A</sub> receptor alpha1 subunit" *J Gen Physiol* vol. 107 (1996): 195–205.
60. Cymes G. D. et al. "Probing ion-channel pores one proton at a time" *Nature* vol. 438 (2005): 975–980.
61. Thompson A. J. et al. "The structural basis of function in Cys-loop receptors" *Q Rev Biophys* vol. 43 (2010): 449–499.
62. Corringer P. et al. "Structure and pharmacology of pentameric receptor channels: from bacteria to brain" *Structure* vol. 20 (2012): 941–956.

63. Walstab J. et al. "5-HT<sub>3</sub> receptors: role in disease and target of drugs" *Pharmacol Ther* vol. 128 (2010): 146–169.
64. Livesey M. R. et al. "Rings of charge within the extracellular vestibule influence ion permeation of the 5-HT<sub>3A</sub> receptor" *J Biol Chem* vol. 286 (2011): 16008–16017.
65. Hansen S. B. et al. "An ion selectivity filter in the extracellular domain of Cys-loop receptors reveals determinants for ion conductance" *J Biol Chem* vol. 283 (2008): 36066–36070.
66. Moroni M. et al. "In glycine and GABA<sub>A</sub> channels, different subunits contribute asymmetrically to channel conductance via residues in the extracellular domain" *J Biol Chem* vol. 286 (2011): 13414–13422.
67. Hibbs R. E. et al. "Principles of activation and permeation in an anion-selective Cys-loop receptor" *Nature* vol. 474 (2011): 54–60.
68. Bocquet N. et al. "X-ray structure of a pentameric ligand-gated ion channel in an apparently open conformation" *Nature* vol. 457 (2009): 111–114.
69. Kelley S. P. et al. "A cytoplasmic region determines single-channel conductance in 5-HT<sub>3</sub> receptors" *Nature* vol. 424 (2003): 321–324.
70. Peters J. A. et al. "Novel structural determinants of single channel conductance and ion selectivity in 5-hydroxytryptamine type 3 and nicotinic acetylcholine receptors" *J Physiol (Lond)* vol. 588 (2010): 587–596.
71. Bouzat C. et al. "Structural basis of the different gating kinetics of fetal and adult acetylcholine receptors" *Neuron* vol. 13 (1994): 1395–1402.
72. Zuber B. et al. "Structure and super organization of acetylcholine receptor rapsyn complexes" *Proc Natl Acad Sci USA* vol. 110 (2013): 10622–10627.
73. Legendre P. et al. "The glycinergic inhibitory synapse" *Cell Mol Life Sci* vol. 58 (2001) 760–793.

74. Lynch J. W. et al. "Molecular structure and function of the glycine receptor chloride channel" *Physiol Rev* vol. 84 (2004): 1051–1095.
75. Langosch, D. et al. "Conserved quaternary structure of ligand gated ion channels: the postsynaptic glycine receptor is a pentamer" *Proc Natl Acad Sci USA* 85 (1988): 7394–7398
76. Rajendra S. et al. "The glycine receptor" *Pharmacol Ther* vol. 73 (1997): 121–146.
77. Laube B. et al. "Modulation of glycine receptor function: a novel approach for therapeutic intervention at inhibitory synapses?" *Trends Pharmacol Sci* vol. 23 (2002): 519–527.
78. Grudzinska, J. et al. "The  $\beta$  subunit determines the ligand binding properties of synaptic glycine receptors" *Neuron* vol. 45 (2005): 727–739.
79. Vandenberg, R. et al. "Antagonism of ligand-gated ion channel receptors: two domains of the glycine receptor  $\alpha$  subunit form the strychnine-binding site" *Proc Natl Acad Sci USA* vol. 89 (1992): 1765–1769.
80. Bode A. et al. "The impact of human hyperekplexia mutations on glycine receptor structure and function. *Mol Brain* vol. 7 (2014): 2.
81. Hibbs R. E. et al. "Principles of activation and permeation in an anionselective Cys-loop receptor" *Nature* vol. 474 (2011): 54–60.
82. Yoluk, O. et al. "Stabilization of the GluCl ligand-gated ion channel in the presence and absence of ivermectin" *Biophys. J.* vol. 105 (2013): 640–647.
83. Nelson, M. E. et al. "Alternate stoichiometries of  $\alpha 4\beta 2$  nicotinic acetylcholine receptors" *Mol. Pharmacol.* Vol. 63 (2003): 332–341.
84. Tapia, L. et al. "Ca<sup>2+</sup> permeability of the  $(\alpha 4)_3(\beta 2)_2$  stoichiometry greatly exceeds that of  $(\alpha 4)_2(\beta 2)_3$  human acetylcholine receptors" *Mol. Pharmacol.* vol. 71 (2007): 769–776.

85. Lester, H. A. et al. "Nicotine is a selective pharmacological chaperone of acetylcholine receptor number and stoichiometry. Implications for drug discovery" *AAPS J.* vol. 11 (2009): 167–177.
86. Zhou, Y. et al. "Human  $\alpha 4\beta 2$  acetylcholine receptors formed from linked subunits" *J. Neurosci.* vol. 23 2003: 9004–9015.
87. Karlin, A. et al. "Emerging structure of the nicotinic acetylcholine receptors" *Nature Rev. Neurosci.* vol. 3 (2002): 102–114.
88. Dougherty, D. A. et al. "The cation- $\pi$  interaction" *Acc. Chem. Res.* vol. 46 (2013): 885–893.
89. Becchetti, A. et al. "The role of nicotinic acetylcholine receptors in autosomal dominant nocturnal frontal lobe epilepsy" *Front. Physiol.* vol. 6 (2015): 22.
90. Celentano, J. J. et al. "Multiphasic desensitization of the GABA<sub>A</sub> receptor in outside-out patches" *Biophys. J.* vol. 66 (1994): 1039–1050.
91. Léna, C. et al. "Allosteric modulations of the nicotinic acetylcholine receptor" *Trends Neurosci.* vol. 16 (1993): 181–186.
92. Paradiso, K. G. et al. "Nicotine is highly effective at producing desensitization of rat  $\alpha 4\beta 2$  neuronal nicotinic receptors" *J. Physiol.* vol. 553 (2003): 857–871.
93. Labriola, J. M. et al. "Structural sensitivity of a prokaryotic pentameric ligand-gated ion channel to its membrane environment" *J. Biol. Chem.* vol. 288 (2013): 11294–11303.
94. Garavito, R.M. et al. "Detergents as Tools in Membrane Biochemistry" *Journal of Biol. Chem.* vol. 276, 35 (2001): 32403–32406.
95. Zulauf, M. et al. "Crystallization of Membrane Proteins (Michel, H., ed)" *CRC Press, Inc., Boca Raton, FL.* (1991); 54–71.
96. Tanford, C. et al. "The Hydrophobic Effect" *John Wiley & Sons, Inc.* (1980): 1
97. Rosen, M. J. et al. "Surfactants and Interfacial Phenomena" *John Wiley & Sons, Inc.* (1978): 1



98. Zhou, Y. "Chemistry of ion coordination and hydration revealed by a K<sup>+</sup> channel–Fab complex at 2.0 Å resolution" *Nature* vol. 414 (2001): 43–48.
99. Rosen, M. et al. "Surfactants and Interfacial Phenomena" 3rd ed. Hoboken, John Wiley & Sons, Inc. 2004: 1.
100. Allen, S. J. et al. "Folding Kinetics of an  $\alpha$  Helical Membrane Protein in Phospholipid Bilayer Vesicles" *J. Mol. Biol.* vol. 342 (2004): 1279-1291.
101. Compton, E. L. R. et al. "Kinetics of an individual transmembrane helix during bacteriorhodopsin folding" *J Mol Biol* vol. 357, 1 (2006): 325-338.
102. Krugliakov, P. et al. "Hydrophile-Lipophile Balance of Surfactants and Solid Particles: Physicochemical Aspects and Applications" *Amsterdam, Elsevier Science.* vol. 1 (2000): 1.
103. Egan, R. W. et al. "Hydrophile-lipophile balance and critical micelle concentration as key factors influencing surfactant disruption of mitochondrial membranes" *J. Biol. Chem.* vol. 251, 14 (1976): 4442-4447.
104. Umbreit, J. N. et al. "Relation of detergent HLB number to solubilization and stabilization of D-alanine carboxypeptidase from *Bacillus subtilis* membranes" *Proc Natl Acad Sci USA.* 70, 10 (1973): 2997-3001.
105. Davies, J. et al. "A quantitative kinetic theory of emulsion type, I. Physical chemistry of the emulsifying agent" *Proceedings of the International Congress of Surface Activity, 2nd, ed. J. Schulman, New York, Academic Press.* vol. 1 (1957): 1.
106. Davies, J. T. et al. "Interfacial Phenomena" *New York, Academic Press.* vol 1 (1961): 1.
107. Nicholson, D. W. et al. "Triton solubilization of proteins from pig liver mitochondrial membranes" *Biochim Biophys Acta.* vol. 856, 3 (1986): 515-525.

108. Dickie, P. et al. "Purification and characterization of membrane-bound fumarate reductase from anaerobically grown *Escherichia coli*" *Can J Biochem.* vol. 57, 6 1979: 813-821.
109. Seddon, A. M. et al. "Membrane proteins, lipids and detergents: not just a soap opera." *Biochim Biophys Acta (BBA) -Biomembranes.* vol. 1666, 1-2 (2004): 105-117.
110. le Maire M, "Interaction of membrane proteins and lipids with solubilizing detergents" *Biochim Biophys Acta.* vol. 1508, 1-2 (2000): 86-111.
111. Evanics, F. et al. "Topology of an outer-membrane enzyme: Measuring oxygen and water contacts in solution NMR studies of PagP" *J Am Chem Soc.* vol. 128, 25 (2006): 8256-8264.
112. Hwang, P. M., et al. "Solution structure and dynamics of the outer membrane enzyme PagP by NMR" *Proc Natl Acad Sci USA* vol. 99, 21 (2002): 13560-13565.
113. Lee, A. G. et al. "How lipids affect the activities of integral membrane proteins" *Biochimica et Biophysica Acta* vol. 1666 (2002): 62– 87.
114. Lee, A. G. et al. "Lipid–protein interactions in biological membranes: a structural perspective" *Biochim. Biophys. Acta* vol. 1612 (2003): 1 – 40.
115. Belrhali, H. et al. "Protein, lipid and water organization in bacteriorhodopsin crystals: a molecular view of the purple membrane at 1.9 Å resolution" *Structure* vol. 7 (1999): 909– 917.
116. Valiyaveetil F.I. et al. "Lipids in the structure, folding and function of the KcsA K<sup>+</sup> channel" *Biochemistry* vol. 41 (2002): 10771–10777.
117. L. Heginbotham, L. et al. "Functional reconstitution of a prokaryotic K<sup>+</sup> channel" *J. Gen. Physiol.* vol. 111 (1998): 741– 749.
118. Nogi, T. et al. "Crystal structures of photosynthetic reaction center and high-potential iron–sulfur protein from *Thermochromatium tepidum*: thermostability and electron transfer" *Proc. Natl. Acad. Sci.* vol. 97 2000: 13561– 13566.

119. Hamouda, A.K. "Assessing the Lipid Requirements of the *Torpedo californica* Nicotinic Acetylcholine Receptor" *Biochemistry* vol. 45 (2006): 4327-4337.
120. daCosta, C. J. "A Lipid-dependent Uncoupled Conformation of the Acetylcholine Receptor" *J. Biol. Chem.* vol. 284, 26 (2009): 17819–17825.
121. Burger, K. et al. "Regulation of receptor function by cholesterol" *Cell. Mol. Life Sci.* vol. 57 (2000): 1577-1592.
122. Barrantes, F. J. et al. "Structural basis for lipid modulation of nicotinic acetylcholine receptor function" *Brain Res. Rev.* vol. 47 (2004): 71-95.
123. Tillman, T. et al. "Effect of membrane lipids on ion channel structure and function" *Cell Biochem. Biophys.* vol. 38 2003: 161-190.
124. Corringer, P. J. et al. "Nicotinic receptors at the amino acid level" *Annu. Rev. Pharmacol. Toxicol.* vol. 40 (2000): 431-458.
125. Karlin, A. et al. "Emerging structure of the nicotinic acetylcholine receptors" *Nat. Rev. Neurosci.* vol. 3 (2002): 102-114.
126. Fong, T. M. et al. "Correlation between acetylcholine receptor function and structural properties of membranes" *Biochemistry* vol. 25 (1986): 830-840.
127. daCosta, C. J. B. et al. "Lipid-protein interactions at the nicotinic acetylcholine receptor" *J. Biol. Chem.* vol. 277 (2002): 201-208.
128. Baenziger, J. E. et al. "Effect of membrane lipid composition on the conformational equilibria of the nicotinic acetylcholine receptor" *J. Biol. Chem.* vol. 275 (2000): 777-784.
129. Barrantes, F. J. et al. "Structural basis for lipid modulation of nicotinic acetylcholine receptor function" *Brain Res. Reviews* vol. 47 (2004): 71-95.
130. Baier, C. J. et al. "Disclosure of cholesterol recognition motifs in transmembrane domains of the human nicotinic acetylcholine receptor" *Scientific Reports* vol. 1 (2011):1-7.

131. Gimpl, G. "Interactions of G protein coupled receptors and cholesterol" *Chemistry and Physics of Lipids* vol. 199 (2016): 61-73.
132. Guzman, G. R. et al. "The polarity of lipid-exposed residues contributes to the functional differences between Torpedo and muscle-type nicotinic receptors" *J Membr Biol* vol. 214 (2006): 131-138.
133. Baez-Pagan, C. A. et al. "Potential role of caveolin-1-positive domains in the regulation of the acetylcholine receptor's activatable pool: Implications in the pathogenesis of a novel congenital myasthenic syndrome" *Channels* vol. 2 (2008): 180-190.
134. Asmar-Rovira, G. A. et al. "Biophysical and ion channel functional characterization of the Torpedo californica nicotinic acetylcholine receptor in varying detergent-lipid environments" *J Membr Biol* vol. 223 (2008): 13-26
135. Padilla-Morales, L. F. et al. "Effects of lipid-analog detergent solubilization on the functionality and lipidic cubic phase mobility of the Torpedo californica nicotinic acetylcholine receptor" *J Membrane Biol* vol. 243 (2011): 47-58.
136. Padilla-Morales, L. F. et al. "Assessment of the functionality and stability of detergent purified nAChR from Torpedo using lipidic matrixes and macroscopic electrophysiology" *Biochim Biophys Acta*. vol. 1858, 1 (2016): 47-56.
137. Ai, X. "Membrane Protein Crystallization in Lipidic Mesophases: Detergent Effects" *Biophysical Journal* vol. 79 (2000): 394-405.
138. Caffrey, M. et al. "Crystallizing membrane proteins using lipidic mesophases" *Nature Protocols* vol. 4, 5 (2009): 706-731.
139. Padilla-Morales, L.F. et al. "Functionality and stability data of detergent purified nAChR from Torpedo using lipidic matrixes and macroscopic electrophysiology" *Data in Brief* vol. 6 (2016): 433-437.

## CHAPTER 2. Thesis Aims

The nicotinic acetylcholine receptor (nAChR) from *Torpedo californica* is a heteropentamer transmembrane protein composed of four homologous subunits ( $2\alpha$ ,  $\beta$ ,  $\gamma$ , and  $\delta$ ), the torpedo nAChR belongs to the family of ligand-gated ion channels (LGICs) such as GABA<sub>A</sub> receptor and the glycine receptor (GlyR) [1]. Since LGIC receptors are critical components of the signal transduction mechanism; they are important targets to treat several neurodegenerative disorders/diseases such as Alzheimer's and Parkinson's, as well as cardiovascular diseases, cancer and inflammation [2,3]. However, one of the most widely studied ion channels, the nAChR, is a prime example of a multimeric membrane complex of which a high-resolution native structure is still unavailable [1]. A comprehensive approach focused on detergent structure, and solubilization conditions could provide valuable information on the preparation of functionally active complex membrane proteins.

Our laboratory has carried out functional/lipidomics/stability studies with *Torpedo californica* nAChR that has been solubilized and affinity-purified using different detergents. Our results indicate that lipid-like detergent structures seems to be more suited for *Torpedo californica* nAChRs solubilization. Recently, we have significantly expanded this lipid-based approach by assessing the function and stability of nAChR-detergent complex (nAChR-DC) with the primary goal of understanding how detergent structure affects the ion channel function, agonist binding, aggregation state of the solubilized nAChR, and ultimately the ability to form three-dimensional crystals [4,5,6]. The **hypothesis** was that certain detergents could alter the native environment of solubilized membrane proteins to induce structural alterations that lead to destabilization, potentially irreversible denaturation and aggregation. During solubilization, a detergent may selectively exclude critical lipid species present in the native cell membrane that is essential for protein function or stability [7]. This detergent-specific lipid alteration could produce a partial structural change in the hydrophobic domains

of the protein that could lead to destabilization, partial or full denaturation and eventual aggregation. Thus, our efforts were focused on designing an effective strategy to isolate the nAChR from *Torpedo californica* in a functional manner, followed by crystallization trials using lipidic cubic phase (LCP) as *in-meso* crystallization matrix [4,5,6].

Our strategy employed the use of lipid analog detergents to isolate the nAChR, purify it using affinity column, and perform functionality and soluble-stability studies using planar lipid bilayer (PLB) and analytical size exclusion chromatography, respectively. In addition, we determined nAChR mobile fractions and diffusion coefficients using LCP coupled with Fluorescent Recovery After Photo-Bleaching (FRAP) as a parameter for stability. The following were our specific aims:

**Aim 1. Study the effect of lipid and cholesterol analog detergents families on the functionality and soluble stability of the nAChR from *Torpedo californica*.** The objective of this aim was to define which detergents preserve ligand binding and ion-channel functionality. Our working hypothesis was that the functional state of the nAChR is dependent on the lipid environment of detergent-solubilized protein and consequently, is dependent on detergent structure. The approach was to 1) record single-channel events of the *Torpedo* nAChR in detergent-solubilized, affinity-purified samples using a planar bilayer system [4,5,6]; and 2) assess ligand binding using the  $\alpha$ -Bungarotoxin ( $\alpha$ -BTx) binding assay coupled to analytical size-exclusion chromatography (A-SEC), as described by Asmar-Rovira, *et al.*, 2008 [1]. Solubilization conditions that produced stable and functional nAChRs were used for conventional vapor diffusion crystallization screening. The outcome of this aim was the establishment of lipid-based strategies to preserve function and stability in detergent-solubilized membrane proteins.

Sub-Aims Outline:

- 1 Record single channel events for each of the detergents' isolation conditions using planar lipid bilayer (PLB).
- 2 Examine the state of aggregation of the nAChR using analytical size exclusion chromatography (A-SEC).
- 3 Conventional vapor diffusion crystallization screening.

**Aim 2. Elucidate the effect detergents on nAChR long-term stability, and mobile fraction and diffusion coefficient in the LCP.** Diffusion of a membrane protein (i.e., mobile fraction) is critical for crystal formation [8]. Therefore, the screening of suitable crystallization conditions for membrane proteins was achieved by coupling LCP to FRAP (LCP-FRAP). We performed LCP-FRAP experiments with detergent-solubilized/fluorescently-tagged nAChR-DC and estimated the mobile fraction and diffusion coefficient [4,5,6]. The outcome of this aim was the establishment of correlations with other aggregation studies, but also to define suitable conditions for nAChR crystallization in LCP.

Sub-Aims Outline:

1. Assess mobile fraction and diffusion coefficient in LCP crystallization conditions by coupling.
2. Examine the long-term stability of detergent-solubilized nAChR within the LCP matrix.
3. Crystallization trials of the nAChR using the most favorable crystallization conditions in the LCP matrix.

## Thesis Aims References

1. Asmar-Rovira, G. A. et al. "Biophysical and ion channel functional characterization of the *Torpedo californica* nicotinic acetylcholine receptor in varying detergent-lipid environments" *J Membr Biol* vol. 223 (2008): 13-26.
2. Báez-Pagán, C.A. et al. "Activation of the Macrophage  $\alpha 7$  Nicotinic Acetylcholine Receptor and Control of Inflammation" *Journal of Neuroimmune Pharmacology* vol. 10, 3 (2015): 468–476.
3. Grando, S. A. "Connections of nicotine to cancer" *Nature Reviews Cancer* vol. 14 (2014): 419 - 429.
4. Padilla-Morales, L. F. et al. "Effects of lipid-analog detergent solubilization on the functionality and lipidic cubic phase mobility of the *Torpedo californica* nicotinic acetylcholine receptor" *J Membrane Biol* vol. 243 (2011): 47–58.
5. Padilla-Morales, L.F. et al. "Assessment of the functionality and stability of detergent purified nAChR from *Torpedo* using lipidic matrixes and macroscopic electrophysiology." *Biochim Biophys Acta*. vol. 1858, 1 (2016): 47-56.
6. Padilla-Morales, L.F. et al. "Functionality and stability data of detergent purified nAChR from *Torpedo* using lipidic matrixes and macroscopic electrophysiology" *Data in Brief* vol. 6 (2016): 433–437.
7. Quesada, O. et al. "Uncovering the lipidic basis for the preparation of functional nicotinic acetylcholine receptor detergent complexes for structural studies" *Sci. Rep.* vol. 6 (2016): 32766.
8. Cherezov, V. et al. "LCP-FRAP Assay for Pre-Screening Membrane Proteins for in Meso Crystallization" *Cryst Growth Des.* vol. 8, 12 (2008): 4307-4315.



## CHAPTER 3. Materials and Methods

### 1. Detergent Purification of the nAChR from the *Torpedo Californica*

Our methodology used affinity bind-and-elute chromatography to extract nAChR from the *Torpedo Californica's* *electroplax* tissue as previously described by Asmar-Rovira et al. 2008 [1]. Affinity purification to isolate nAChR from *Torpedo Californica* (an abundant natural source; **Figure 1**) has been employed since the 70's by Weil et al. 1974 [2]. However previous procedures oversee the significant contribution that lipids could have during isolation of the nAChR. We employed a comprehensive lipid-based approach by using lipid analog detergents to extract the nAChR from the membranous tissue successfully. We considered detergent structure, physical properties, and the *Torpedo Californica's* lipid distribution to determine suitable lipid analog detergent structures that would allow the isolation of a functional nAChR prompt for crystallization. Since our approach used native nAChR from a natural source, the purified nAChR remained unaltered in contrast with cell cultured and engineered nAChR protein constructs that have been previously crystallized.

#### 1.1 *Torpedo Californica* Electroplax Homogenization and Crude Membrane Preparation

*Torpedo Californica electroplax* tissue was thawed and weighed at 4.0 °C in the cold room. The homogenization process was also completed at temperature conditions of 4.0 °C within the cold room; ice was used to sustain temperature when working outside of the cold room. Buffer H (10mM Sodium Phosphate, 5mM EDTA, 5mM EGTA, 15mM DTPA, 400mM NaCl, 0.02% Sodium Azide) was used to homogenize the tissue at a proportion of 0.5 g per mL of buffer H. The buffer was supplemented with iodoacetamide at 0.094 mg/mL and 1 $\mu$ /mL of 200mM PMSF to avoid protein degradation.

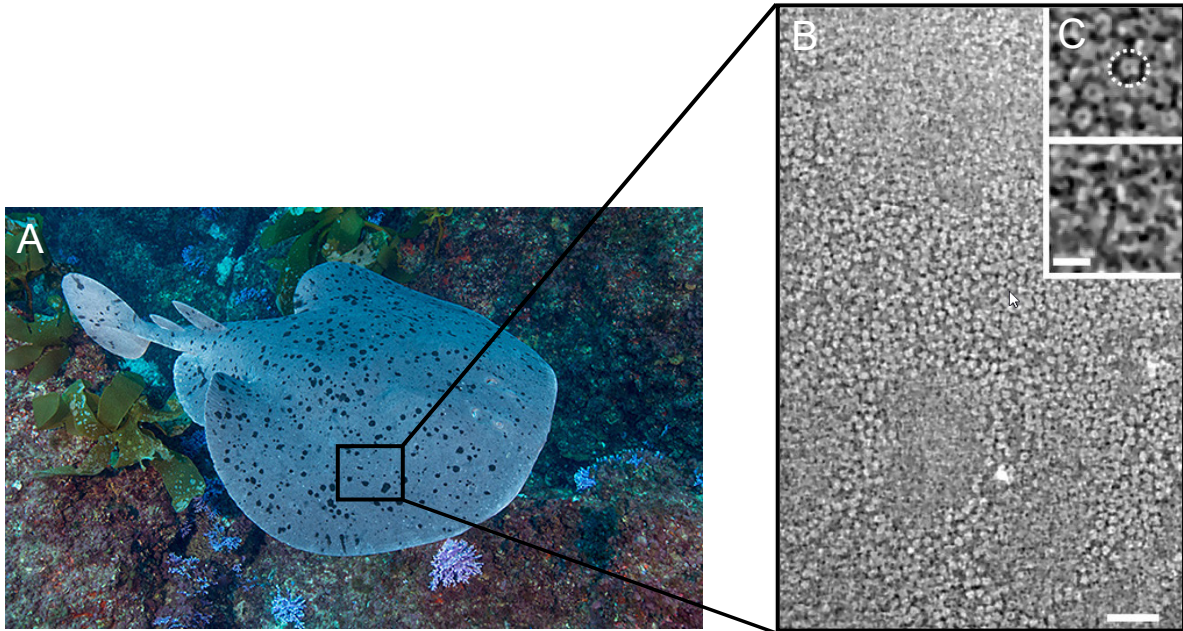


**Figure 1:** Shows the content and the quasi crystallographic arrangement of nAChR in the Torpedo electroplax tissue. A) A picture of the Torpedo California a type of Pacific Electric Ray and a natural source of nAChR. B) A tomographic slice cross-sectioning of the extracellular domain of the nAChRs. The picture evidences the high density of nAChR across the tissue. C) Magnification of the tomographic image, the donut arrangement is noticed very clearly in this image. [Scale bars: 50 nm B frame; 10 nm C frame].

The tissue was homogenized using a blender set up in “hi” for 4 minutes. The foam generated during the process was gently removed, and the homogenized tissue let to settle for no more than 15 minutes to avoid protein degradation. The homogenate was then transferred into 50 mL tubes and centrifuged at 6500 rpm for about 25 min at 4.0 °C. After centrifugation, the supernatant was transferred into a 500 mL beaker using sterile gauze as a filter to prevent membranous material from accessing the solution. The filtered supernatant was subsequently transferred into Ti70 ultracentrifuge tubes (Beckman Coulter) for ultracentrifugation. The ultracentrifuge, which was pre-cooled at 4.0 °C, was set to run at 40,000 rpm for 30 min at 4.0 °C. The resulting protein pellet is re-suspended in buffer K (10mM Sodium Phosphate, 5mM EDTA, 5mM EGTA, 5mM DTPA, 0.02% Sodium Azide) using a small syringe; the pellets were always handled gently.

The resuspended pellet mixture was poured into 2 x 50 mL tubes and placed in a pre-cooled centrifuge. The samples were centrifuged at 6,500 rpm for 25 min at 4.0 °C. After the centrifugation was completed, the tubes were removed from the centrifuge and placed immediately on ice. A white pellet in the peach-colored supernatant was obtained. This pellet was "softer" than the previous pellet and is composed of unfolded protein. Therefore, extreme care was necessary to prevent pellet disruption during sample handling. The supernatant was carefully transferred into 500 mL beaker. Subsequently, the supernatant in the 500 mL beaker was transferred into cleaned Ti70 tubes. Equal amounts of supernatant were transferred to each Ti70 tube to balance the weight. The samples were then centrifuged at 40,000 rpm for 30 min at 4.0 °C (the centrifuge was pre-cooled). Once the centrifugation step was over, the tubes were removed and immediately placed on ice. The supernatant was clear, and the pellet was off-white. Approximately 5 mL of previously prepared 40% sucrose Buffer K solution supplemented with 200 µL of PMSF) was added into one of the tubes. The pellet was resuspended by gently shaking the tubes this step was repeated as needed to resuspend all the pellets available, transferring the solution from one tube into the other. All the resuspended

pellets were transferred into a 250 mL beaker, and a syringe was used to disrupt them. Formation of bubbles (foaming) was prevented to avoid protein degradation. The syringe charge and discharge process were performed until no colloidal particles were noticed. The resulting material was transferred into 50 mL cryotubes and stored at -70 °C. **Figure 2** outlines the process step by step.

## **1.2 Acetylcholine Affinity Column Preparation**

The resin used was customized to purify the nAChR via ligand binding selectively. Bio-Rad Affi-Gel-10 (Bio-Rad; Hercules, CA) resin was used as backbone and bromoacetylcholine was covalently attached to the resin to act as a fixed ligand. **Figure 3** outlines the complete column preparations process.

To prepare the resin, 1 bottle (25mL) of Bio-Rad Affi-Gel-10 was thawed at 4.0 °C in the cold room until a homogeneous liquid was noticed. The resin was well mixed and poured into a large column (Bio-Rad Econo Column (2.5 x 20 cm)). The storage solution (isopropanol) was drained to the resin level, and resin dryness was avoided.

A 150 mL wash of cold isopropanol was applied to the resin; any residual resin was rinsed from the bottle using isopropanol (2-propanol, Sigma 190764) and poured into the column, which was then drained completely. The resin was washed with cold distilled water for 20 minutes. While the amount of water used during the rinse was not relevant, the contact time was crucial. Therefore, the 20-minute time frame was never exceeded. A MOPS-Cystamine solution (1.05 g of cystamine dihydrochloride dissolved in 100 mL MOPS at pH=8.0) was added to the column; 10 mL was saved for column rinse. This solution was prepared fresh (while the Bio-Rad resin was thawed). The resin was resuspended using a harmonious shaking movement; vigorous shaking was avoided. Afterward, the resin was poured into a beaker with a stir bar; the column was rinsed twice with the remaining MOPS-Cystamine solution to recover most of the resin from the walls. The resin was stirred at medium speed (gently) for ~4.5 hours in the cold room.

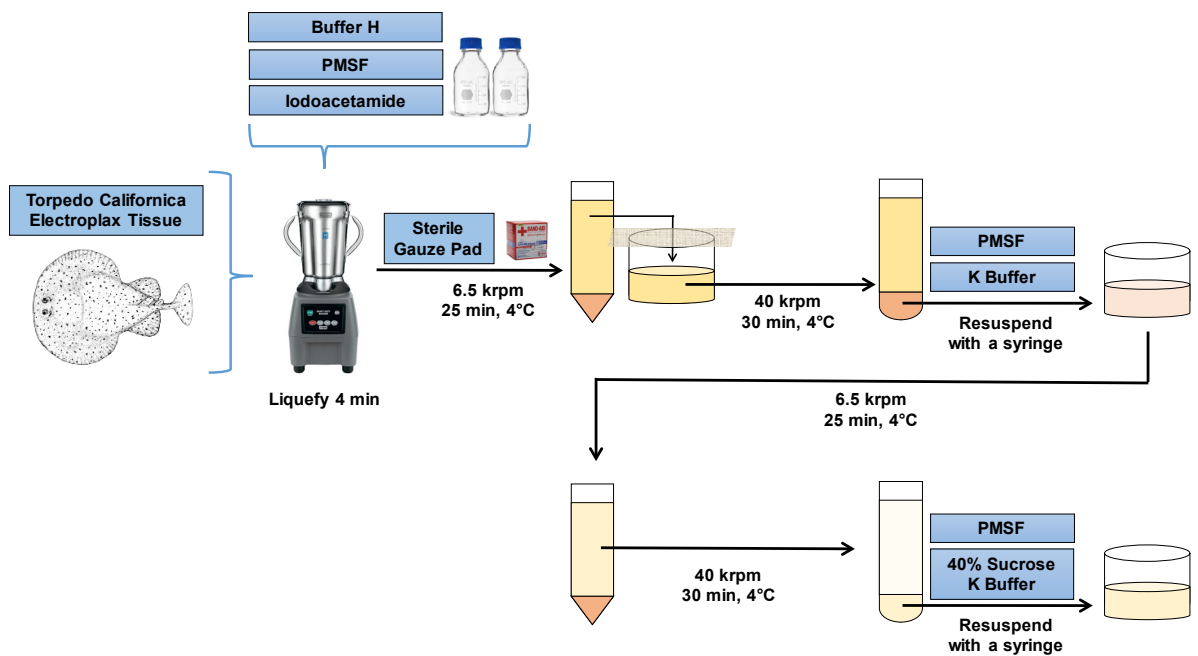


**Figure 2:** This image outlines the overall process of crude membrane isolation. The complete process was executed at 4 °C in the cold-room to avoid additional stress to the nAChR when solubilized. The *Torpedo Californica* tissue was provided by Aquatic Research Consultant.

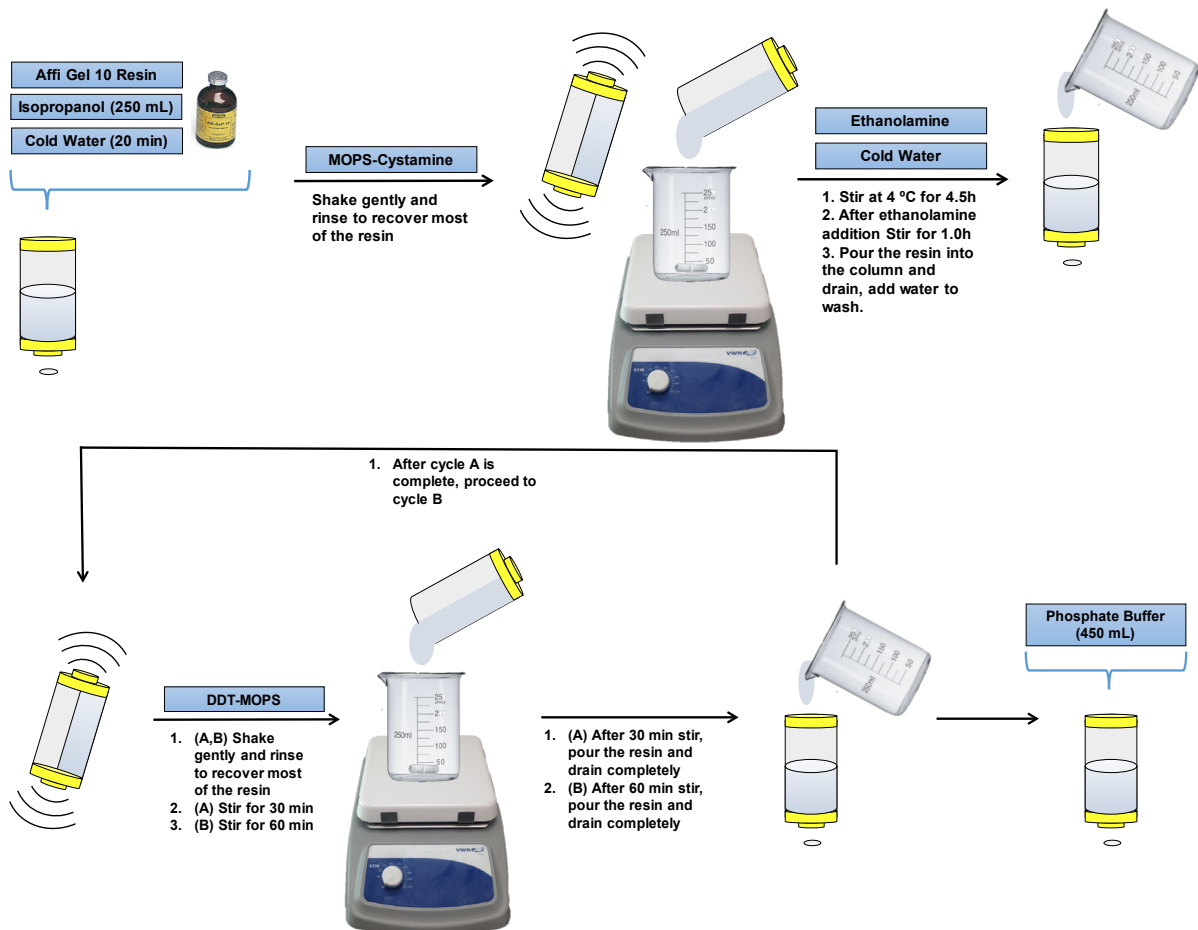


**Figure 3:** This image outlines the overall process of affinity column preparation. The procedure was executed at 4 °C.

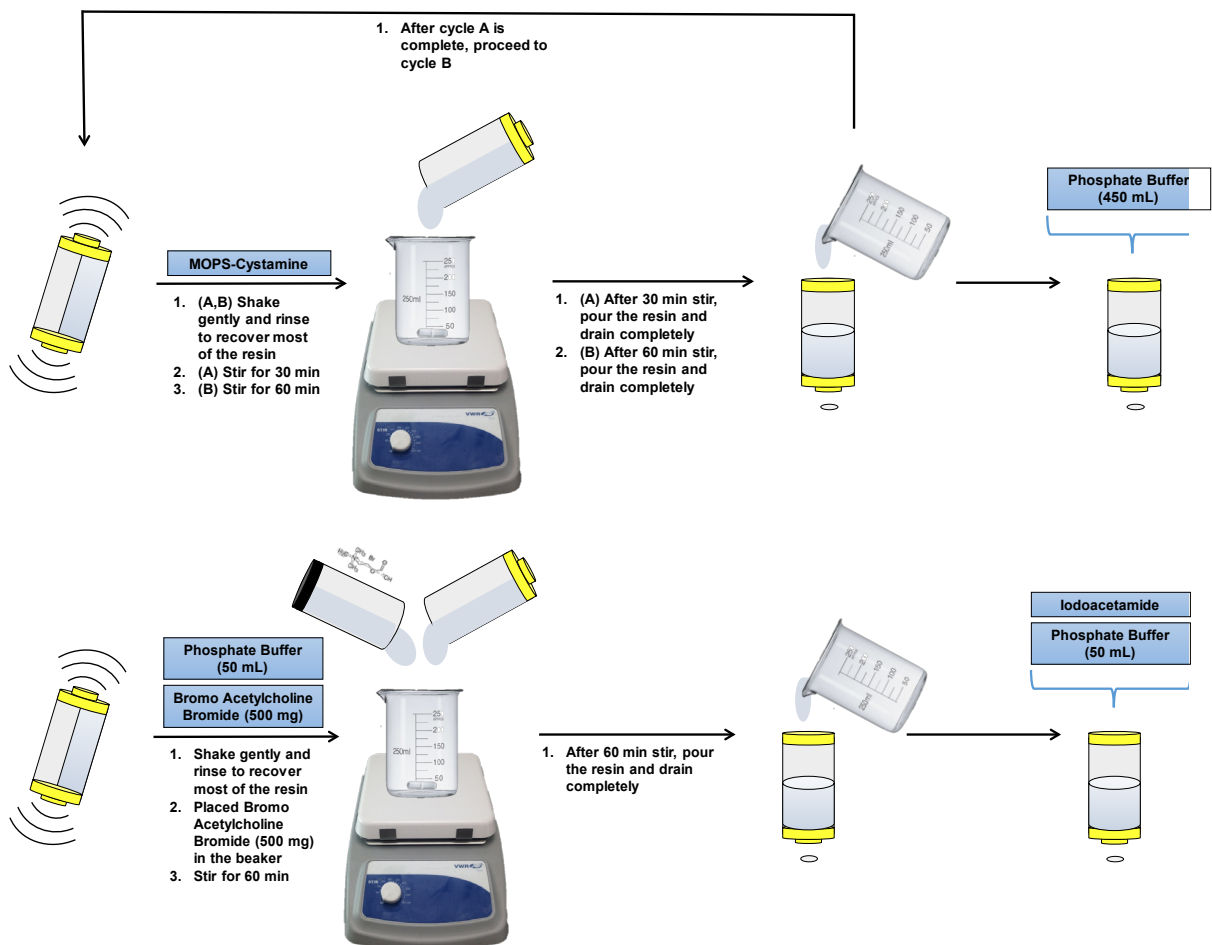


**Figure 3 continuation:** This image outlines the overall process of affinity column preparation.

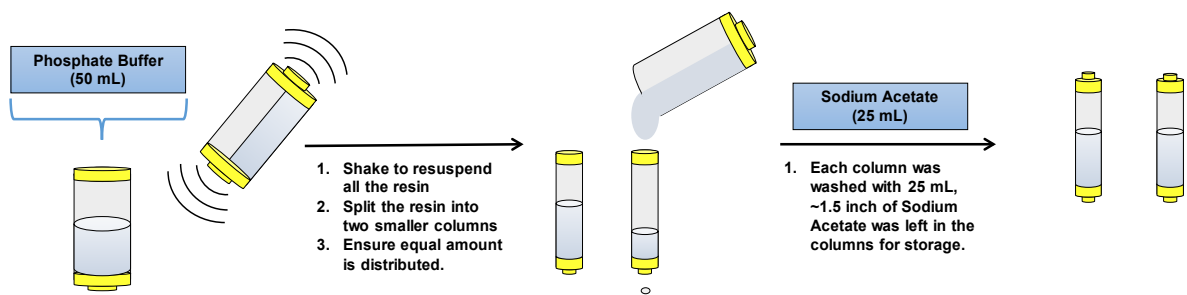


**Figure 3 continuation:** This image outlines the overall process of affinity column preparation. Columns are subsequently stored at in the cold-room (4 °C).



After the 4.5 hours, 5 mL of 1.0 M ethanolamine (pH=8.0) was added and stirred for 1 hour in the cold room to ensure blocking any remaining reactive groups. The resin was poured into the large column and drained thoroughly. Subsequently, 150 mL of cold filtered water was used to rinse any remaining ethanolamine; 20 mL of water was used to flush the beaker to ensure maximum resin recovery.

From this step forward, all procedures were performed at room temperature. A solution of DDT-MOPS was prepared (2.1 g DTT in 100 mL MOPS at pH=8.0). This solution was usually made during the 4.5h reaction timeframe. The resin was resuspended with DTT-MOPS solution and poured into a beaker; the column was rinsed twice with DTT-MOPS solution to recover most of the resin from the column's walls. The resin was stirred at medium speed for 30 minutes at room temperature. Subsequently, the resin was poured into a column, and the DTT solution was drained completely. The resin was resuspended for a second time with room temperature DTT-MOPS solution and poured into a beaker; the column was rinsed twice with DTT-MOPS solution. Once the resin was placed in the beaker, it was stirred at medium speed for 60 minutes at room temperature.

Our next step was to pour the resin into a column and exchange the DTT solution with 450 mL of room temperature 50 mM phosphate buffer (pH=7.0). The column cap and bottom seal were washed with water and with the 50 mM phosphate buffer to ensure that no residual DTT was present in the following steps. The resin was resuspended with 50 mL of 50 mM phosphate buffer (pH=7.0) at room temperature and poured into a beaker containing 500 mg of bromoacetylcholine; the column was rinsed twice to recover most of the resin from the walls. The reaction was stirred at medium speed for 1 hour at room temperature. While the resin was stirring, 50 mg of iodoacetamide was dissolved in 50 mL of cold, filtered water (this solution was prepared fresh to avoid iodoacetamide degradation). After 1 hour, the resin was transferred into a column, and the bromoacetylcholine was drained. The column was washed with the previously prepared iodoacetamide solution to methylate any remaining reactive

groups. The beaker was rinsed with the iodoacetamide solution to recover most of the resin from the beaker's walls. The wash solution was drained completely, and the resin was resuspended with 50 mL of 50 mM Sodium Acetate storage buffer (pH=4.0). The resuspended resin was poured in equal amounts into two small columns (25 mL); this step was performed rapidly to prevent resin settlement. The columns were washed with 25 mL of 50 mM Sodium Acetate storage buffer (pH=4.0), the buffer was drained until leaving enough to cover the resin for long-term storage.

### **1.3 Affinity Purification of nAChR Using Lipid Analog Detergents**

For more than a decade our group has been able to successfully purify the nAChR using lipid analog detergent [1]. The nAChR purification was accomplished using a selectively bind and elute style chromatography; the wash step was executed using the same lipid analog detergent as used for the crude membrane extraction. The primary role of this wash was to ensure a substantial reduction of impurities such as associated proteins and non-functional (binding capable) nAChR. All the purification process was executed in the cold room; otherwise, samples were handled on the ice when exposed to laboratory room environment. The complete process is outlined in **Figure 4**.

Detergent extraction was as follows: 13 mL of DB-1 (10 mM 3-(N-Morpholino)propanesulfonic acid (MOPS), 100 mM Sodium Chloride (NaCl), 0.1 mM ethylenediamine tetra-acetic acid (EDTA) and 0.02% Sodium Azide ( $\text{NaN}_3$ ) buffer, 2 mL of 10% lipid analog detergent solution and 5 mL of crude membrane protein were combined in a ~26 mL Ti-70 ultracentrifuge tube. The order was considered critical because the nAChR should not be exposed to high concentrations of detergent. Extreme detergent concentrations could alter the native state of the nAChR.

The DB-1 volume can be adjusted according to the crude membrane volume as long as the detergent:protein ratios are kept equal in proportion. The resulting detergent concentration was as follows: 1% for LDAO, DDM, FC-12, FC-14 FC-16, LFC-12, LFC-14 and LFC-16; 2%

for Cholate, CHAPS, CHAPSO and OG; and 4% for BigCHAP. The mixture was shaken gently for 1 hour at 4.0 °C to avoid aggregation. The solubilized membrane protein was ultracentrifuged (Beckman L-100 XP) at 40,000 rpm for 52 min (Beckman 70 Ti rotor); full brake was applied to stop the spinning. **Figure 4** describes the overall process. The next steps were executed while the ultracentrifuge was running:

1. The storage buffer was drained completely from affinity columns.
2. Column flush: As a flush step, 50 mL of cold distilled water was applied to each column through the edge of the funnel to avoid column bed disruption and then the columns were drained completely.
3. Column conditioning: 50 mL of 1.5 x CMC detergent solution were added to each column. The columns were ready for use after the CMC detergent solution was drained completely.

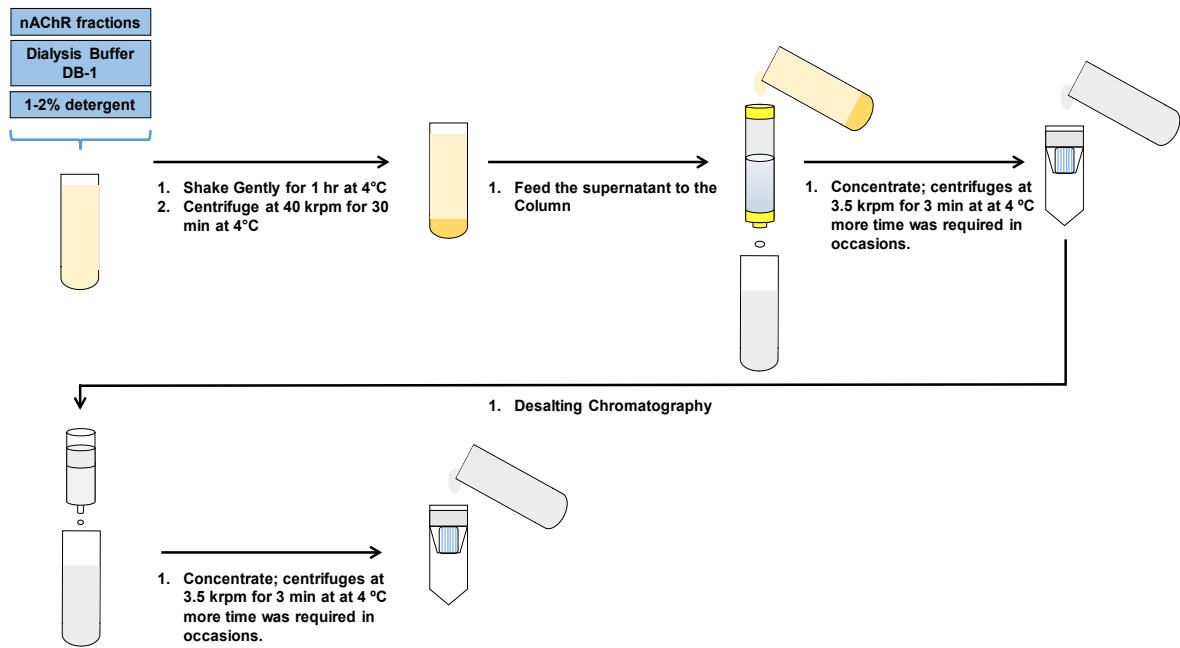


**Figure 4:** This image outlines the overall process of affinity column execution to purified nAChR from homogenized *Torpedo Californica* membranes. Detergent purification process is executed in the cold-room at 4 °C. After collection, sample is measured to determine nAChR concentration.

After ultracentrifugation of extracted protein, the samples were applied to the column using a pipette to avoid foaming and allowed to drain almost entirely. The flow-through was collected for troubleshooting purposes. A total of 50 mL of 1X DB-1 detergent buffer was added to the column through the edge of a funnel and allowed to drain almost entirely. This previous step was the detergent wash; flow-through was again collected for troubleshooting purposes. The column flow-through was used in occasions to test for protein concentration and perform SDS-Page to determine if the nAChR was not bound to the column or to assess the degree of purity.

While the column was draining, the elution buffer was prepared:

1. In a 50 mL tube, 90 mg of Carbamylcholine Chloride and 292 mg of NaCl were added.
2. A total of 50 mL of 1X DB-1 detergent buffer was added just before use. This procedure was required as the Carbamoylcholine (Carb) could be degraded in the detergent buffer.

A total of 50 mL of elution buffer was added to the column through the edge of a funnel; the elution was recovered in clean 50 mL tubes. While the nAChR was eluted from the affinity column, the PD-10 desalting column was equilibrated with 25 mL of 1X DB-1 detergent buffer. The affinity column was rinsed with 50 mL of distilled water (dH<sub>2</sub>O) and drained completely; subsequently, 50 mL of 50 mM Acetic Acid Storage buffer (pH=4.0) were added; the funnel was removed, and the columns were sealed.

The purified protein sample was concentrated using concentrating filters units (Millipore 100K NMWL) in the centrifuge at 3500 rpm at 4.0 °C; filters were pre-rinsed with ~2.5 mL of dH<sub>2</sub>O before use. Subsequently, the concentrated protein sample was processed through a pre-equilibrated desalting column. The desalting column was drained entirely and flushed with 5 mL of 1X DB-1 detergent buffer to maximize protein yield. The flow-through was collected in filter concentrators (Millipore Amicon Ultra). The purified protein was concentrated down to a 150-200 µL range, transferred to a microtube and stored in the cold room at 4.0 °C.

## 2. Characterization of Detergent Purified nAChR

The characterization was focused on testing the functionality and stability of the purified-nAChR to determine suitable purification conditions for crystallization. The goal was to purify nAChR from *Torpedo Californica* electroplax tissue using lipid analog detergents to produce functional and stable detergent-nAChR complexes for further crystallization trials.

Protein identity was determined by SDS-PAGE, as the comparison of weight standards with receptor subunits allows for positive identification. The similarity between nAChR subunits required the use of gradient acrylamide gels coupled to high voltage exposure. The nAChR functionality was examined by planar lipid bilayer; this technique uses commercially available lipids to create a man-made lipid bilayer membrane in an electronic cell. The setup allows for electrophysiological studies where single ion channel openings and ion flux can be studied. Lipid analog detergents have shown to sustain ion channel functionality in the planar lipid bilayer as previously observed by Asmar-Rovira et al. 2008 [1]. Nevertheless, our methods are designed to understand further how the structural properties of lipid analog detergents might influence the nAChR ion channel functionality. As a result, the planar lipid bilayer technique allows the determination of the best isolation conditions, through a lipid-based approach that sustains ion channel functionality. Soluble stability was examined by comparing aggregation levels of detergent-nAChR samples using analytical size exclusion chromatography. Protein stability directly correlates with the number of aggregates in a sample. The detergent purification that showed the lowest levels of protein aggregation was considered adequate to sustain nAChR stability when isolated from the native lipidic membrane.

In addition, nAChR crystallization experiments were performed using Lipidic Cubic Phase (LCP). The LCP provides a membranous environment that can sustain the stability of integral membrane proteins while delivering a crystallization mechanism that favors the formation of membranous proteins crystals. However, the LCP mechanism relies on constant mobility of

the membranous proteins across the lipidic media. Our methods examined the suitable detergent purification of the nAChR that maintains protein mobility after 30-days of preparation. If crystallization conditions are appropriate, based on available published data a 30-day time frame should be enough to notice signals of crystal formation.

After the suitable conditions for crystallization of the nAChR were determined, the samples were submitted for crystallization trials in Lipidic Cubic Phase - 1-monoolein matrix, Lipidic Sponge Phase (LSP) - hydrated 1-Monoolein matrix, and Vapor diffusion (Sitting Drop and Hanging Drop). The crystals were transported under cryo conditions to a high-power particle accelerator synchrotron facility for protein diffraction. The synchrotron facility allows for high definition diffraction and selective area scanning. By using these tools, we were able to scan segments of the harvested crystals that contained the best reticle arrangement, thus increasing the chances for high-resolution diffraction.

Finally, a holistic analysis of crystallization data, stability data and functional data was performed to better understand the fundamental contributions of each variable to the production of high-quality diffracting crystals. A model was created using multivariate analysis in SAS-JMP software and assuming a linear behavior for each regression.

### **2.1 SDS-Page and Protein Concentration Analysis by BCA**

Samples from each purified protein condition were subjected to SDS-PAGE. The samples were mixed with loading buffer at a 1:1 ratio and boiled (100 °C) for ~ 1.5 min in a heating block. Samples were then run in a pre-cast acrylamide gel for 45 minutes at 200 volts in the cold room and analyzed along with a molecular weight marker (161-0395 Precision Plus Protein; BIORAD) to identify nAChR subunits.

A Pierce BCA Protein Assay Kit was used to determine protein concentration (BCA Protein Assay Kit 23225; Thermo Scientific). A standard curve was generated ranging from 0.5 to 12.0 mg/mL, and the linear regression was performed using Microsoft Excel.

## 2.2 Ion Channel Functionality Assessment in Planar Lipid Bilayer Assays

Functional readings were executed in a Warner Instruments (Hamden, CT) model BC-525D Bilayer Clamp Amplifier with an 8-pole Low-pass Bessel filter (LPF-8). Signal was translated through an Axon Instruments Digidata 1322-A interface (Sunnyvale, CA) and processed in a PC based computer. Approximately 100  $\mu$ L of purified nAChR were coated with PMAL-C8 (Poly (maleic anhydride-alt-1- decene) substituted with 3-(Dimethylamino) propylamine) detergent (Anatrace; Maumee Ohio). Data were successfully analyzed using Clampfit software 10.0/11.0 (Molecular Devices Corporation, Union City, CA). The complete process is outlined in **Figure 5**.

A mixture of Brain PC (L- $\alpha$  Phosphatidylcholine), PE (L- $\alpha$ -ethanolamine) (Avanti Polar Lipids; Alabaster, AL) and cholesterol (Anatrace; Maumee Ohio) was prepared at  $\sim$ 75 mg/mL (using a 3:1:1 ratio) in chloroform. The mixture was then evaporated under nitrogen and resuspended in decane to a concentration of  $\sim$ 75 mg/mL. A 1:1 dilution in decane was applied to a 200  $\mu$ m aperture in a cup-shaped Teflon chamber and allowed to air dry before reopening under nitrogen. The cup chamber was fitted into the rear cavity of a rectangular plastic holder to create the bipolar system, containing electrode apertures which were filled with 1 M KCl. Previously prepared salt bridges were used to complete the system connection. To prepare the salt bridges, a 1 M KCl solution was heated to  $\sim$ 70  $^{\circ}$ C to dissolve agarose to a 2% final concentration. Capillary tubes were cut to  $\sim$  2.5-inch length and bent into a U shape using an open flame. The U-shaped tubes were filled with heated 1 M KCl, 2% agarose solution and cooled at room temperature. The resulting salt bridges tubes were stored in the cold room submerged in a 1 M KCl solution.

The Teflon chamber and front plastic holder cavity were filled with  $\sim$ 1 mL of bilayer buffer solution: 10 mM HEPES, 1 mM  $MgCl_2$ , and 150 mM NaI at pH 7.2. Salt bridges were used to connect the electrodes to the chambers, and the Teflon chamber aperture was re-coated with lipid mixture until a seal was detected resulting in a membrane capacitance = 90–170 pA.



Approximately 1–25  $\mu\text{g}$  of PMAL-coated nAChR vesicles were added to the front chamber and stirred for  $\sim 15$  min. while verifying protein incorporation through a 5–10 pA change in membrane capacitance.

Stirring was stopped for data recording. The membrane potential was gradually increased (+10mV steps) to +70 mV for 1 min and switched gradually (-10mV steps) to -70 mV for 1 min to record a baseline signal with protein and no agonist induction. Then, the membrane potential was turned off before adding 0.5  $\mu\text{M}$  Carb., gradually increasing to +70 mV for 2–5 min or until steady currents were observed, switching to -70 mV for the same timeframe and continuing these cycles until the membrane broke. Clampfit 10.0/11.0 software (Molecular Devices Corporation, Union City, CA) was used to analyze 5–30 min file segments, manually searching for 100–1000 ion channel opening-closing events, which were integrated and processed with a PC based computer, generating mean open channel current and mean open channel time histograms from which values for these parameters were obtained for each detergent purification.

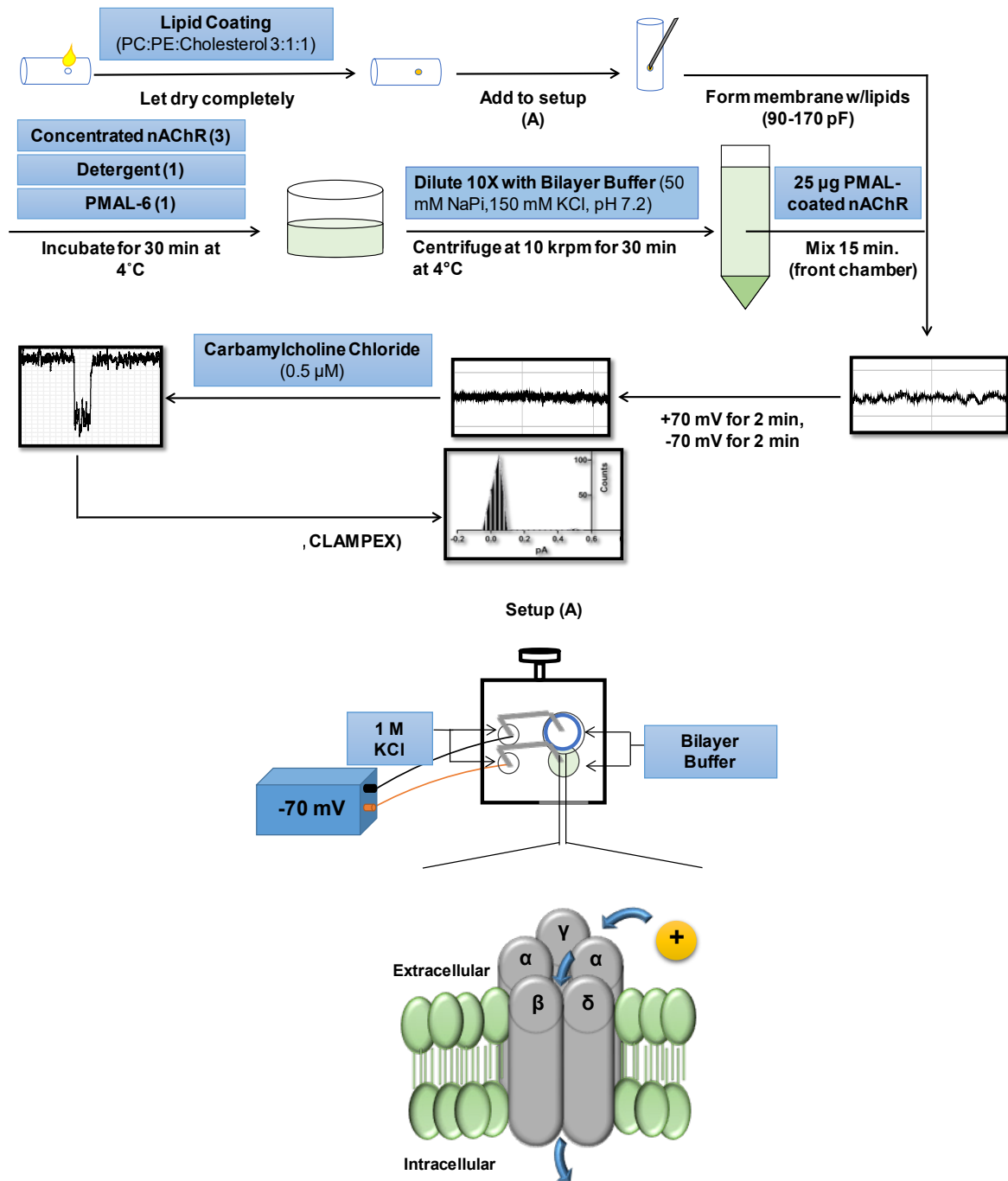


**Figure 5:** Outline of the overall process for the functionality assessment of detergent purified nAChR. Single channel currents were recorded and examined to compare receptor functionality after detergent purification.

### 2.3 Two Electrode Voltage Clamp Experiments (TEVC) on Oocytes

For the TEVC experiments, we used a modified version of previous protocols published by our group [3]. **Figure 6** outlined the process to execute the TEVC experiments. Briefly, membrane current recordings were performed at room temperature (rt) (21–25 °C) for 16–36 h after injection; longer incubation times were tested, however oocyte viability was compromised for some detergents. Therefore we choose a favorable timeframe for all the detergents in this study. Oocytes were placed in a 200  $\mu$ L chamber that was continuously perfused with 5 mL/min of a calcium-depleted OR-2 (containing in mM: 82 NaCl, 2.5 KCl, 1 MgCl<sub>2</sub>, 5 HEPES; and adjusted to 7.6 pH with a NaOH solution) to elude the activation of an endogenous Ca<sup>2+</sup> dependent chloride current. The macroscopic currents were induced by a 5s application of a non-saturating concentration of acetylcholine (100  $\mu$ M, to make sure that we are not underestimating the amplitudes because of desensitized receptors) through a computer control 8 channel perfusion system (VC-8, Warner Instruments, Hamden, CT) connected to a 8 – 1 perfusion mini manifold, at a holding potential of –70 mV using a Gene Clamp 500B amplifier (Axon Instruments, Foster City, CA). Electrodes were filled with a 3 M KCl solution, and the resistances were calculated to average 1.3 m $\Omega$ . The nAChRs macroscopic currents were filtered at 100 Hz and digitized at 1000 Hz using a Digidata 1440A interface (Axon Instruments, Foster City, CA). Data was processed and analyzed using the Clampex 10.2, (pCLAMP 10.2 software, Molecular Devices) running on a Microsoft Windows-based computer.

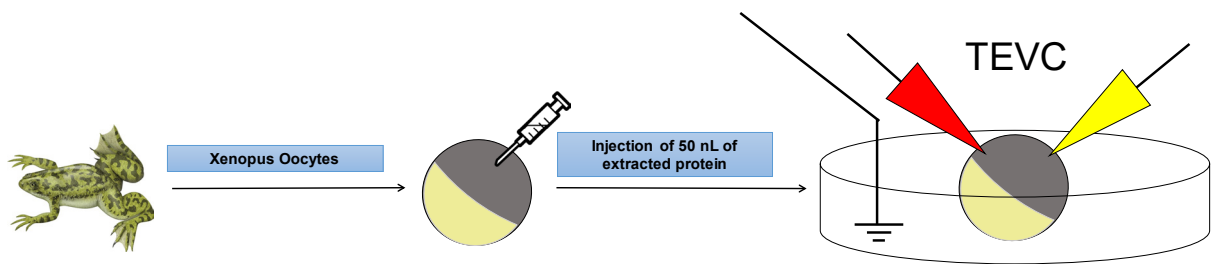


**Figure 6:** This flow diagram shows the overall process of TEVC evaluation to determine macroscopic functionality of detergent purified nAChR. Macroscopic currents are evaluated for comparison.

## 2.4 Lipidic Cubic Phase Mobility Analysis using Fluorescence After Photo Bleaching

Lipidic Cubic Phase mobility analysis was executed using Fluorescence After Photo Bleaching (FRAP) experiments that were performed following the protocols and conditions described by Cherezov, et al., 2008 [5] with the following modifications: 1) 50  $\mu\text{L}$  of a solution containing 2.0 - 7.0 mg/mL of ligand-affinity purified nAChRs was incubated with  $\alpha\text{BTX}$  conjugated with Alexa 488 in a 1:2.5 ratio respectively for 1.5-2 hours in the dark at 4.0  $^{\circ}\text{C}$ ; and 2) the nAChR-  $\alpha\text{-BTX}$  complex was mixed with molten monoolein (1-oleoyl-*rac*-glycerol, Sigma) in a 2:3 volume ratio, using a lipid mixer (Hamilton Syringe) and mixed until clear in appearance. The complete process is outlined in **Figure 7**. The nAChR- $\alpha\text{-BTX}$  in LCP was placed on a 75 mm x 25 mm slide and washed with 1.5 mL of detergent buffer solution three times before recovering the LCP-nAChR with a syringe. The LCP-nAChR was transferred into an automatic sampler, and  $\sim 0.2$   $\mu\text{L}$  of LCP-nAChR was dispensed into a 7 mm diameter well. The well was formed by punching holes into 50  $\mu\text{m}$  thick transfer tape (3M, 9482PC) and pressing into the glass slide. The wells were then covered by pressing a coverslip against the slide and flattened with a rubber roll (Caffrey and Cherezov 2009) [4]. This procedure was performed quickly to ensure a tight seal; otherwise, the LCP could dry out compromising matrix integrity. The experimental procedure was conducted in a controlled environment where humidity was not lower than 40-50% at any time. In order to prevent interference from unbound  $\alpha\text{BTx}$  fluorescence, 3  $\mu\text{L}$  of a 1.0 mg/mL  $\alpha\text{BTx}$ -PBS solution was diluted with 100  $\mu\text{L}$  of detergent buffer, and 50  $\mu\text{L}$  of this  $\alpha\text{BTx}$ -detergent solution was used to perform LCP with the lipid monoolein. After coupling each syringe with the mixer, one containing the  $\alpha\text{BTx}$ -detergent solution and the other containing monoolein, the sample was mixed until clear in appearance. After the cubic phase formation, the media was washed 3 times with 1.5 mL of detergent buffer, recovered with a syringe, transferred into a 75 mm x 25 mm glass slide, and

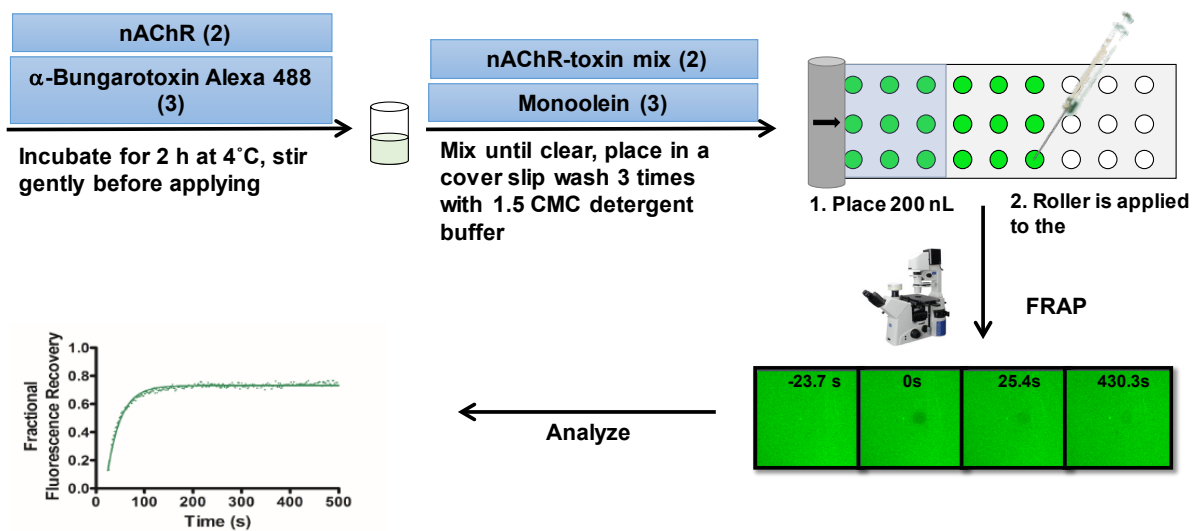


**Figure 7:** This flow diagram shows the overall process of LCP sample preparation for FRAP experiments. Diffusion and mobility is evaluated for detergent purified nAChR inserted into the LCP. Data is analyzed and evaluated for comparison.

covered with a 25 mm x 25 mm coverslip which was tightly pressed and sealed to prevent loss of moisture.

Data collection for FRAP was performed at room temperature using a Zeiss LSM 510 confocal microscope. Fluorescence baseline was established using five (5) pre-bleach images, and the laser was triggered to bleach at 75% power, immediately followed by a sequence of 500 images scanning at 2.6% power with a 600 ms laser scanning delay. Images obtained were processed using the LSM 510 Meta ZEN software. Moreover, data analysis from each sample was integrated within a 14.0  $\mu\text{m}$  diameter circular region of interest ( $\text{ROI}_1$ ). Averaged integrated intensity of another 14.0  $\mu\text{m}$  circular region of interest ( $\text{ROI}_2$ ), positioned near the bleached  $\text{ROI}_1$ , was used to correct/normalized for irradiated- photobleaching during the acquisition sequence. Fluorescence intensity was adjusted by dividing the integrated intensity value of  $\text{ROI}_1$  in the bleached spot by the average integrated intensity of  $\text{ROI}_2$ . As described by Cherezov, et al., 2008 [5], fractional fluorescence recovery curves  $F(t)$  were calculated using Eq 1:

$$F(t) = [(f_t - f_0)/f_\infty - f_0] \quad (\text{Eq 1})$$

In Eq 1,  $F(t)$  is the corrected fluorescence intensity of the bleached spot,  $f_0$  is the corrected/normalized fluorescence intensity of the bleached spot during the 600 ms after bleaching, and  $f_\infty$  is the average of corrected fluorescence intensity in the five pre-bleached images. Fractional Mobility values were obtained by calculating the average of the last 50 values of  $F(t)$ . The fractional fluorescence recovery curves were fitted with a one dimensional exponential Plot (Eq 2) where  $A_i$  is the amplitude of each component,  $K$  is a constant related to the degree of bleaching,  $t$  is time and  $B$  is a constant related to the mobile fraction of receptors (Axelrod et al, 1976) [6].

$$f(t) = \sum_{i=1}^n A_i (1 - \exp(-Kt)) + B \quad (\text{Eq 2})$$

The fractional fluorescence recovery curves were fitted with a one-dimensional equation (one Phase Exponential Plot) provided by Graph Pad statistical analysis software. The Diffusion coefficient value was calculated using Eq 3; where R is the half width at half maximum of the Gaussian [ $R=r(2\ln 2)^{0.5}$ ] and K is a constant calculated using Eq 2 as described by Cherezov, et.al, 2008 [5] and Pucadyil, et.al, 2006 [7].

$$D = [R^2/4K] \quad (\text{Eq. 3})$$

### **2.5 Lipidic Cubic Phase Mobility Analysis using FRAP to Determine nAChR Stability on the Lipidic Cubic Phase**

Stability assessment in the LCP was achieved by using FRAP experiments as described in the previous section 3.3. The procedure for sample preparation was similar although the samples to determine the long-term stability assessment required controlled storage under high humidity conditions and low light exposure until the next time point analysis. The confocal imaging facility room provided the ideal temperature conditions to sustain environmental control, while a humidified chamber ensure high levels of humidity. The process is outlined in **Figure 8**.



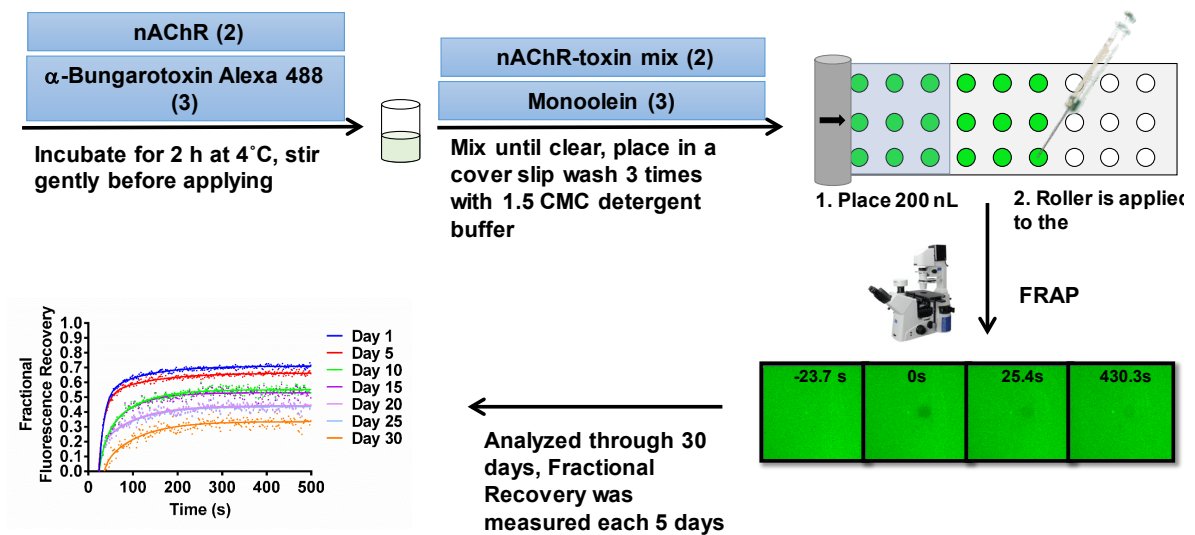


**Figure 8:** This flow diagram shows the overall process of LCP sample preparation for FRAP experiments and the continuous evaluation of diffusion and mobility along a 30 day period. Detergent purified nAChR inserted into the LCP is continuously evaluated to compare nAChR stability per detergent purification.

This procedure was also similar to the protocol described by Caffrey and Cherezov on 2009 [4], with minor modifications. Fluorescence baseline was established using five (5) pre-bleach images: the laser is triggered to bleach at 75% laser power, immediately followed by a sequence of 500 images scanning at 2.6% laser power, with a 600 ms laser scanning delay. All images were obtained and processed by the LSM 510 Meta ZEN program. All experiments were done at room temperature (21-23°C). This procedure was repeated 7 times for a 30 day period, using a 5-day interval.

## **2.6 Hanging Drop and Sitting Drop Crystallization of Purified nAChR**

Detergent purified nAChR was used for crystallization using Hanging Drop and Sitting Drop vapor diffusion crystallization techniques. Detergent purifications with concentrations higher than 3.0 mg/mL were used for both vapor diffusion crystallization techniques as it is widely known that lower concentrations are not likely to generate protein crystals. The nAChR was isolated and purified as previously described. Samples were treated with  $\alpha$ BTx labeled with Alexa 488 to immobilize the receptor into a unique closed conformation and increase the probability for reticle formation. Moreover, the Alexa 488 fluorophore aids in the identification of nAChR crystals in the confocal microscope. The process is outlined in **Figure 9**.

The Alexa 488-labeled  $\alpha$ BTx (Invitrogen) was added to detergent purified nAChR at a 2:1 ratio ( $\alpha$ BTx:nAChR); approximately 600  $\mu$ L of nAChR were used. Samples were incubated for approximately 2h in the cold room while covered with aluminum foil to avoid light exposure; from this step forward, samples were managed with minimal light exposure to avoid fluorophore quenching. After the 2-hour incubation, the samples were washed 3 times with 1.5 mL of the detergent buffer using the concentrator filters Amicon Ultra centrifugal filter units Ultra-15 (Millipore) that allow pass-through of the unbound  $\alpha$ BTx and retain labeled nAChR. Pass through solution fluorescence was monitored using the LSM 510 Meta to determine if the all the unbound  $\alpha$ BTx was completely removed. About 200  $\mu$ L of the flow through were placed on a slide and covered with a coverslip; the slide was sealed with a small amount of

fast drying glue. If fluorescence was noticed, the solution was rewashed; however, a minimal amount of wash was desired to avoid excessive lipid removal.

After  $\alpha$ BTx removal, the solution was concentrated, and sample concentration was measured to determine if the 3.0 mg/mL milestone was achieved. After confirmation, the Mosquito® TTP Labtech® liquid handler was used to perform a high throughput crystal screening. The mosquito allows for fast screening conditions, minimizing the amount of protein sample required for analysis. The nAChR samples were placed in a Polystyrene MRC Crystallization Plate (Molecular Dimensions). This plate is compatible with the mosquito equipment and allows for two sitting drop experimental conditions to be tested simultaneously; 1:1 and 1:2 nAChR:Buffer conditions were used for each experiment. For the hanging drop experiments 96-2 well, INTELLI-PLATE ® flat bottom (Molecular Dimensions) plates were used. This type of plate was also compatible with the Mosquito® TTP Labtech® liquid handler. Crystal Screen®, Crystal Screen 2®, and Index® (Hampton) crystallization conditions were used.

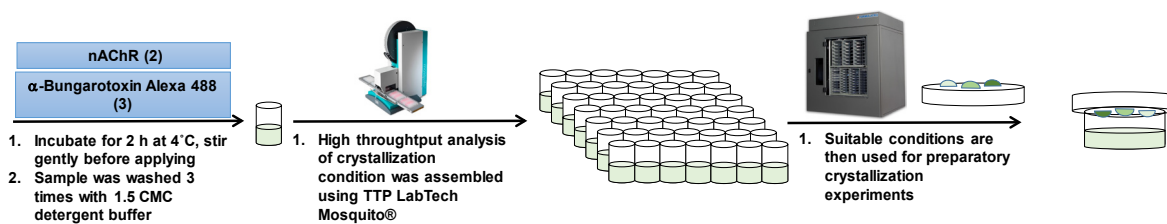


**Figure 9:** This figure shows a flow diagram of the overall process for the preparation of Hanging Drop crystallization trials. Detergent purified nAChR is assembled in 96 well plates and stored in the incubator. Nucleation and bulk crystal development was monitored using rock imager software to determine suitable conditions for crystallization. After suitable conditions were identified, preparatory crystallizations trials were executed to allow for crystal harvest.

After conditions prompt for crystallization were determined, preparatory crystallization experiments were executed. VDX® Plates with incorporated sealant (Hampton) were used for the preparatory crystallization. Approximately 50-100  $\mu\text{L}$  of protein sample was placed on round Siliconized Glass Cover Slides (Hampton) and mixed with 50, 25, 10  $\mu\text{L}$  of crystallization condition, to create a total of 3 drops at an increasing concentration gradient. The siliconized glass cover was placed on the VDX plate previously filled with 1 mL of the crystallization condition. Samples were placed on a ROCK Imager 54 (Formulatrix), the robotic incubator allowed for constant monitoring and ambiance control. After a crystal hit was noticed, the crystals were harvested and diffracted on a Rigaku RU-H3R X-ray generator, Osmic mirrors, a Saturn92 CCD detector, and an X-Stream 2000 low-temperature system. **Figure 10** outlines the crystal diffraction setup.

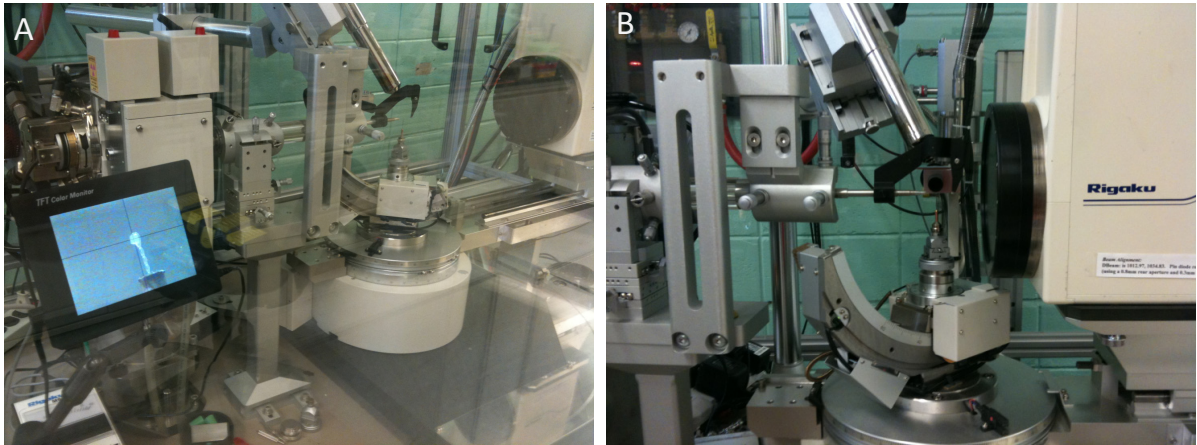


**Figure 10:** Images A and B show the crystal diffraction assembly in the Rigaku RU-H3R X-ray generator. Harvested crystals were mounted and diffracted. Data was collected and analyzed to determine the quality of crystals. The X-Ray power was regulated to 80% and the diffraction was examined from 5 to 60s of exposure to determine the existence of single unit cell arrangements.

## 2.7 Lipidic Cubic Phase Crystallization of Purified nAChR

The LCP combines the use of crystallization conditions with the advantage of lipids to provide an appropriate environment to sustain integral membrane protein stability while delivering a supporting mechanism towards protein crystal development. The critical aspect of this technique is that it relies on a lipidic environment for protein crystallization and aligns with the lipid-based approach used for nAChR crystallization. The LCP technique uses monoolein lipid (Nu-Chek Prep) as a central component of the lipidic matrix. The mechanism of action is based on the transformations of the lipid environment as the water content within the lipidic matrix changes once the crystallization conditions are applied. The LCP technique has two major advantages against traditional vapor diffusion techniques: 1) Hanging drop and Sitting drop crystallization mechanism are based on reducing the quantity of space of a defined aqueous volume to trigger a spontaneous arrangement of proteins; whereas the LCP provides a better approach towards crystallization of integral membrane proteins by allowing for a more organized mechanism of crystallization based on membranous like support; and 2) Hanging drop and Sitting drop techniques usually require higher protein concentrations to achieve a successful crystallization, while the LCP has proven to support protein crystallization with small amounts of sample and lower protein concentrations. This is highly desirable because our purification approach, which relies on native nAChR isolation from natural tissue, usually yields low protein concentrations ~3 mg/mL. The LCP for our experiments is generated and handled following the recommendations and procedures described by our colleagues Vadim Cherezov and Wei Liu in the video graphic article “Crystallization of Membrane Proteins in Lipidic Mesophases” *J. Vis Exp* 2011 (49) 2501 [8]. **Figure 11** outlines the complete process for the crystallization of the nAChR in the LCP.

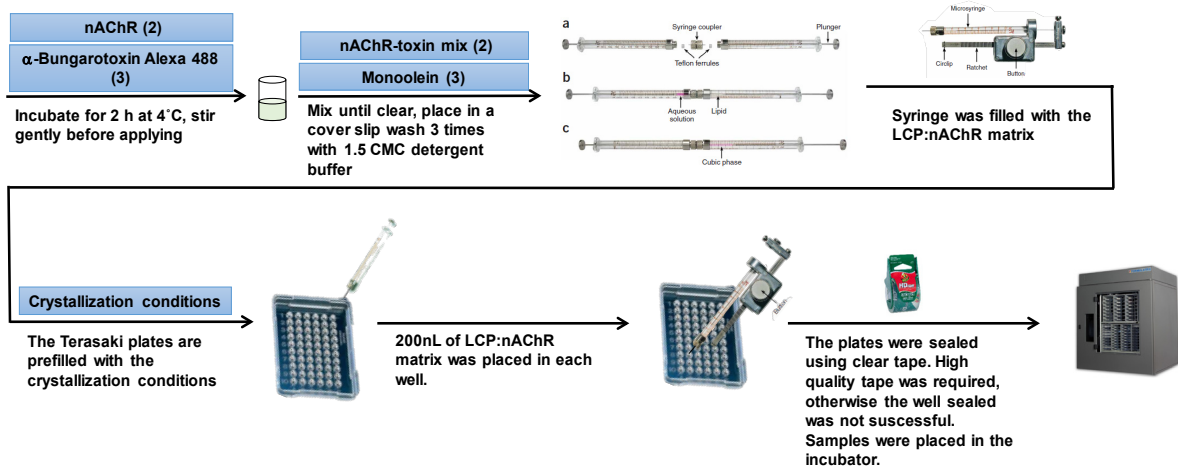


**Figure 11:** This flow diagram shows the process to prepare the LCP crystallization trials using detergent purified nAChR and monoolein. Preparation was executed as described by our colleagues Vadim Cherezov and Wei Liu in the videographic article “Crystallization of Membrane Proteins in Lipidic Mesophases” J. Vis Exp 2011 (49) 2501. Crystallization trials were stored in the formulatrix incubator to control vibration, humidity and temperature.



Detergent purified nAChR was used for crystallization experiments on LCP; purification was performed as described earlier in this document. The first step was the nAChR labeling:  $\alpha$ BTx with Alexa 488 fluorophore (Invitrogen) was used to label approximately 100  $\mu$ L of detergent purified nAChR in a 1:1 ratio  $\alpha$ BTx:nAChR. The sample was incubated at 4.0  $^{\circ}$ C in the cold room for approximately 3 hours while covered with aluminum foil to avoid fluorophore quenching as a result of light exposure. Meanwhile, the monoolein (1g), previously stored at  $-70^{\circ}$ C, was melted using an incubator at  $37^{\circ}$ C. Humidity control to sustain a low humidity environment during this procedure is essential to avoid lipid degradation. After approximately 15 minutes, the liquefied monoolein was transferred into a sealable 25 mL flask.

The Wizard Cubic LCP Kit (Rigaku) was used to create the LCP. A total of 75  $\mu$ L of molten monoolein was placed in the syringe; suction can be applied to load the monoolein into the syringe. However both needle and monoolein need to be sustained at  $37^{\circ}$ C. All hardware was pre-heated to minimize the formation of bubbles within the liquid. After the desired volume was placed into the 250  $\mu$ L syringe (Hamilton), the needle was placed angled towards the plunger inside the incubator ( $37^{\circ}$ C); this allowed the liquefied monoolein to move towards the syringe plunger and any trapped air towards the needle. The liquefied monoolein was then pushed towards the needle eliminating any air trapped within the syringe. Air bubbles could disrupt the LCP arrangement causing experimental failure; in this case, the LCP would not achieve complete clearness during mixing. The needle was then kept stored in the incubator with humidity control, while the protein samples were prepared.

After incubation, the nAChR sample was transferred into a different 250  $\mu$ L syringe (Hamilton). Both needles are joined together via a mixing bridge between the two needles. A Symmetric Mixer Union (Rigaku) was used to couple the two needles. When coupling the needles, a small amount of liquefied monoolein was transferred into the coupler before connecting to avoid the insertion of air bubbles into the mix. The material was then mixed in continuous slow motion, moving the content from one needle to the other until a clear

appearance was observed. From this step forward, a humidifier was used to sustain environment humidity higher than 85% to avoid LCP dehydration. Samples were placed on a slide, and the material was washed 3X times with 1.5 mL of buffer solution to remove any traces of unbound  $\alpha$ BTx. The LSM 510 Meta was used to monitor the successful removal of unbound  $\alpha$ BTx. Samples were then recovered and placed into an automated Ratchet Dispenser (Rigaku) that controlled the amount of LCP sample to be placed into the crystallization plates. Terasaki Style Microtrays (Rigaku) were used for LCP crystallization trials; 0.2  $\mu$ L of LCP was placed into each well, containing 2 $\mu$ L of the crystallization conditions; Wizard® (Rigaku), Cristal Screen® (Hampton) and Cristal Screen 2® (Hampton) were used for this screening. The plates were sealed using Duck Tape® (Rigaku) to seal the individual wells and allow the LCP crystallization mechanism to occur. The plates were stored in an air table or in the formulatrix incubator to avoid undesired vibration and samples were only removed from the air table to scan for any fluorescence signal of nucleation using the LSM 510 Meta.

After a positive identification was performed, samples were harvested from the plates using the Micro-Tool™ (Hampton) and Crystal Wand™ (Hampton). The Crystal Wand was used to install an appropriate Cryo Loop™ (Hampton) based on crystal shape and size. The crystal was harvested and immediately submerged into a Cryo Dewar (Hampton) filled with liquid nitrogen; extreme caution was required in this step to prevent the crystal from falling from the Cryo Loop. Subsequently, a Vial Clamp™ (Hampton) containing the Vial Cap™ (Hampton) was submerged into the liquid nitrogen. The Vial Cap and the Cryo Loop were joined under the liquid nitrogen and transferred into Cryo Canes™ for further storage under liquid nitrogen conditions. All equipment used was ALS style because the robotic arms and equipment in the Argonne National Laboratory-Advanced Photon Source (APS) only handled ALS style hardware.

Next, to complete the harvest and successfully reach 200+ crystals hits, samples were transferred via Cryo shipping using next day mail service to the Argonne National Laboratory – Advanced Photon Source for further analysis. The x-ray diffraction experiments were executed on beamlines 23-ID-B and 23-ID-D; beamlines specialized in x-ray diffraction of small crystals of lipidic matrixes. The technical properties that contributed to the suitability of such beamlines for LCP crystal diffraction were:

1. The beamlines were equipped with a powerful X-ray beam that could be focused as low as 5  $\mu\text{m}$ ; this capability was perfect for diffracting independent segments of protein crystals, allowing concentrating on crystals prone to diffract with better quality.
2. Attenuation at 20.00 coupled with 20  $\mu\text{m}$  excitation area was perfect for diffraction of small crystals without damaging or altering crystal integrity.
3. The raster software. This software programs the robot arm to scan the Cryo Loop to look for crystal segments with areas prone to diffract, based on protein fluorescence under X-ray exposure.

After data acquisition, the data were analyzed using ADXV software to view the diffraction patterns and scatter diffraction data characterization was analyzed using both autoPROC and XDS software. These tools were provided by the GM/Ca CAT team at the Argonne National Laboratory. Generated images and data models were then visually inspected; manual input was required on occasions to determine if the scatter diffractions were positive to protein crystal diffraction.

### **2.8 Lipidic Cubic Phase Crystallization of Purified nAChR Under Potentiated Environment**

According to years of kinetic and electrophysiology studies, the nAChR conformations are understood to respond to actual membrane potential because of depolarization. Our team took advantage of this feature and designed the first lipid base crystallization approach in a potentiated environment. The lipid matrix with the detergent purified nAChR was prepared as

described in section 2.6. Only LFC-16 and FC-16 detergents were used for this experiment, and all samples were above the 4.0 mg/mL of protein concentration. The preparation of the LCP sample is outlined in **Figure 12**.

The potentiated environment was provided by an AXOPATCH 2008 Amplifier (Axon Instruments), the probe was connected to a multi-link connecting rod that allows to connect up to 10 experiments at the same time without increasing the current. A 0.25 mm thick platinum/silver thread was used as an electrode to contact the sample. The thread was weld into the copper rod connectors using tin from the highest purity 99.9% to close the system. Once the electrodes were ready, the sample was prepared and inserted into a previously cut ~2.0 inch, 1.5 mm borosilicate tube (Warner Instrument). The tubes were half filled with the crystallization condition. Approximately 10  $\mu$ L of the nAChR:LCP mixture was placed in the middle of the tube while ensuring that no bubbles were present in the sample, as bubbles would affect the potentiated gradient. The electrodes were then placed into the tube until the crystallization condition was touched. The tube was immediately sealed using capillary wax and a wax pen (Hampton Research); a small “disconnecting-like” force was applied to the electrodes to ensure a secure seal was achieved. Setup image is outlined in **Figure 12**.

The sample was then transferred into a small rubber pad; electrodes were inspected and connected into the current amplifier assemble. The voltage used for the experiments ranged from -8 mV, -10 mV and -15 mV. Samples were monitored daily in the microscope until crystals were observed. After identification, samples were examined under the LSM 510 Meta to confirm that crystals were fluorescent.

After positive identification, crystals were harvested. A small crystal tube was used to push the samples from inside the tube, and the sample was placed on a slide. This procedure was performed very smoothly to avoid crystal damage. The crystals were harvested and analyzed as previously described in section 2.7.

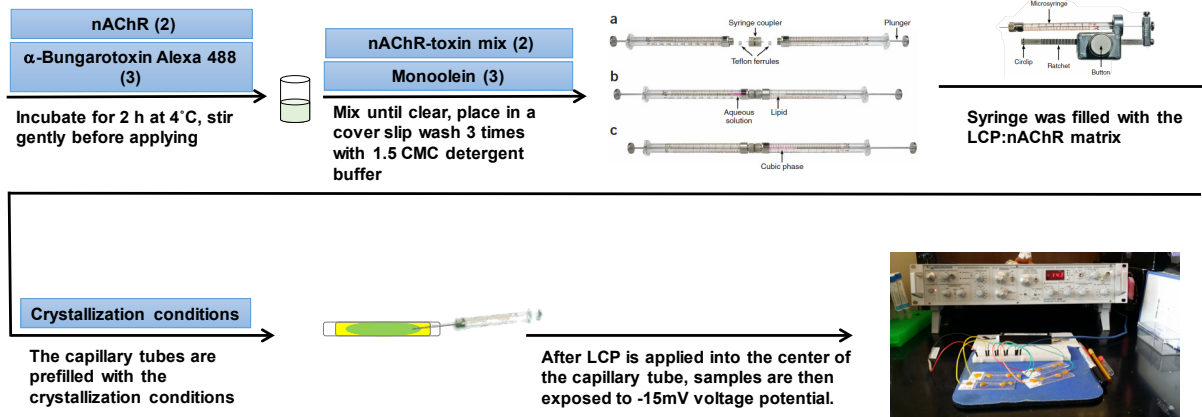


**Figure 12:** The flow diagram describes the assembly for the crystallization trials under applied voltage potential. LCP is generated as described by our colleagues Vadim Cherezov and Wei Liu in the videographic article “Crystallization of Membrane Proteins in Lipidic Mesophases” *J. Vis Exp* 2011 (49) 2501. Crystallization trials were stored at room temperature. Images A and B show the complete setup; red arrows in figure A show electrode connections and the green box show the multi-distribution to allow the assembly of a maximum of 4 trials at the same time. The red box in image B shows the final setup.

## Materials and Methods References

1. Asmar-Rovira, G. A. et al. "Biophysical and Ion Channel Functional Characterization of the *Torpedo californica* Nicotinic Acetylcholine Receptor in Varying Detergent–Lipid Environments" *J Membrane Biol* vol. 223, 1 (2008): 13–26.
2. Weill, C. L. et al. "Affinity labeling of purified acetylcholine receptor from *Torpedo californica*" *Biochem. Biophys. Res. Commun.* vol. 61 (1974): 997–1003
3. Santiago, J. et al. "Tryptophan scanning mutagenesis in the TM3 domain of the *Torpedo californica* acetylcholine receptor beta subunit reveals an alpha-helical structure" *Biochemistry (Mosc)*. vol. 43 (2004): 10064–10070.
4. Caffrey, M. et al. "Crystallizing membrane proteins using lipidic mesophases" *Nature Protocols* vol. 4, 5 (2009): 706-731.
5. Cherezov, V. et al. "LCP-FRAP Assay for Pre-Screening Membrane Proteins for in Meso Crystallization" *Cryst Growth Des.* vol. 8, 12 (2008): 4307-4315.
6. Axelrod, D. et al. "Mobility measurement by analysis of fluorescence photobleaching recovery kinetics" *Biophys J.* vol. 16, 9 (1976): 1055-1069.
7. Pucadyil, T.J. et al. "Effect of cholesterol on lateral diffusion of fluorescent lipid probes in native hippocampal membranes" *Chem. Phys. Lipids.* vol. 143 (2006): 11-21.
8. Cherezov V. et al. "Crystallization of Membrane Proteins in Lipidic Mesophases" *J. Vis Exp.* vol. 49 (2011): 2501.

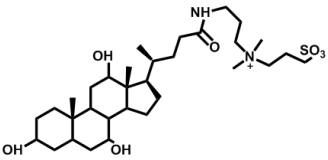
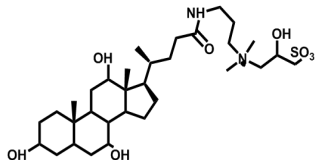
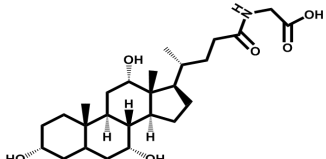
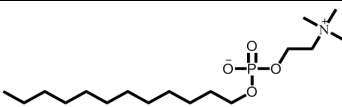
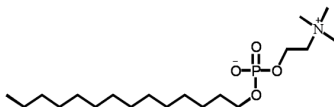
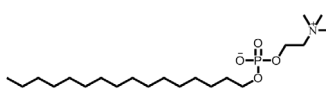
## CHAPTER 4. Results

### 1. Affinity Purification Using Lipid Analog Detergents

Purification of nAChR was executed as a preparatory activity to solubilize the nAChRs in the crude membranes from the *T. californica* electroplax tissue. The solubilization required a series of centrifugations and ultracentrifugation steps, as well as mechanical homogenization to extract crude membranes from the Torpedo's tissue. Lipid analog detergents were used to solubilize the nAChR from crude membranes. As lessons learned from previously reported data (Asmra-Rovira et al. 2008), our analysis is focused on the lipid analog detergents. Detergents in **Table 1** were used in our experiments and demonstrated to isolate nAChR from the Torpedo's tissue successfully. Affinity purification was accomplished for all detergents, demonstrating that agonist binding was not affected by detergent solubilization. These detergents supported nAChR isolation, although previously reported data [1] data showed that there are detergents more suitable for nAChR solubilization/purification, some detergents have shown to sustain nAChR ion channel functionality and soluble stability, and this could be based on the detergent physical properties. Our results outlined the capability of each detergent to isolate a functional and stable nAChR and demonstrated that detergent physical properties play an essential role in the solubilization of nAChR for further crystallographic studies.

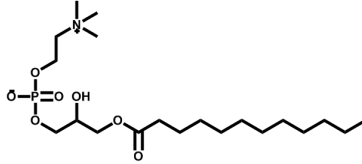
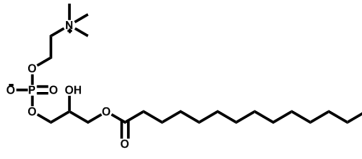
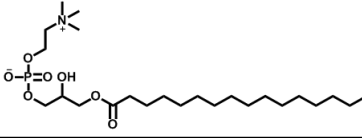
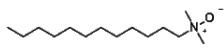
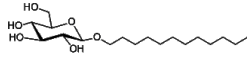
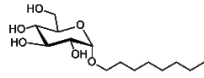
According to our results, both cholesterol and phospholipid analog detergents were successful in isolating the nAChR from lipid membranes. In addition, the functional and stability data, the structural features of the phospholipid analog detergents seemed to be more suited for nAChR isolation.

**Table 1:** Chemical and physical properties of the lipid and non-lipid analog detergents.

Name	CMC (mM)	Aggregation Number	Crude Membrane Solubilization Concentration (mM)	Affinity Column Wash Buffer Concentration (mM)	Structure
<b>Cholesterol-Analog Detergents</b>					
<b>CHAPS</b>	~8	10	32.5 (2%)	12	
<b>CHAPSO</b>	~8	11	32.5 (2%)	12	
<b>Cholate</b>	2.1	2	8.6 (2%)	3.15	
<b>Phospholipid-Analog Detergents Fos-Choline</b>					
<b>FC-12</b>	1.5	54	28.4 (1%)	2.25	
<b>FC-14</b>	0.12	108	26.4 (1%)	0.18	
<b>FC-16</b>	0.013	178	24.5 (1%)	0.20	



**Table 1:** Chemical and physical properties of the lipid and non-lipid analog detergents.

Phospholipid-Analog Detergents Lyso Fos-Choline					
<b>LFC-12</b>	0.32	n/a	7.3 (1%)	0.48	
<b>LFC-14</b>	0.036	n/a	7.7 (1%)	0.054	
<b>LFC-16</b>	0.0032	n/a	20.2 (1%)	0.0048	
Non Lipid-Analog Detergents					
<b>LDAO</b>	1	76	43.59 (1%)	1.5	
<b>DDM</b>	0.17	78	28.69 (1%)	0.26	
<b>OG</b>	10	n/a	68.39(2%)	15	

SDS-PAGE and BSA (protein concentration) data also supported that isolation using lipid analog detergents is plausible for retaining receptor sub unit composition. SDS-PAGE gels were comparable to previous studies by Asmar-Rovira et al. 2008 [1] (**Figure 1-6**). Each SDS-PAGE showed four receptor subunits in adequate proportion. Affinity purification concentrations were comparable with previous studies by Asmar-Rovira et al. 2008 [1] and ranged from 2.0 mg/mL to 17.0 mg/mL.

## **2. Soluble Stability and Ion Channel Functionality of Detergent Purified nAChR**

Analytical size exclusion chromatography (A-SEC) was used to test the soluble stability of the nAChRs when using lipid analog detergent to purify the nAChRs from the *T. californica* crude membranes. A-SEC allowed us to assess the capability of each detergent extraction condition to stabilize the solubilized nAChR by analyzing the nAChR aggregation state. This approach determined which detergent, phospholipid or cholesterol analog provided the appropriate conditions to sustain soluble stability. By using  $\alpha$ BTx tagged with Alexa 488, we were able to identify nAChRs monomer, dimer, and aggregate species as well as the free/unbound tagged  $\alpha$ BTx. All detergents used to solubilize the nAChR were successfully labeled with  $\alpha$ BTx-Alexa 488; this demonstrated that the antagonist binding capability of solubilized nAChRs remains unaffected following detergent purification. The percentage of composition for the nAChRs monomer, dimer and aggregated species was calculated from fluorescence-chromatography spectra to compare the distribution of the mentioned species. The stability of the nAChR was examined for each detergent condition by comparing the enrichment of aggregated species.

In our analysis, both cholesterol and phospholipids analog detergents showed some degree of aggregated species, suggesting that both types of lipid analog detergents contain unfolded nAChRs. This could be associated either with sample handling during the shipping process (samples were analyzed at the Scripps Research Institute, San Diego California) or

aggregates could have been formed during crude membrane addition, even though the crude membranes were added slowly through the complete characterization some degree of aggregation is always expected. However, phospholipid analog detergents showed a lower percentage of aggregated species than cholesterol analog detergents. Thus, the phospholipid analog detergents structure and residual lipids seem to be favorable to support solubilized nAChR stability than cholesterol analog detergents.

Residual Lipids have always been crucial when isolating integral membrane proteins especially as complex as the nAChR, where residual lipids have shown to be very important in sustaining nAChRs functionality and stability [1]. Therefore, during the purification process, lipid depletion is a crucial aspect to consider when purifying nAChRs from *T. californica* crude membranes. Thus far several studies have suggested that the nAChR is highly sensitive to the lipid environment and that lipid identity/structure can influence ion channel functionality, thus affecting nAChR stability [1, 2]. Findings from such studies support the differences in aggregate composition observed in our results (**Figures 1-6**). Lipid depletion, as a result of detergent micelle interaction, could be subtracting activity essential lipids from solubilized nAChR and consequently inducing aggregate formation by de-stabilizing the nAChR-lipid-detergent complexes. Recent findings by Quesada et al. 2016 established a comprehensive lipid analysis lipid-like detergent-solubilized nAChR. Their study showed that lipid depletion leads to unstable nAChR and that lipid identity/composition could affect receptor functionality and stability. Our results showed that cholesterol analog detergents seem to generate higher levels of lipid-depleted species and consequently induce higher aggregations levels. On the other hand, phospholipid analog detergents contribute to nAChR soluble stability producing lower levels of aggregated species.

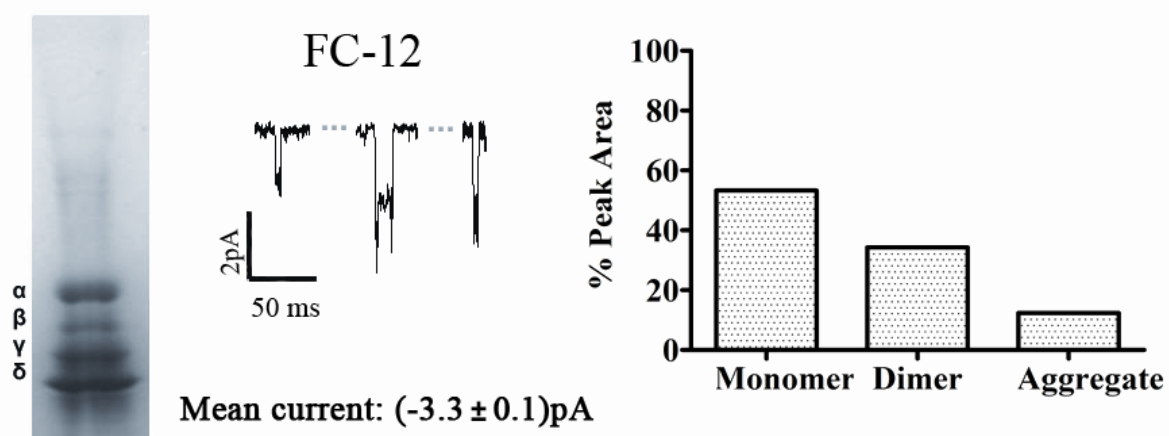


**Figure 1:** FC-12 detergent functional and soluble stability data. PLB current traces of affinity-purified nAChR at -70 mV membrane potential with 0.5 M of carbamylcholine chloride (middle panel), SDS-PAGE gels (left panel) and A-SEC stability assays (right panel); monomer (53.3%)/dimer (34.3%)/aggregate (12.4%). An average of three independent bilayer experiments with a duration of 20 min each was performed.

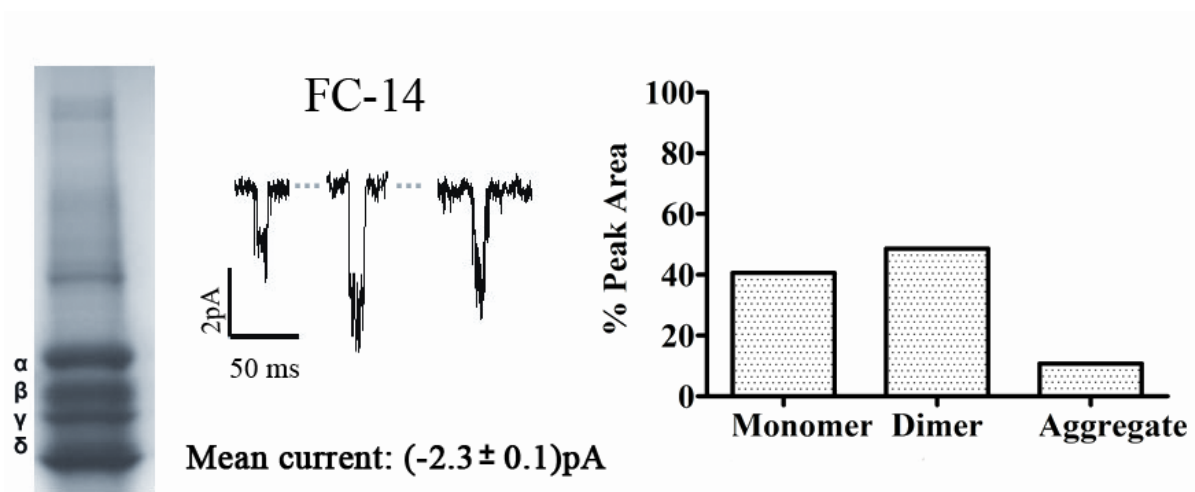


**Figure 2:** FC-14 detergent functional and soluble stability data. PLB Current traces of affinity-purified nAChR at -70 mV membrane potential with 0.5 M of carbamylcholine chloride (middle panel), SDS-PAGE gels (left panel) and A-SEC stability assays (right panel); monomer (40.6%)/dimer (48.6%)/aggregate (10.8%). An average of three independent bilayer experiments with a duration of 20 min each was performed.

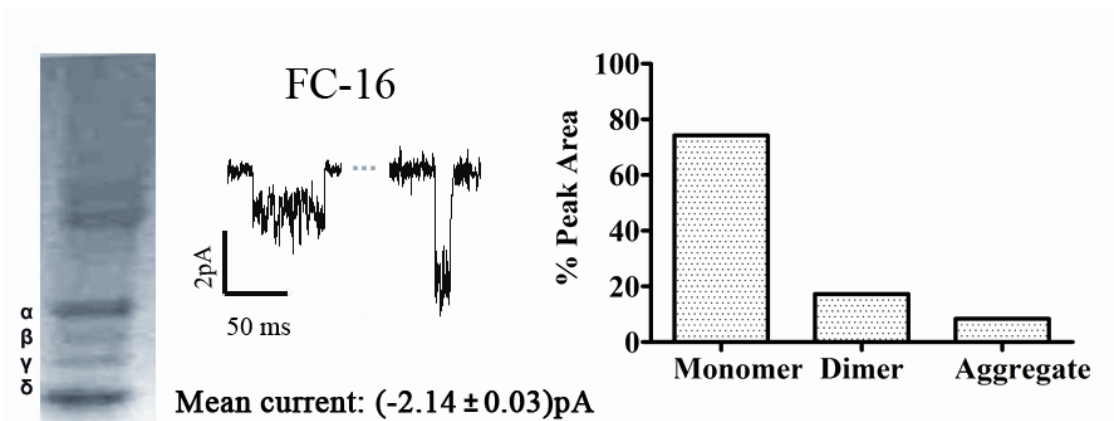


**Figure 3:** FC-16 detergent functional and soluble stability data. PLB Current traces of affinity-purified nAChR at -70 mV membrane potential with 0.5 M of carbamylcholine chloride (middle panel), SDS-PAGE gels (left panel) and A-SEC stability assays (right panel); monomer (74.3%)/dimer (17.3%)/aggregate (8.4%). An average of three independent bilayer experiments with a duration of 20 min each was performed.

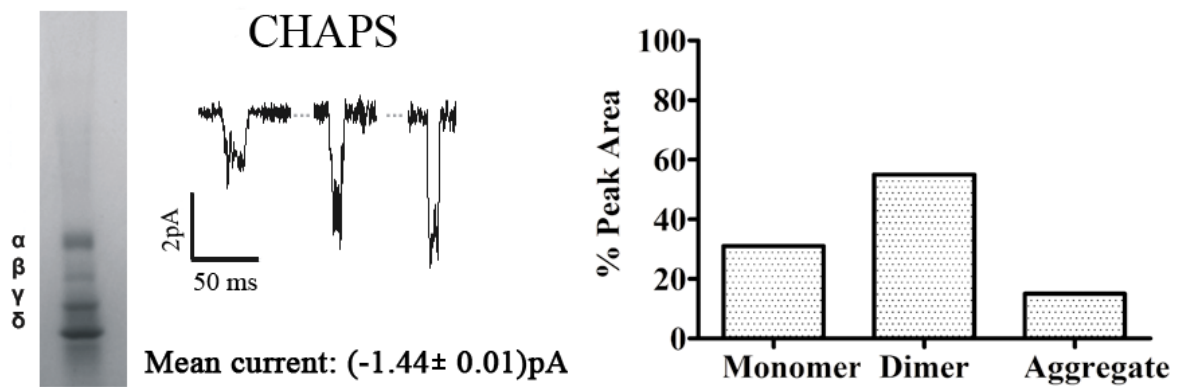


**Figure 5:** CHAPS detergent functional and soluble stability data. PLB Current traces of affinity-purified nAChR at -70 mV membrane potential with 0.5 M of carbamylcholine chloride (middle panel), SDS-PAGE gels (left panel) and A-SEC stability assays (right panel); monomer (30%)/dimer (55%)/aggregate (15%). An average of three independent bilayer experiments with a duration of 20 min each was performed.

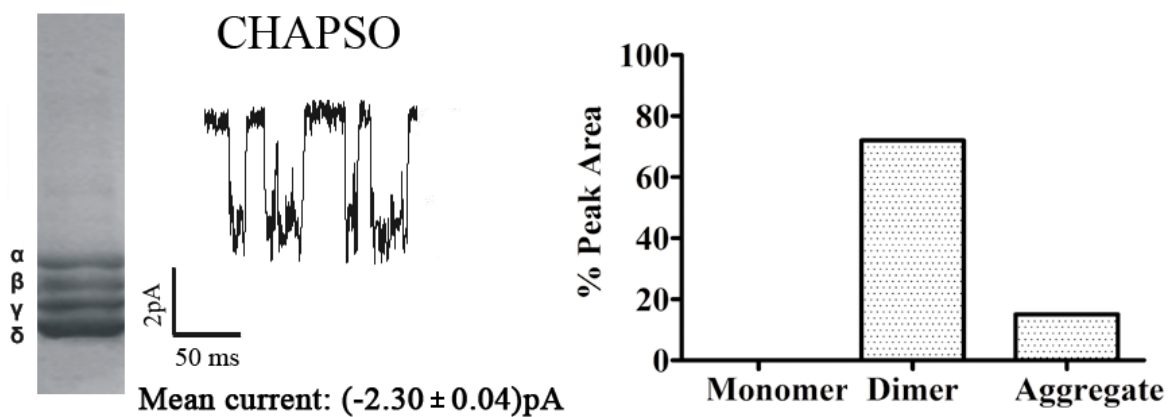


**Figure 6:** CHAPSO detergent functional and soluble stability data. PLB Current traces of affinity-purified nAChR at -70 mV membrane potential with 0.5 M of carbamylcholine chloride (middle panel), SDS-PAGE gels (left panel) and A-SEC stability assays (right panel); monomer (0.0%)/dimer (72.7%)/aggregate (27.3%). An average of three independent bilayer experiments with a duration of 20 min each was performed.



The ion channel functionality of the detergent purified nAChRs was examined through planar lipid bilayer electrophysiology (PLB). This technique allows the examination of detergent purified nAChR single channel openings after insertion into a membranous environment and as a result, determines the capability of lipid analog detergent on sustaining nAChRs functionality. The receptors were inserted into a membrane composed of PC:PE:Cholesterol lipids and highly sensitive sensors were used to measure microscopic currents resulting from ion channel opening (See methods section for a detailed description of the PLB assembly). Such ion channel openings occur as a consequence of carbamylcholine (Carb) binding, a cholinergic agonist capable of nAChR activation for more extended periods of time than acetylcholine; it has been extensively used for the nAChR characterizations when using PLB [1,3,4]. Since this strategy mimics the native functionality of nAChR, higher and stable currents correlate with functional and stable nAChR.

Our results showed that all phospholipid analog detergents were capable of sustaining ion channel functionality in different degrees, since ion channel openings appeared as well-defined opening/closing events in a consistent manner through the PLB experiment. The opening/closing events were equivalent with previous data from Asmar-Rovira et al. 2008 [1], Nelson et al. 1980 [3], Labarca et al. 1984 [4]. Experimental controls results validated the PLB capability to measure single channel currents, no considerable ion channel current was observed at -70 mV voltage potential under the following conditions: (1) affinity-purified nAChR using LFC-16 no Carb, and (2) in affinity-purified nAChR using LFC-16 exposed to 0.5  $\mu$ M Carb and 0.5  $\mu$ M  $\alpha$ BTx (**Figure 7**). Our data indicate that despite lipid depletion occurring as a result of detergent purification, the purified nAChR retains antagonist binding functionality and ion channel capability. Even though phospholipid analog detergents only differ by two or four acyclic carbons in the hydrophobic chain (FC-12, FC-14, FC-16), notable differences can be observed in the fluidity of ion channel events as well as mean channel currents results (**Figure 1-6**). These findings suggest there is a correlation between, ion

channel currents and the length of the hydrophobic acyl chain. Differences between currents could be due to the unique residual lipid composition that each detergent purification has during receptor solubilization. Recent findings by Quesada et al. 2016 [2] support that each detergent sustains a unique residual composition of lipids after detergent solubilization and this lipid environment could be influencing nAChR functionality in the PLB. In addition, the detergent itself could be altering receptor functionality, by either allosteric interaction through the membranous domain, or by interacting with hydrophilic domains in the nAChR. In both cases the detergent could be affecting ion channel functionality, thus disturbing ion channel currents.

Although the LFC-16 structure has a similar head group when compared to all FC-12, FC-14 and FC-16 detergents mentioned, the LFC-16 has a unique structural characteristic: LFC-16 is a lysophospholipid of PC instead of a phosphate ether. Despite the structural difference between the polar head group and the acyl chain of LFC-16 and FC-16, their mean currents are comparable.

The cholesterol analog detergents have previously shown functionality in the PLB. CHAPS, Cholate and BigCHAP showed to retain ion channel functionality, although BigCHAP mean currents were significantly lower than those in CHAPS and Cholate [1], 1 out of 6 membranes formed for PLB showed minimal to none functionality while induced with Carb. In our experiments, CHAPS and CHAPSO detergent purifications also retain ion channel functionality and agonist binding capability. CHAPS currents were comparable to those previously observed in Rovira et al. 2008 [1] (**Figure 5-6**), thus confirming that our methodology was consistent with previously tested purifications. The resulting currents observed for CHAPS and CHAPSO were comparable: mean ion channel current of  $-1.44 \pm 0.01$  pA for CHAPS and of  $-1.92 \pm 0.04$  pA for CHAPSO.

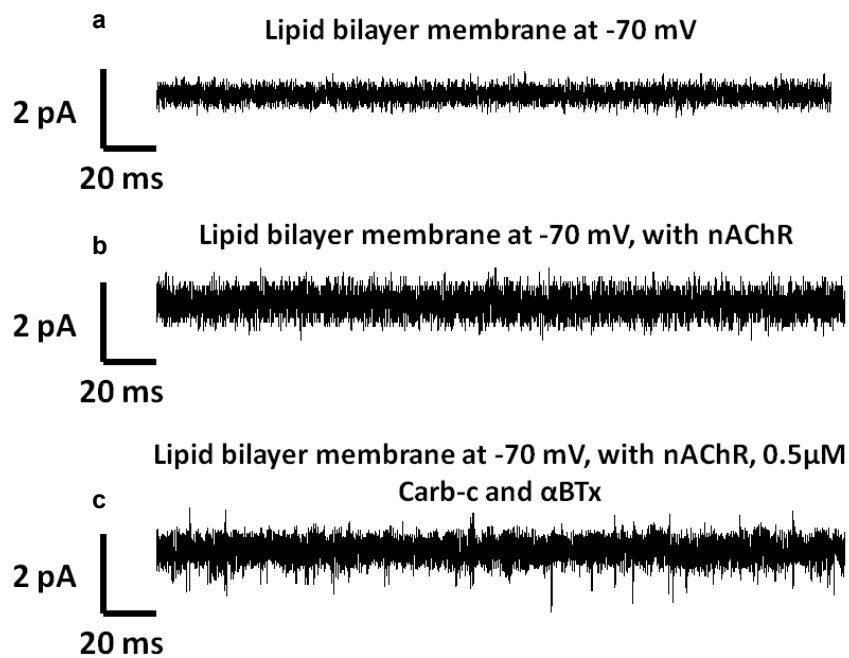


**Figure 7:** Planar Lipid Bilayer experimental controls using LFC-16 fatty acid analog detergent at -70mV membrane potential. No significant ion channel current was observed in the lipid bilayer membrane at -70 mV membrane potential (a), in a lipid bilayer with affinity-purified nAChR using LFC-16 (b), or in a lipid bilayer with affinity-purified nAChR using LFC-16 exposed to 0.5 μM Carb-c and 0.5 μM αBTx (c).

### 3. Macroscopic Ion Channel Functional Assessment of Detergent Solubilized and Affinity Purified nAChR Using Lipid and Non-lipid Analog Detergents.

Ion channel functionality was examined in a macro scale for detergent purified AChRs from *T. californica*. We used the injection of the crude membrane and purified nAChR using non-lipid, phospholipid and cholesterol analog detergents, into *Xenopus laevis* oocytes to characterize the capability of each detergent in sustaining the nAChRs functionality of the nAChRs protein pool. Acetylcholine (ACh), a natural cholinergic agonist, was used as stimuli; macroscopic currents were measured using the TEVC as described in the methods section (see method section for a detailed description of the assembly). Injection of the crude membrane was used to determine experimental feasibility, and to establish a macroscopic based line to analyze the detergent effects. After 5.0 s of exposure with 100  $\mu$ M ACh, the oocyte injected with *T. californica* crude membrane reported a mean amplitude response of  $-274 \pm 36$  nA; n = 10 (**Figure 8**). After recording all the events related to ACh stimuli and performing 5.0 s washes with 1  $\mu$ M  $\alpha$ -BTX, the currents were suppressed effectively blocking the response. Only 1 out of 5 oocytes gave a measurable response of  $-17$  nA following the  $\alpha$ -BTX wash (**Figure 8**). This indicates that currents measured in the oocytes from *Xenopus laevis*, as a result of ACh addition were from functional nAChRs inserted into the oocyte membranes from *T. californica* crude membranes. These experiments confirm that nAChRs functionality in macro can be assessed by injecting raw nAChR from *T. californica* to *Xenopus laevis* oocytes. The mechanism of nAChR insertion into the oocytes membranes is not fully understood.

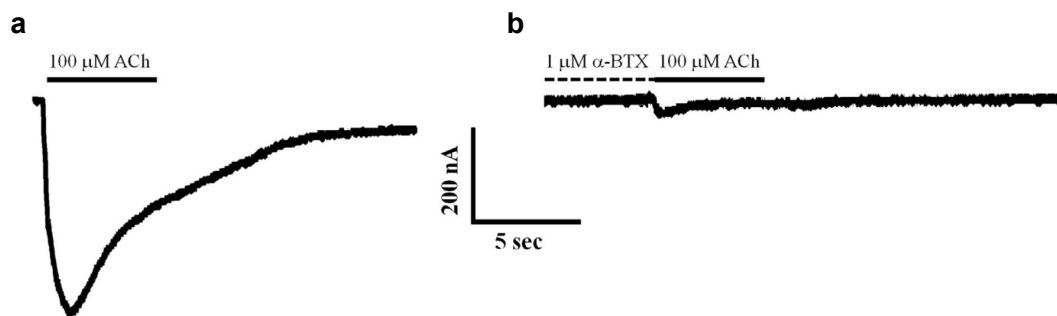


**Figure 8:** Macroscopic ion channel functional assay of crude membrane extracts from Tc nAChRs. Crude membranes extracted from *T. californica* were microinjected into *Xenopus laevis* oocytes and macroscopic ACh evoked currents were measured at  $-70$  mV using TEVC. A, Representative response to a 5 s application of  $100 \mu\text{M}$  ACh (represented by a bar) of oocytes injected with crude membrane extracts. B. Representative response to a 5 s application of  $100 \mu\text{M}$  ACh (represented by a bar) following a 5 s pre-application of  $1 \mu\text{M}$   $\alpha\text{BTx}$ .

*T. californica* crude membranes and solubilized nAChRs purified with detergents lipid/non-lipid analog through affinity chromatography produced results that are consistent with previously reported data using planar lipid bilayer; i.e. single channels current amplitudes are comparable; events shapes are very similar. These results validate the effectiveness of our study to characterize the nAChRs pools when using different detergents. Non-lipid detergent solubilization did not produce a stable and functional nAChRs; similar results were previously reported by our group in Asmar-Rovira et al. 2008 [1] and Padilla et al. 2011 [5] in the planar lipid bilayer. Data shows evident results were the mean amplitudes are considered poor responses of nAChR. DDM ( $-12 \pm 2$  nA, n=4) and OG (only 1 out of 4 oocytes gave a measurable response of  $-10$  nA) as a result of ACh application (**Figure 9**). This data suggests that non-lipid detergents are inadequate at sustaining nAChR function.

Applying the same solubilization procedure with cholesterol analog detergents, such as Cholate, induced nAChR responses ( $-338 \pm 43$  nA, n = 13) (**Figure 9**). Cholesterol analogs have been shown to sustain nAChR functionality. This is the case for sodium cholate, which has previously been reported to support nAChR function in the PLB in Asmar-Rovira et al. 2008. Interestingly, the mean current is very close in magnitude to the crude membrane control, although closing kinetics seems to be noticeably different. Perhaps the closing kinetics are affected either by the residual amount of lipids associated with the affinity purification using Cholate, or the detergent itself could be influencing the ion channel functionality by a lipid-like interaction with the nAChRs.

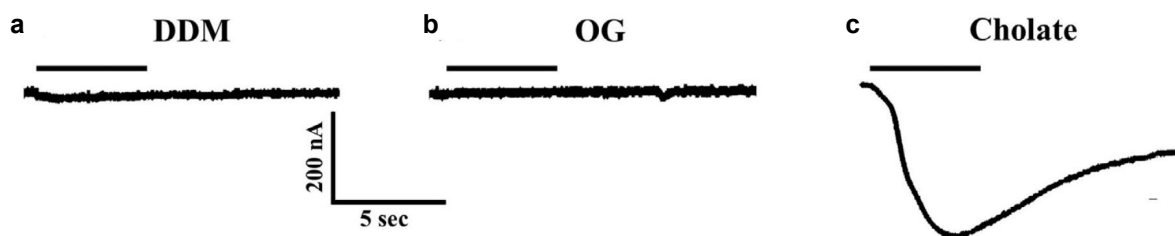


**Figure 9:** Macroscopic ion channel functional assays of detergent solubilized and affinity purified nAChR DCs using a, DDM; b, OG; c, Cholate. Responses were evoked by a 5 s application of 100  $\mu\text{M}$  ACh (represented by a solid bar) at  $-70\text{mV}$  on oocytes injected with detergent solubilized purified nAChR-DCs.

Detergent purifications using the phospholipid analog detergent family foscholine (FC), showed that detergent structural features and physicochemical properties are crucial to sustaining proper nAChRs function. When comparing the mean amplitude of nAChR currents for FC-12 ( $-177 \pm 23$  nA,  $n = 7$ ) with both FC-14 ( $-60 \pm 10$  nA,  $n = 3$ ) and FC-16 ( $-26 \pm 10$  nA,  $n = 9$ ) (**Figure 10**), it is apparent that a small change in the length of the detergent's acyl chain can induce a major change in nAChR function. Interestingly, changes in the acyl chain length of lysofoscholine (LFC) detergents also affect the mean amplitude of nAChR responses in oocytes. However, the effects were opposite to those seen with FC detergents, with the shorter acyl chain LFC-12 displaying smaller mean amplitudes (only 1 out of 4 oocytes gave a measurable response of  $-10$  nA) than the longer side chain LFC-14 ( $-488 \pm 64$  nA,  $n = 4$ ) and LFC-16 ( $-446 \pm 44$  nA,  $n = 5$ ) (**Figure 11**). These results suggest that the longer acyl chain containing detergents in this family (LFC-14 and LFC-16) are able to support nAChR functionality better than the shorter acyl chain LFC-12. Moreover, detergent length could be influencing the nAChR mechanism.

A normalized approach was used due to the high variability in the amplitude results to execute an impartial comparison to assess detergent ability to sustain nAChRs function independently. The amplitude data were normalized to the respective crude membranes used for each detergent solubilization (**Figure 12**). The resulting analysis is consistent with previously published data showing that sodium cholate is able to sustain nAChR function. In addition, when using sodium cholate, results suggest nAChR function is similar to that observed prior to detergent extraction. Furthermore, we found that detergents such as LFC-14, LFC-16, and FC-12 are able to sustain functionality; indicating that these detergents might be better suited than detergents such as LFC-12, FC-14, and FC16 that cannot maintain the same levels of nAChR functionality.



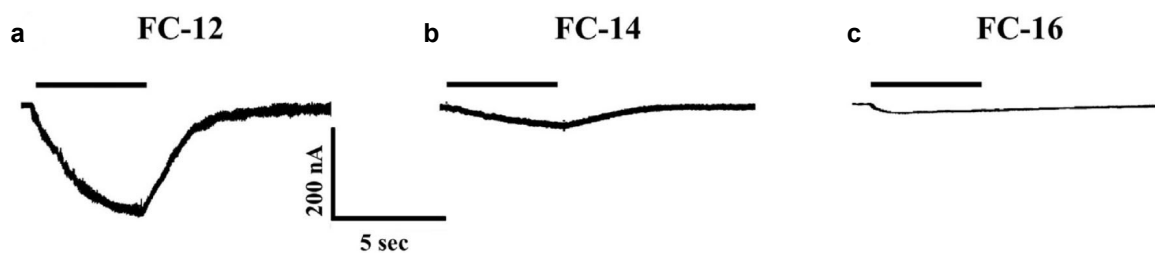


**Figure 10:** Macroscopic ion channel functional assays of detergent solubilized and affinity purified nAChR DCs using a, FC-12; b, FC-14; c, FC-16. Responses were evoked by a 5 s application of 100  $\mu$ M ACh (represented by a solid bar) at  $-70$ mV on oocytes injected with detergent solubilized purified nAChR-DCs.

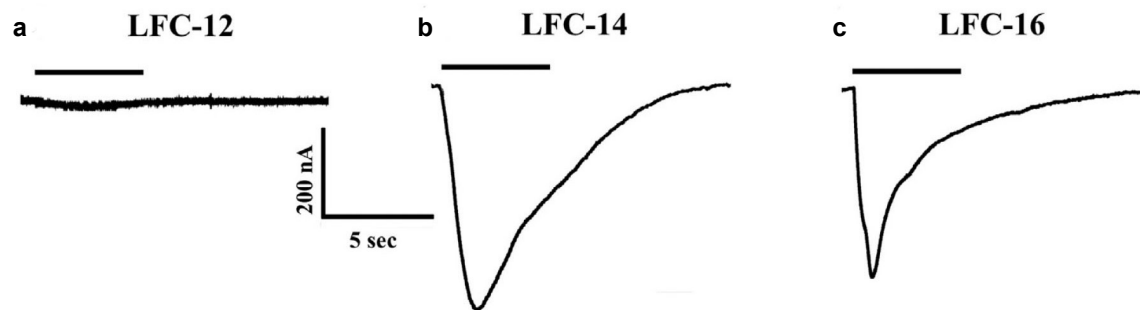


**Figure 11:** Macroscopic ion channel functional assays of detergent solubilized and affinity purified nAChR DCs using a, LFC-12; b, LFC-14; c, LFC-16. Responses were evoked by a 5 s application of 100  $\mu$ M ACh (represented by a solid bar) at  $-70$ mV on oocytes injected with detergent solubilized purified nAChR-DCs.

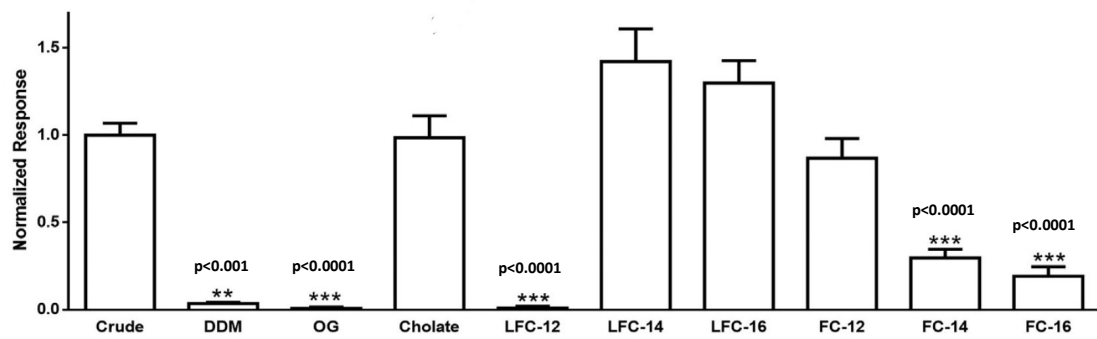


**Figure 12:** Responses for all detergents were normalized to the respective crude membranes used for solubilization, plotted as mean  $\pm$  SEM, and compared using an unpaired t-test in Graph Pad Prism 6; \*\*\*p < 0.0001; \*\*p < 0.001.

#### 4. Mobility Assessment of Detergent Purified nAChR in LCP Using Lipid Analog Detergents

Mobility assessment in the LCP was accomplished following the protocols and conditions described by Cherezov et al. 2008 [6]. Fluorescence Recovery After Photobleaching (FRAP) was employed to determine the fractional recovery and the diffusion coefficient of detergent purified nAChR. Mobility/diffusion of the nAChR is key to deciding suitable conditions for *in-meso* crystallization. The crystal formation mechanism described by Cherezov and Caffrey 2007 [7] rely on protein mobility to reach a bulk mesophase that will further evolve into a crystal. The LCP crystal formation mechanism is portrayed mainly as a lateral diffusion through a lamellar phase, where protein flexibility and dynamics are essential for successful displacement. Consequently, protein fluidity in the LCP is essential to overcome this mechanism stages as described Cherezov and Caffrey et al. 2007 [7] during crystal formation. Each detergent purification provides a unique lipid environment that would give the receptor with the flexibility needed to move along the lipidic matrix. Thus, is essential to assess nAChR mobility in the LCP. Our data shows the differences in mobility between affinity purified nAChR using different lipid analog detergents.

Following our strategy, first, we evaluated the fluorescence contribution from the unbound  $\alpha$ BTx-Alexa 488. By using confocal imaging, we were able to determine that fluorescence contribution by unbound  $\alpha$ BTx-Alexa 488 was eliminated by three consecutive washes into the already prepared LCP using a detergent buffer. This procedure was performed to ensure the removal of any unbounded  $\alpha$ BTx-Alexa 488. The flowing liquid from the washes was examined in the confocal microscope to determine residual fluorescence.

Moreover, **Figure 13** shows that there was no significant interaction/binding between the free  $\alpha$ BTx-Alexa 488 and the lipidic matrix, proving that free  $\alpha$ BTx-Alexa 488 is not a considerable source of background fluorescence. Traces of free  $\alpha$ BTx-Alexa 488 were identified by irradiating the slides with a 488 nm Argon laser at 5% power. The scanning was

performed manually using a 40X magnification lens in search for any sign of fluorescence source. Fluorescence was noticed in the regions surrounding the LCP matrix, showing that  $\alpha$ BTx-Alexa 488 remains in the water interface in the perimeter of the lipidic mixture. In addition,  $\alpha$ BTx-Alexa 488 binding is not expected to be affected by the detergent's identity because during A-SEC experiments and as showed by Asmar-Rovira et al. 2008,  $\alpha$ BTx-Alexa 488 remains steadily bound to the nAChR.

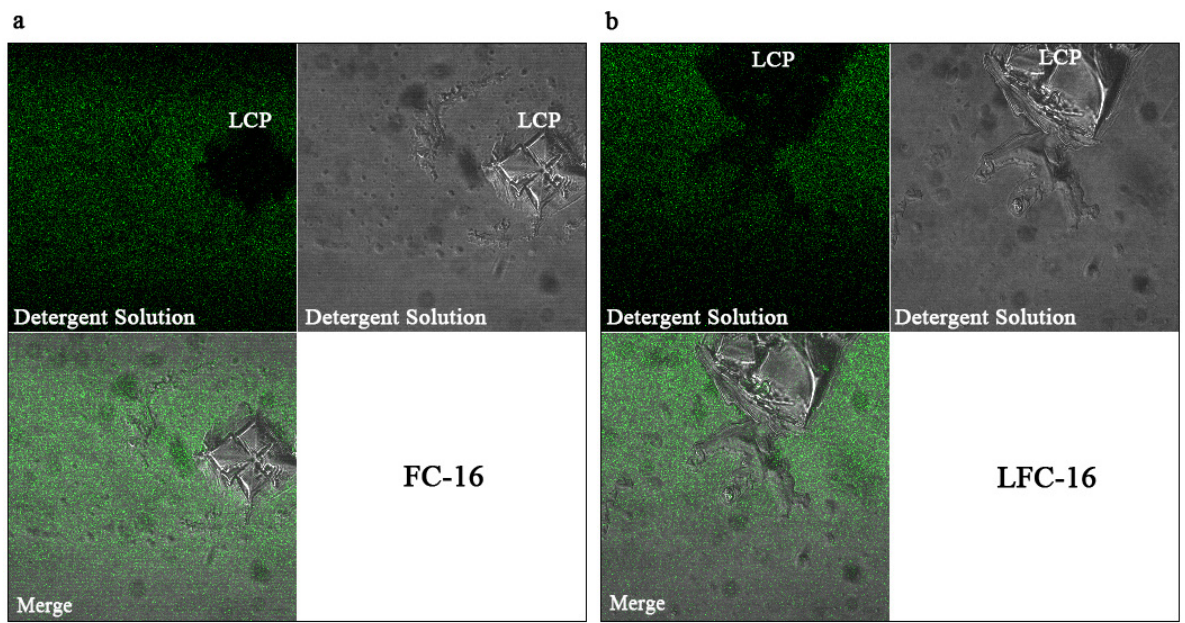
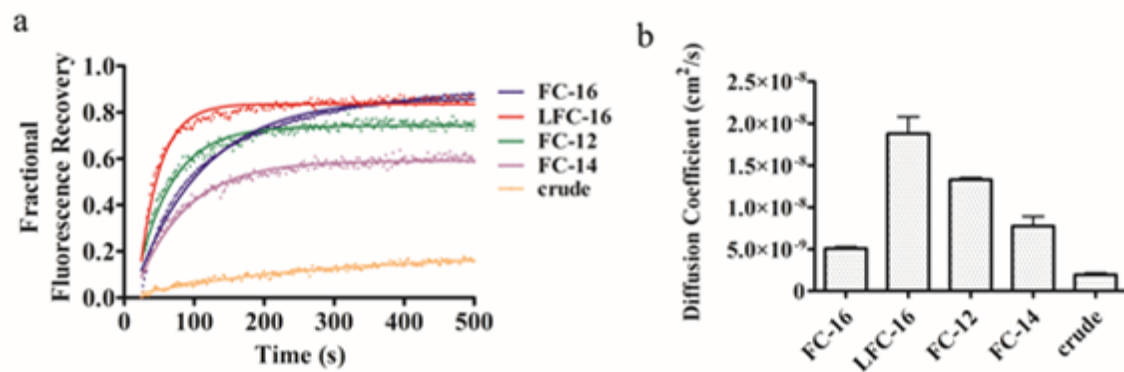


Figure 13: FRAP control experiments show that  $\alpha$ BTx does not bind to or mixes with the LCP matrix in the absence of nAChRs; thus, it is a nonsignificant source of background fluorescence (a,b). The protocol for  $\alpha$ BTx removal is described in “Materials and Methods” section.

Experiments to determine the mobility and diffusion of purified nAChR using phospholipid analog detergents were completed successfully. **Figures 14-16** shows fractional fluorescence recovery data that have been fitted with a single component diffusion equation as previously described in the methods section. The LSM Ziex 510 was used to perform FRAP experiments using 2.6% laser power and regions of interest of 14.0  $\mu\text{m}$ . Noticeable differences were observed for the mobility and the diffusion of purified nAChR using phospholipid analog detergents. Within the first 100 seconds, fractional recoveries vary from 0.4 to 0.75 among the different phospholipid analog detergents. This suggests there is a conglomerate of factors that might be influencing nAChR mobility besides structural differences between the phospholipid analog detergents such as the hydrophobic acyl chain length and the polar head group. Moreover there is a correlation between the percentage of the monomer on the detergent extractions and the fractional recovery; in general, higher levels of monomer state yield higher fractional recovery in the LCP. Solubilization using LFC-16 detergent yielded 85% of fractional recovery, whereas 82% of the nAChR was in a monomeric state. On the other hand, FC-16 produced 87% fractional recovery, with 74% of the nAChR in the monomeric state. These results for the fractional recovery/mobile fraction are comparable with observations by Cherezov and colleagues for the LCP crystallized  $\beta_2$ -Adrenergic receptor– T4L [6]. **Figure 14a** shows the fractional recovery curves for phospholipid analog detergents; the data shows a direct correlation between the monomeric state of the nAChR after detergent purification and the fractional recovery in the LCP. Model in **Figure 15** shows the correlating parameters using linear regression, indicating the grade of change of the fractional recovery as a function of phospholipid analog detergent monomer percentage.



**Figure 14:** Fractional fluorescence recovery and diffusion coefficient of each affinity-purified nAChR using phospholipid-analog detergents. FRAP experiments (a) were recorded for affinity-purified nAChR using the phospholipid-analog detergents FC-16, LFC-16, FC-12 and FC-14. All fluorescence recovery experiments were performed in duplicate, averaging three recoveries on different areas of the LCP with incorporated nAChR. The fractional recovery was calculated for each phospholipid-analog detergent using Eq. 1 from “Lipidic Cubic Phase Mobility Analysis using Fluorescence After Photo Bleaching” for each fractional fluorescence recovery of the duplicates. The diffusion coefficient (b) was calculated using Eqs. 2 and 3 from “Lipidic Cubic Phase Mobility Analysis using Fluorescence After Photo Bleaching” for each phospholipid-analog detergent.



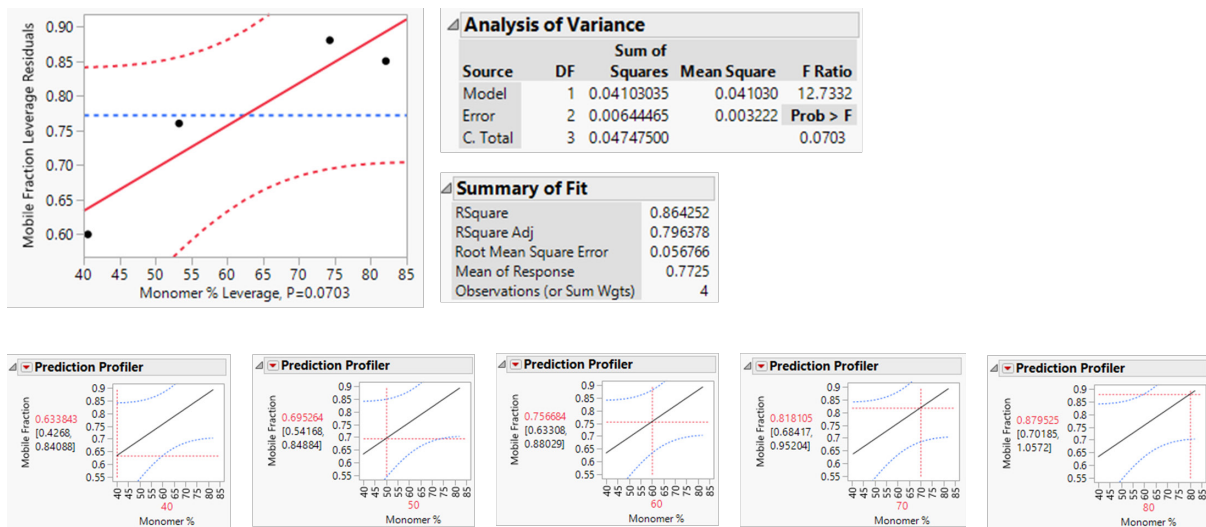


**Figure 15:** Mobile fraction for each phospholipid analog detergent and monomer % of composition were modeled to determine a correlating pattern. The model fitted a linear regression with a  $|r|$  adjusted of 0.7963, this value is closer to 1. Also the resulting root mean square error is 0.0567, this value is less than 0.23, the greatest change in the mobile fraction data, which indicates the absence of lack of fit. Thus, regression can be considered practical significant. An increment in the monomer % correlates with higher values of mobile fraction, as shown in the prediction profilers, when using phospholipid analog detergents to purified nAChRs from *T. californica* crude membranes.

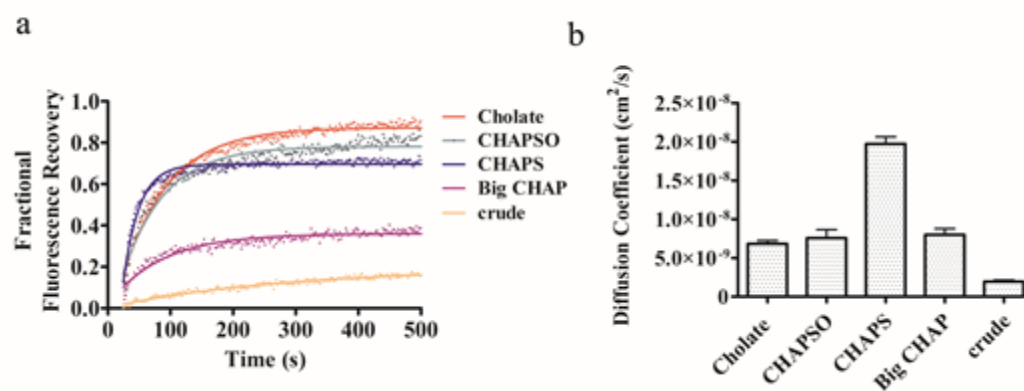


**Figure 16:** Fractional fluorescence recovery and diffusion coefficient of each affinity-purified nAChR using phospholipid-analog detergents. FRAP experiments (a) were recorded for affinity-purified nAChR using the phospholipid-analog detergents FC-16, LFC-16, FC-12 and FC-14. All fluorescence recovery experiments were performed in duplicate, averaging three recoveries on different areas of the LCP with the nAChR incorporated. The fractional recovery was calculated for each phospholipid-analog detergent using Eq. 1 from “Lipidic Cubic Phase Mobility Analysis using Fluorescence After Photo Bleaching” for each fractional fluorescence recovery of the duplicates. The diffusion coefficient (b) was calculated using Eqs. 2 and 3 from “Lipidic Cubic Phase Mobility Analysis using Fluorescence After Photo Bleaching” for each phospholipid-analog detergent.

The nAChR diffusion coefficient in the LCP was analyzed to determine differences in protein displacement as a result of phospholipid analog detergent purification. The diffusion coefficient describes the velocity by which the nAChR is displaced within the membranous matrix. **Figure 14b** shows that there was no considerable difference in the diffusion coefficient or velocity of displacement between the phospholipid analog detergents. However, LFC-16 appears to stand out because it reaches the fractional recovery plateau 10x times faster. Perhaps there is a unique combination of factors such as the polar head group and tail linker that could be causing the observed differences; particularly when compared to FC-16 that reaches the fractional recovery plateau 10x slower and their structural features are very similar. Data showed that there is an apparent correlation between monomer percentage of composition and fractional recovery with the acyl chain length. Crude membrane isolation seems to disrupt the LCP integrity, or the colossal amount of residual lipids restricts the fractional recovery and the diffusion coefficient.

Experiments to determine the mobility and diffusion of nAChR purified using cholesterol analog detergents was successfully completed. The fractional recovery data was well fitted using a single component diffusion equation (**Figure 16**). According to our results, there were no noticeable differences between the diffusion coefficients of CHAPSO, Cholate and BigCHAP, all detergents showed a diffusion coefficient of  $\sim 7.50 \times 10^{-9} \text{ cm}^2/\text{s}$ . However, CHAPS produced a diffusion coefficient of  $1.92 \times 10^{-8} \text{ cm}^2/\text{s}$  (**Figure 16**). Interestingly, despite the high similarities in terms of their chemical and physical properties, CHAPS and CHAPSO showed differences in the diffusion coefficient. Perhaps differences between the acyl chain length and the charge distribution along the detergent tail are impacting nAChR displacement in the LCP.

The total amount of phospholipid and cholesterol was determined previously for each detergent extraction: CHAPS, Big CHAP and Cholate, data was reported in Asmar-Rovira et al. 2008 [1]. These detergents produced different ratios of total phospholipid analogs and

cholesterol in their purifications. We determined the phospholipid to cholesterol ratio of these detergents and compared the resulting value with the diffusion coefficient (**Figure 17**). Results showed a proportion of ~1.4:1 phospholipid to cholesterol would yield a high diffusion coefficient, thus higher nAChR displacement in the LCP when using cholesterol analog detergents. Therefore, lipid ratios might be affecting the LCP matrix or protein motility.

Fractional recovery of cholesterol analog detergents was analyzed to determine nAChR mobile fraction (**Figure 16**). CHAPS and cholate detergents yielded a mobile fraction of 71% and 89%, respectively. CHAPSO produced 81% mobile fraction, whereas Big CHAP showed a mobile fraction of 37% and crude membrane showed ~10% mobile fraction. In contrast with the phospholipid analog detergents, no correlation was observed between the monomer percentage of composition and the different structural features of cholesterol analog detergents. Lipid analysis data from previous experiments showed that purification with CHAPS and cholate produce high yields and a negligible amount of residual lipids. On the other hand, affinity chromatography using Big CHAP showed a significant amount of residual native lipids and SDS-PAGE showed a noticeable amount of contaminants. These findings suggest that the reduction in the mobile fraction observed for Big CHAP could be associated with the significant amount of residual of natural lipids. This conclusion is also supported by the 10% mobile fraction observed for the crude membrane.

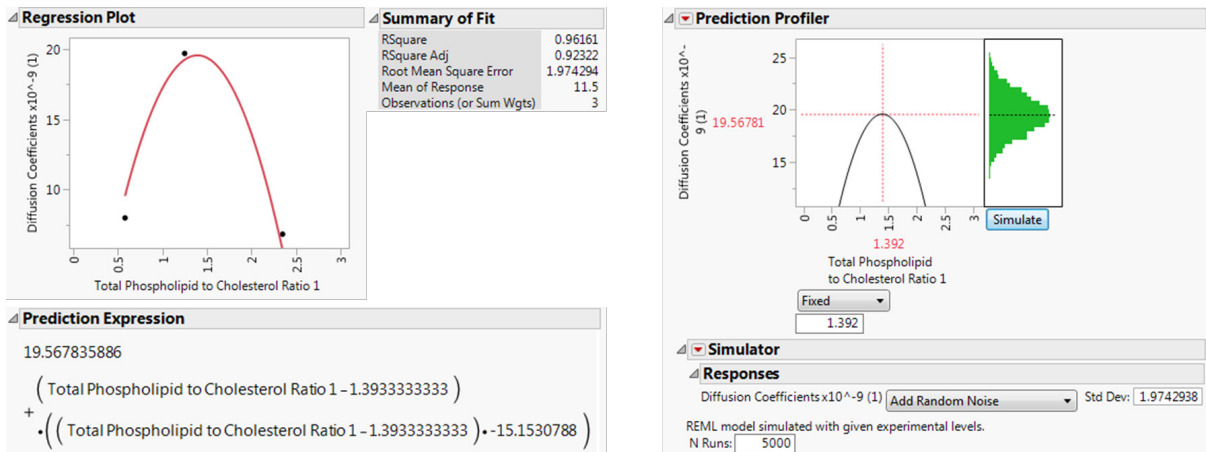


**Figure 17:** Total phospholipid and cholesterol ratios were previously determined for the cholesterol analog detergents by Asma-Rovira et. al. 2008, this data was used to determine the correlation between the diffusion coefficient and the phospholipid to cholesterol ratio. The fit model has an  $|r|$  adjusted of 0.9232, this value is closer to 1. The root mean square error was 1.97, this result is less than the highest change in the diffusing coefficient ( $\sim 10$  units); thus, the model can be considered practical significant. Data showed there is an optimal proportion of phospholipid to cholesterol to maximize the nAChRs diffusion coefficients in the LCP. At approximately 1.4:1 phospholipid to cholesterol ratio the diffusion coefficient is at its maximal, when using cholesterol analog detergents to purified nAChRs from *T. californica* crude membranes.

Cholesterol molecules are well known to influence nAChR functionality; thus, receptor conformation and mobility might be affected as well. Previous experiments reported in Asmar-Rovira et al. 2008 [1], determined the amount of total residual cholesterol in CHAPS, Cholate and Big CHAP purifications. A correlation is evident between the amount of total remaining cholesterol and the mobile fraction using cholesterol analog detergents (**Figure 18**). Conceivably, the remaining amount of cholesterol could be affecting nAChR mobility. According to our findings enriched cholesterol environments, when using cholesterol analog detergents for affinity chromatography, could be noticeably limiting the nAChR mobile fraction in the LCP.

Previous data from Asmar-Rovira et al. 2008 [1] showed that affinity chromatography using non-lipid-analog detergents did not produce functional nAChR. Nevertheless, fractional recovery data in the LCP was successfully fitted with a single component diffusion curve (**Figure 19**). For the non-lipid-analog detergents, no substantial differences were noticed in the mobile fraction and diffusion coefficient results. Diffusion coefficient for LDAO, DDM and OG were  $9.88 \times 10^{-9}$ ,  $1.99 \times 10^{-8}$  and  $1.34 \times 10^{-8}$  cm<sup>2</sup>/s, with a standard deviation of only  $\pm 0.41 \times 10^{-8}$ ; such differences between detergents is considered minimal. These results indicate that nonfunctional nAChR diffuses as well as nAChR solubilized using lipid-analog detergents in the lipidic matrix. Perhaps this nonfunctional nAChR has a structural capability that the functional nAChR lacks and allowed for nAChR displacement with ease.

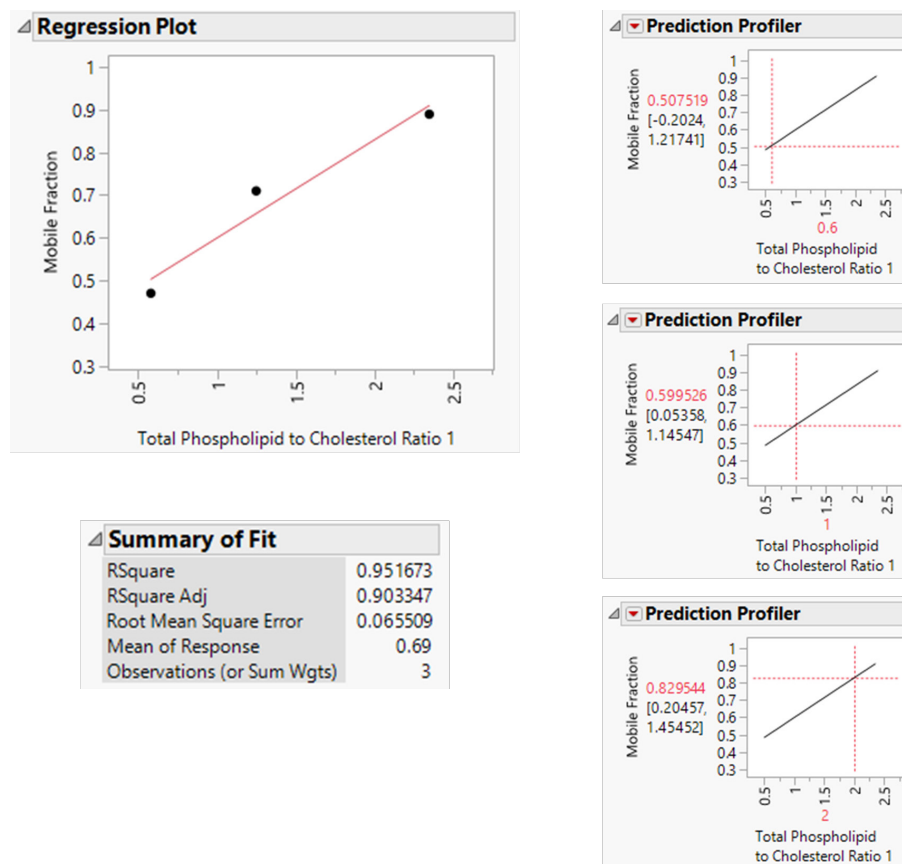


**Figure 18:** Total phospholipid and cholesterol ratios were previously determined for the cholesterol analog detergents by Asma-Rovira et. al. 2008; this data was used to determine the correlation between the mobile fraction and the phospholipid to cholesterol ratio. Model fitted a linear regression with a  $|r|$  adjusted of 0.9033, this value is closer to 1. The root mean square error was 0.06551, this result is less than the highest change in the mobile fraction ( $\sim 0.4$  units); thus, the model is considered practical significant. Data showed that there is an optimal proportion of phospholipid to cholesterol to maximize the nAChRs mobile fraction in the LCP; highest phospholipid to cholesterol ratio promotes higher mobile fractions. At approximately 2:1 phospholipid to cholesterol ratio the mobile fraction is 0.8295, when using cholesterol analog detergents to purified nAChRs from *T. californica* crude membranes.

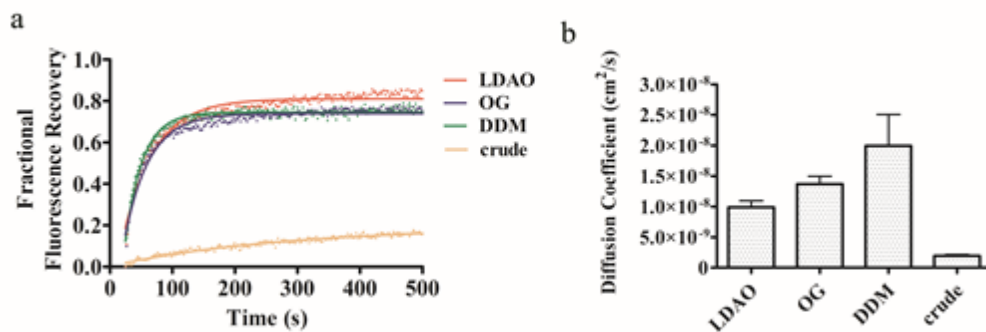


**Figure 19:** Fractional fluorescence recovery and diffusion coefficient of each affinity-purified nAChR using non-lipid-analog detergents. FRAP experiments (a) were recorded for affinity-purified nAChR using the non-lipid-analog detergents LDAO, OG, and DDM. All fluorescence recovery experiments were performed in duplicate, averaging three recoveries on different areas of the LCP with the nAChR incorporated. The fractional recovery was calculated for each non-lipid-analog detergent using Eq. 1, from “Lipidic Cubic Phase Mobility Analysis using Fluorescence After Photo Bleaching” in the materials and methods section, for each fractional fluorescence recovery of the duplicates. The diffusion coefficient (b) was calculated using Eqs. 2 and 3, from “Lipidic Cubic Phase Mobility Analysis using Fluorescence After Photo Bleaching” in the materials and methods section, for each non-lipid-analog detergent.



## 5. LCP Stability Assessment of Detergent Purified nAChR Using Lipid Analog Detergents

FRAP studies performed in the LCP can be interpreted as a stability measurement for transmembrane proteins embedded on lipid matrixes. The strategy involves the calculation of mobile fraction and diffusion coefficient from fractional recovery curves, as described in the methods section, for nAChR affinity chromatography using lipid analog detergents classified as cholesterol analogs and phospholipid analogs. This approach was previously executed by Cherezov et al. 2008 [6], and by our group on Padilla et al. 2011 [5], where continuous mobility on the LCP was assessed for the nAChR using 5 day period intervals for up to 30 days. In order to establish the feasibility of protein mobility and nucleation, which are crucial for nAChR crystallization, a 30-day FRAP assay was carried out for each detergent.

Mobility curves of cholesterol analog detergents fit consistently with a single component diffusion equation (**Figure 20**). All cholesterol analog detergents showed no considerable diffusion differences during the 30-day period; all showed  $10^{-9}$  cm<sup>2</sup>/s diffusion coefficients and most sustained the same diffusion coefficient values during the 30 day period. However, both BigCHAP and CHAPS deviated from this trend (**Figure 21**). Big CHAP diffusion displayed an evident decay from  $\sim 8.0 \times 10^{-9}$  cm<sup>2</sup>/s to  $\sim 2.0 \times 10^{-9}$  cm<sup>2</sup>/s during the first 5 days; whereas during the first 5 days CHAPS showed the highest diffusion coefficient of  $\sim 1.2 \times 10^{-8}$  cm<sup>2</sup>/s, followed by a constant decay to  $\sim 7.5 \times 10^{-9}$  cm<sup>2</sup>/s. On the other hand, CHAPSO and sodium cholate showed a continual diffusion coefficient of the average of  $7.5 \times 10^{-9}$  cm<sup>2</sup>/s (in average) during the 30-day period (**Figure 21**). These values are consistent with previous studies that analyzed the diffusion coefficients for transmembrane proteins on lipidic matrixes [5,6].

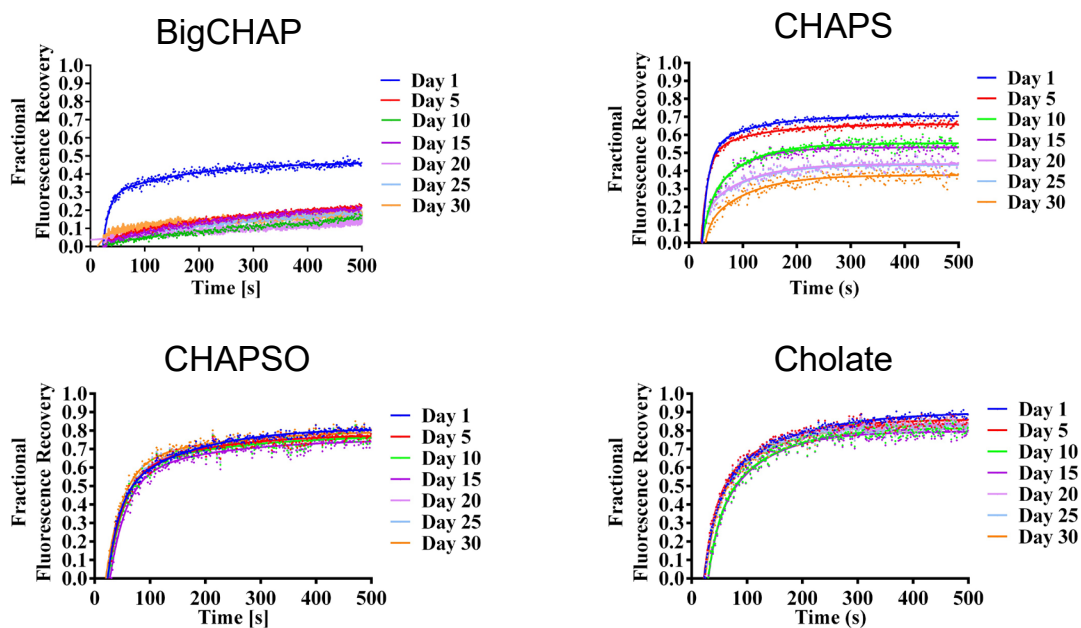


**Figure 20:** LCP-FRAP stability assay for cholesterol analog detergents. Fractional fluorescence recovery and diffusion coefficient of each affinity purified nAChR using cholesterol analog detergents. FRAP experiments of Cholate, BigCHAP, CHAPSO, and CHAPS were recorded every five days for thirty days. All fluorescence recovery experiments were performed in triplicates, averaging five recoveries on different areas of the lipidic matrix with incorporated nAChR.

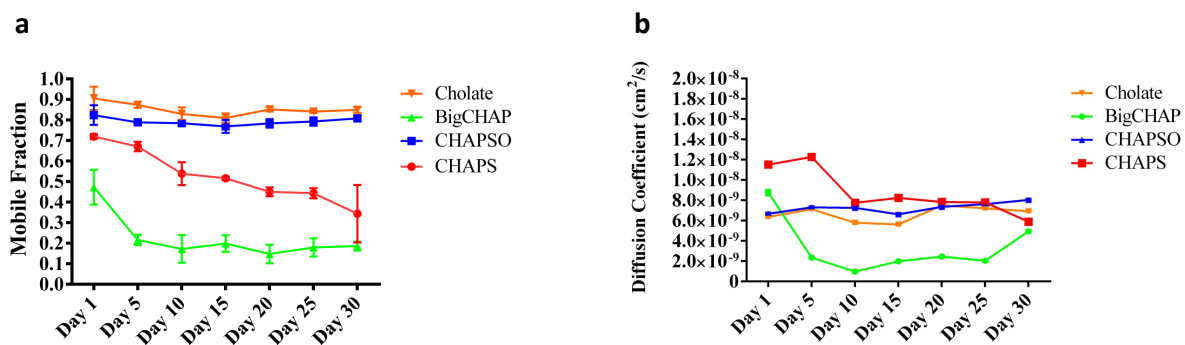


**Figure 21:** LCP-FRAP stability assay for cholesterol analog detergents. The fractional recovery was calculated using Eq. (1), from “Lipidic Cubic Phase Mobility Analysis using Fluorescence After Photo Bleaching” in the materials and methods section, for each fractional recovery of the triplicates. The mobile fraction (a) was obtained by averaging the last twenty points of the fractional recovery obtained in Figure 20. The diffusion coefficient (b) was calculated using Eq. (2) from “Lipidic Cubic Phase Mobility Analysis using Fluorescence After Photo Bleaching” in the materials and methods section.

All phospholipid analog detergents showed a good fit with a single component diffusion equation. For the foscholine family, there were no substantial changes for FC-14 and FC-16 during the 30-day period. Both detergents showed a monthly average of  $6.0 \times 10^{-9} \text{ cm}^2/\text{s}$  and  $8.0 \times 10^{-9} \text{ cm}^2/\text{s}$  respectively (**Figure 22-23**). Nevertheless, FC-12 showed an alternating pattern that contrasts the behavior of the longer acyl chains -14 and -16. During the 30-day period, the diffusion coefficient of FC-12 fluctuated between  $\sim 6.0 \times 10^{-9} \text{ cm}^2/\text{s}$  and  $\sim 1.2 \times 10^{-9} \text{ cm}^2/\text{s}$ . On the contrary, the lysofoscholine family (LFC types) showed no major changes in diffusion coefficients during the 30-day period. LFC-12 and LFC-14 showed similar diffusion coefficient values with a monthly average of  $7.25 \times 10^{-9} \text{ cm}^2/\text{s}$  and  $7.01 \times 10^{-9} \text{ cm}^2/\text{s}$  respectively (**Figure 24-25**). On the other hand, LFC-16 showed a considerable difference in the diffusion coefficient value with a monthly average of  $1.3 \times 10^{-8} \text{ cm}^2/\text{s}$ ; a  $\sim 2$  fold increment compared to LFC-12 and -14, which makes LFC-16 the detergent that produces the fastest population of nAChR-DC mobile on the lipidic matrix.

According to our results, FC-14 and FC-16 did not show a noteworthy change on the mobile fraction during the 30 day period; where FC-14 presented the lowest MF 54% and FC-16 the highest MF 94% (**Figure 22-23**). In contrast, FC-12 showed an alternating behavior with MF values from 70% to 40% during the 30-day period. The phospholipid analog detergents, LFC types, showed no substantial changes among the 30-day period. Although LFC-12 displayed an alternating behavior similar to that of FC-12; the fluctuations go from the 30% to 40% (**Figure 24-25**). In addition, an interesting pattern was observed for the LFC types, according to the present data the population of mobile nAChR-DC augments with the length of the detergent acyl chain. The LFC family showed average mobile fraction during the study period of 34%, 61%, and 90%, for LFC-12, LFC-14, and LFC-16, respectively. Considering these results, a linear increment of the mobile fraction is observed as a function of the detergent acyl chain length.

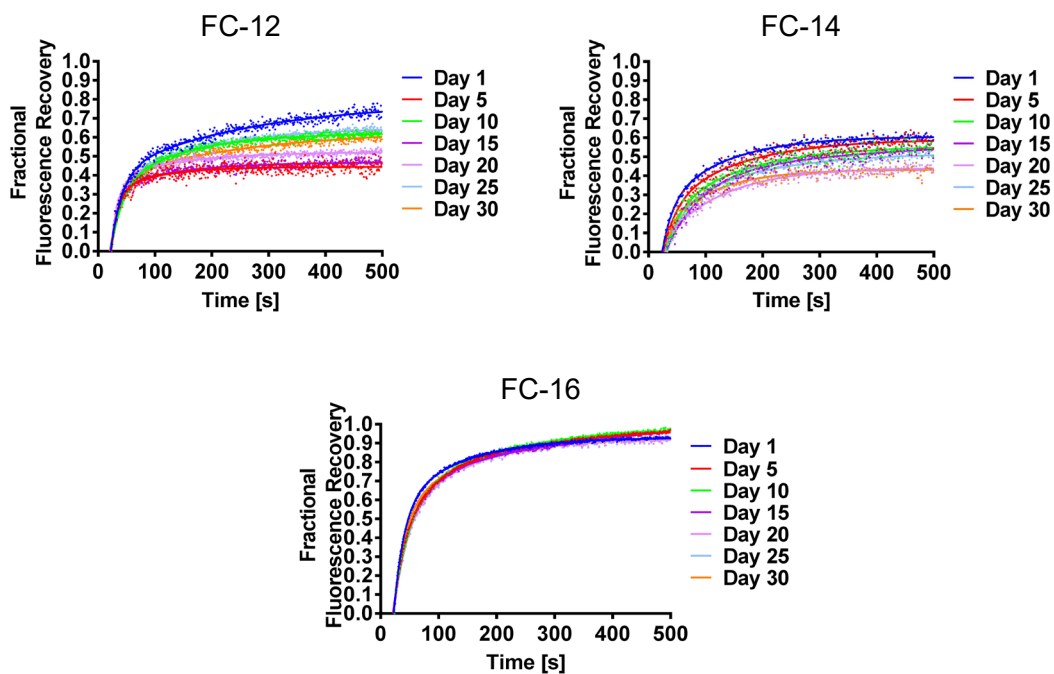


**Figure 22:** LCP-FRAP stability assay for phospholipid analog detergents. Fractional fluorescence recovery and diffusion coefficient of each affinity purified nAChR using phospholipid analog detergents of the Fos choline (FC) family. FRAP experiments of FC-12, FC-14, and FC-16 were recorded every five days for thirty days. All fluorescence recovery experiments were performed in triplicates, averaging five recoveries on different areas of the lipidic matrix with incorporated nAChR.

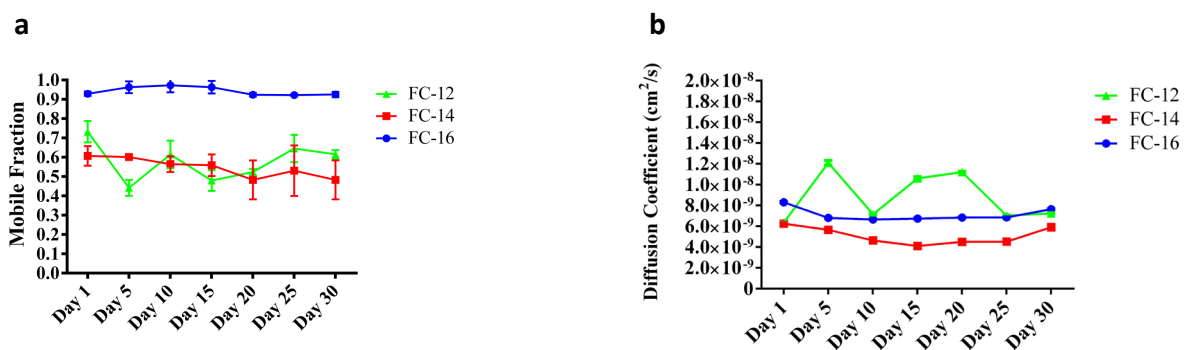


**Figure 23:** LCP-FRAP stability assay for phospholipid analog detergents. The fractional recovery was calculated using Eq. (1), from “Lipidic Cubic Phase Mobility Analysis using Fluorescence After Photo Bleaching” in the materials and methods section, for each fractional recovery of the triplicates. The mobile fraction (a) was obtained by averaging the last twenty points of the fractional recovery obtained in Figure 22. The diffusion coefficient (b) was calculated using Eq. (2), from “Lipidic Cubic Phase Mobility Analysis using Fluorescence After Photo Bleaching” in the materials and methods section.

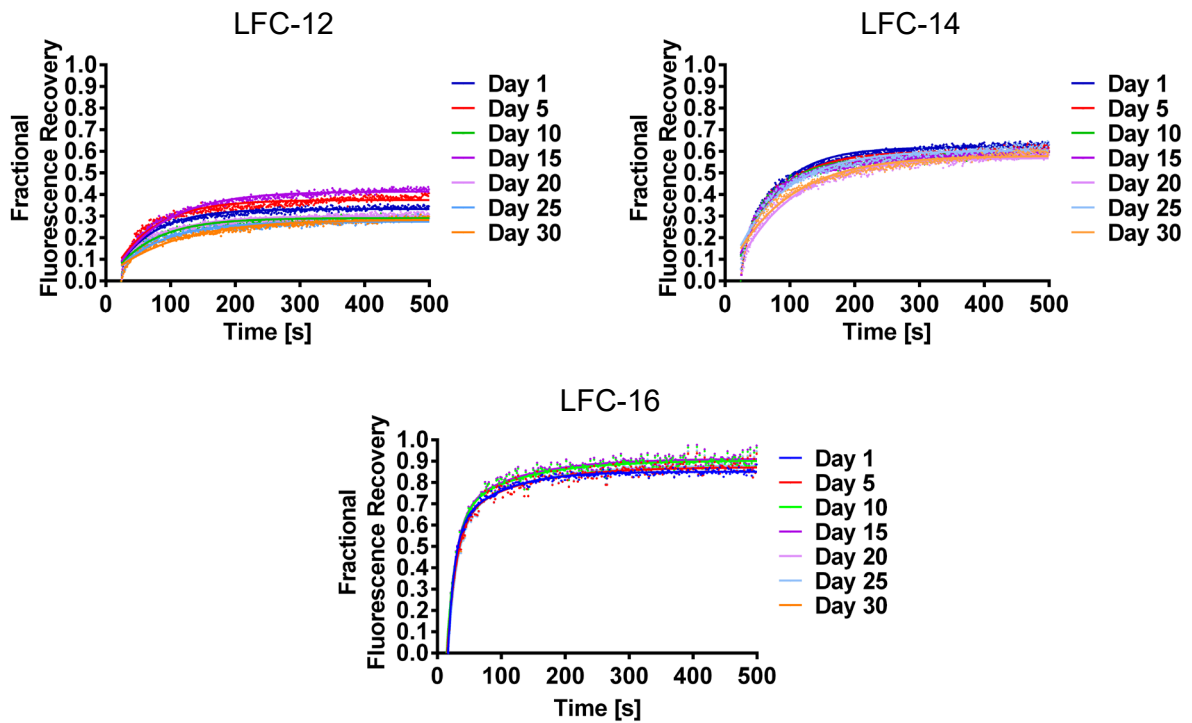


**Figure 24:** Phospholipid analog detergents lipidic matrix stability, LCP-FRAP assay. Fractional fluorescence recovery and diffusion coefficient of each affinity purified nAChR using phospholipid analog detergents of the LysoFos choline (LFC) family. FRAP experiments of LFC-12, LFC-14, and LFC-16 were recorded every five days for thirty days. All fluorescence recovery experiments were performed in triplicates, averaging five recoveries on different areas of the lipidic matrix with incorporated nAChR.

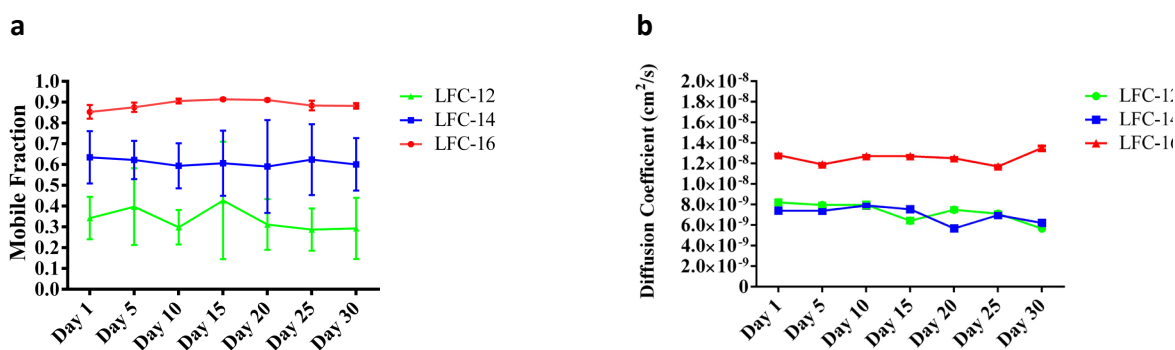


**Figure 25:** The fractional recovery was calculated using Eq. (1), from “Lipidic Cubic Phase Mobility Analysis using Fluorescence After Photo Bleaching” in the materials and methods section, for each fractional recovery of the triplicates. The mobile fraction (a) was obtained by averaging the last twenty points of the fractional recovery obtained in Figure 24. The diffusion coefficient (b) was calculated using Eq. (2), from “Lipidic Cubic Phase Mobility Analysis using Fluorescence After Photo Bleaching” in the materials and methods section.



## **6. Vapor Diffusion Crystallization of Detergent Purified nAChR Using Lipid Analog Detergents**

Protein crystallization was developed in the 19<sup>th</sup> century with the purpose of demonstrating material purity and as a purification tool. The crystallization of macromolecules such as proteins, nucleic acids, and large biological complexes, like viruses, depends on the dual capability of a solution that is supersaturated in the macromolecule but possesses the ideal conditions to sustain the macromolecule's stability and native state. This has been the Achilles heel of this purification/nucleation technique. The supersaturation state is achieved through the addition of mild precipitating agents (crystallant) such as salts or simple polymers, and by the manipulation of various parameters that include temperature, ionic strength, and pH.

Several factors can affect the structural state of the macromolecule during the crystallization process, such as metal ions, inhibitors, cofactors, or other conventional small molecules like detergents. There have been several approaches that combine a spectrum of factors, to control crystallization conditions and promote crystallization. Proteins stabilizers, targeted by molecular modeling have increased the odds to achieve protein crystallization. Positive results among macromolecular crystallization targets have multiplied rapidly in recent years owing to the advent of practical, easy-to-use screening kits and the application of laboratory robotics.

All these advancements have set the foundations for the achievement of vapor diffusion crystals of transmembrane proteins. The use of protein stabilizers allowed the creation of co-crystallizable complexes, which not only provide key salt bridge contacts to generate protein crystals but enhance protein stability allowing for high-resolution diffraction after X-Ray exposure. Molecular engineering has allowed for the modification of transmembrane proteins to improve chemical dynamics prompt to crystal formation while sustaining functionality. Our strategy is based on a lipidic approach to determine the membranous like environment suitable for crystallization of a stable and functional nAChR.

Our results contribute to the pursuit of nAChR crystallization using vapor diffusion technique. In our lipidic based approach, we used phospholipid analog detergents that have shown functionality in the PLB and have also shown to sustain stability in soluble nAChR detergent complex and the lipidic cubic phase. Detergent purifications with LFC-16 and FC-16 were used for vapor diffusion experiments. Results in **Table 2** outline the condition of detergent purifications that have shown crystal formation. In vapor diffusion, FC-16 seems to be more suited than LFC-16 to produce crystals like structures. Although none of the crystals produced well defined diffracting patterns, microdilution of larger crystal-like structures and nanodrop readings, confirmed that these arrangements were composed of proteins. Data shows that conditions in **Table 2** are more prompt to generate crystals using the detergent FC-16 (**Figure 26**). Perhaps there is a multi-factorial contribution that would be impacting the quality of developed crystals, or the power source used for crystal diffraction was not adequate. Experimental variability due to inconsistent handling during dilution could be a factor influencing reproducibility; although the use of the mosquito robot minimalizes the impact.

**Table 2:** Crystallization conditions used in Vapor Diffusion (Hanging drop) that produced low quality nAChRs crystals.

Detergent ID	Protein Concentration (mg/mL)	Protein Dilution Factor (Protein:Buffer)	Buffer	Crystallant/Precipitant	Salt
FC-16	5.60	1:1	Sodium cacodylate, 0.1M (pH = 6.5)	2-Methyl-2-pentenediol, 30% v/v	Magnesium acetate, 0.2M
FC-16	4.88	1:1	Sodium cacodylate, 0.1M (pH = 6.5)	2-Methyl-2-pentenediol, 30% v/v	Magnesium acetate, 0.2M

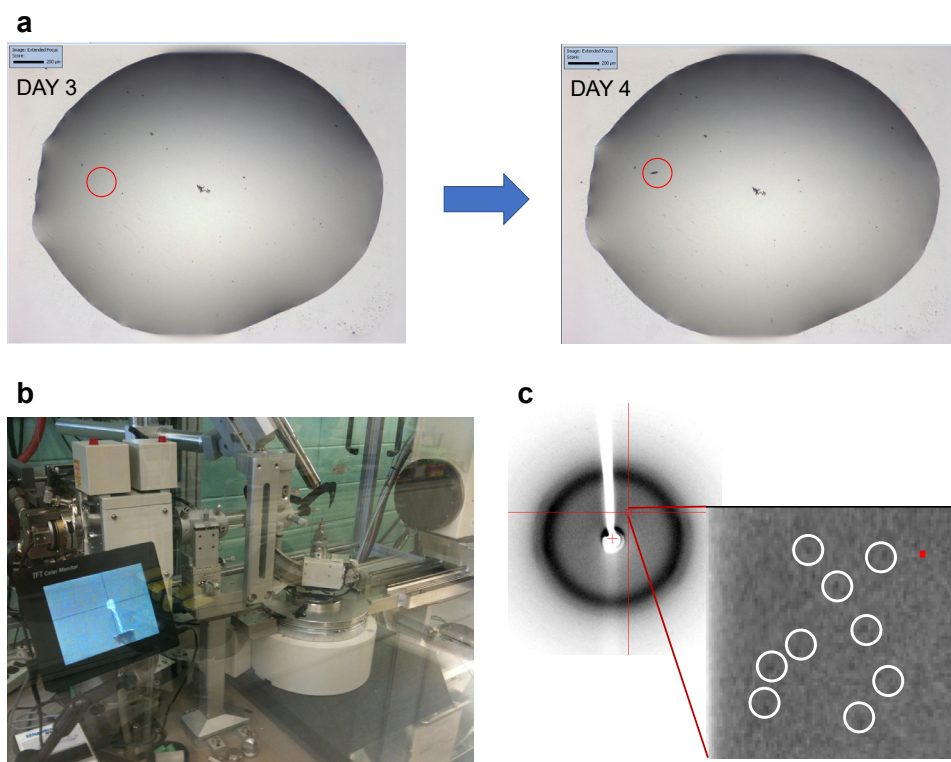


**Figure 26:** Low Quality nAChR crystals generated under vapor diffusion (Hanging Drop). The time frame image (a) was collected in the ROCK Imager 54 (Formulatrix) robotic incubator under constant monitoring and ambience control. After a crystal hit was noticed, the crystals were harvested and diffracted on a Rigaku RU-H3R X-ray generator (b). However, poor diffraction patterns were observed (c) and only few diffraction dots were observed in the collected phase.

## 7. Lipidic Cubic Phase Crystallization of Detergent Purified nAChR Using Lipid Analog Detergents

Lipid cubic phase or *in meso* technique has become a robust approach for integral membrane protein crystallization. This technique has trended rapidly since its great achievements back in the early to mid-2000s, particularly after the contribution to elucidating the structure of the first functional chimeric GPCR receptors. Mechanistically, there is still a great deal to learn and understand. Nevertheless the technique has provided excellent results with transmembrane protein.

The critical elements for LCP crystallization success are based on two crucial characteristics: (1) provides a native-like membranous environment throughout the membrane protein crystallization process instead of being exposed to chemically distinct environment and (2) crystals grown in LCP allows proteins to make contact not only through hydrophilic but also through hydrophobic domains, and as a results lowers solvent content and improves crystal organization.

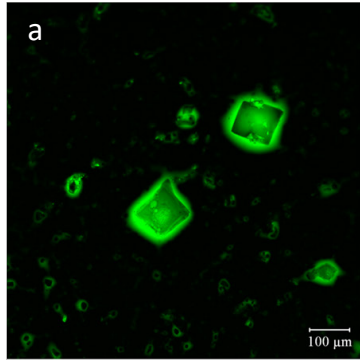
LCP matrix has been used for the crystallization of the nAChR in the past. Electron microscopy images demonstrate the capability of the nAChR to form microcrystals in a lipidic matrix [8]. However, such crystals were not from diffractive quality. Perhaps a deeper understanding of lipidic matrixes mechanisms and of nAChR stability in lipidic environments could have provided key elements/controls to obtain high-quality crystals.

Our lipid-based approach, *in-meso* crystallization of the nAChR, provided a critical stabilizing environment that supports nAChR stability better than traditional vapor diffusion techniques. As our LCP mobility and stability assessments confirm, the chemical-physical properties of residual lipids and detergents affect the stabilizing capabilities of the LCP. Therefore, it is important to thoroughly analyze the isolation process before using the LCP as crystallization media. According to our results, LFC-16 and FC-16 are detergents that could withstand nAChR functionality and sustain both soluble and LCP stability. Therefore, our

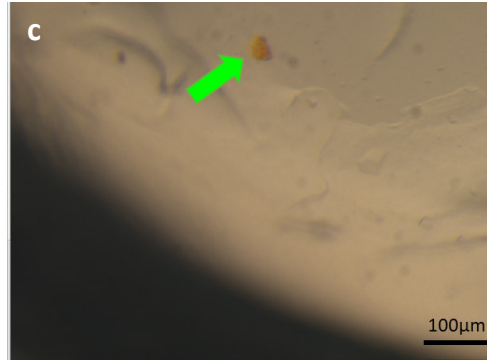
crystallization trials will be focused on using nAChR that has been purified using LFC-16 and FC-16.

Our results showed LFC-16 and FC-16 consistently generated protein crystals in the LCP (**Figure 27**). Experiment consistency was evaluated and resulted in a 1 out of 3 experiments produce crystals to produce a 33% consistency, where most of the experiment produced about 6 protein crystals. However, not all experiments were able to produce protein crystals as much as previously described: only 5 out of 6 total experiments produced more than 5 nAChR crystals. This 83% consistency between experiments that generate AChR crystals could be related to the hardware, as the LCP is sensitive to humidity and the micro-batch preparations are highly dependent in a duck tape® seal. Visual assessment of several experiments confirmed that the use of duck tape® did not always provide the efficient seal necessary to isolate the crystallization conditions. Several tape brands were tested but none provided better performance than the duck tape ®.

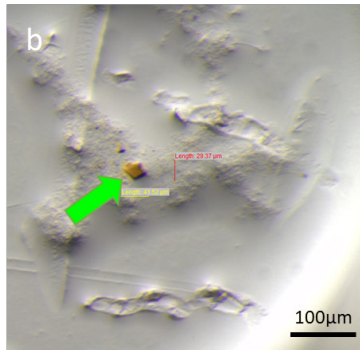
All harvested crystals were diffracted under high power light source at the National Laboratories as described in the materials and method section. Despite the lack of high-resolution data, several crystals were confirmed to be composed of protein per 280 nm readings in the nanodrop. Non-diffractive crystals were consistently achieved showing the LCP capability to crystallize affinity purified nAChR using lipid analog detergents. Receptor crystals were in general between 20 – 40 µm. In terms of appearance, crystals were expected to have sharp edges although the crystal shape was hard to determine due to LCP density and blurriness. As expected, the color was Ambar/Green (**Figure 27**). This color was anticipated due to the αBTx fluorescent tag - Alexa 488; the αBTx solution was green to the naked eye, thus in nucleation this color is likely to intensify into an Ambar/Green. Several diffraction images showed possible diffracting patterns from protein arrangement (**Figure 28**). Nevertheless, our results suggest that higher controls and structural stability of the nAChR might be required to increase the diffraction quality of crystals.



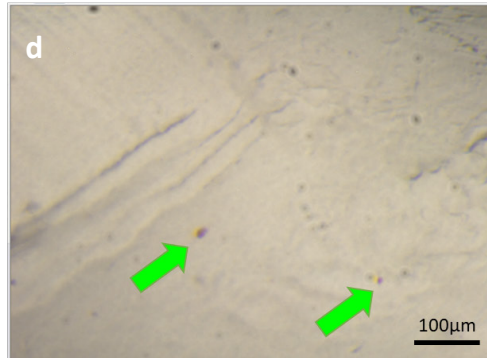
**Precipitant:** 20% (w/v) PEG-3000  
**Buffer:** MES  
**Salt:** 0.2 M MgCL<sub>2</sub>  
**pH:** 6.0  
**Detergent:** LFC-16  
**Concentration:** 4.89 mg/mL  
**Time:** 30 days



**Precipitant:** 30% w/v Polyethylene glycol 4,000  
**Buffer:** 0.2M Ammonium acetate  
**Salt:** 0.1M Sodium citrate tribasic dihydrate  
**pH:** 5.6  
**Conductivity:** 10 mS/cm  
**Detergent:** FC-16  
**Concentration:** 12.27 mg/mL  
**Time:** 10 Days

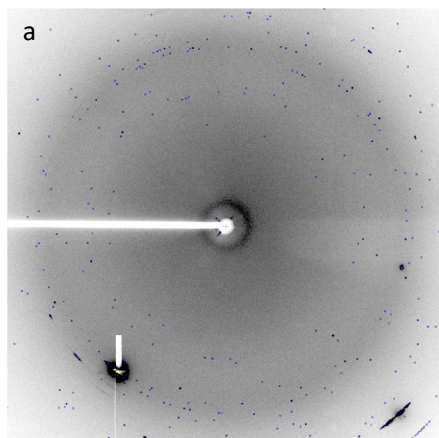


**Precipitant:** 30% w/v Polyethylene glycol 4,000  
**Buffer:** 0.2M Ammonium acetate  
**Salt:** 0.1M Sodium citrate tribasic dihydrate  
**pH:** 5.6  
**Conductivity:** 10 mS/cm  
**Detergent:** LFC-16  
**Concentration:** 6.09 mg/mL  
**Time:** 9 Days

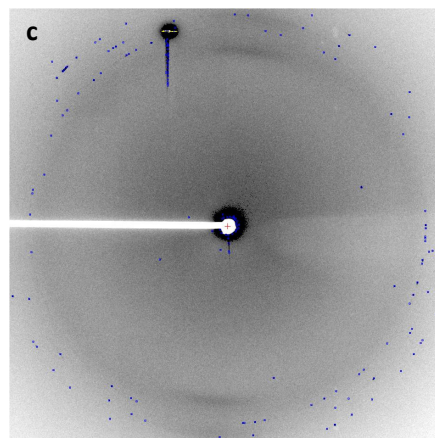


**Precipitant:** 30% w/v Polyethylene glycol 4,000  
**Buffer:** 0.2M Ammonium acetate  
**Salt:** 0.1M Sodium citrate tribasic dihydrate  
**pH:** 5.6  
**Conductivity:** 10 mS/cm  
**Detergent:** FC-16  
**Concentration:** 8.12 mg/mL  
**Time:** 13 Days

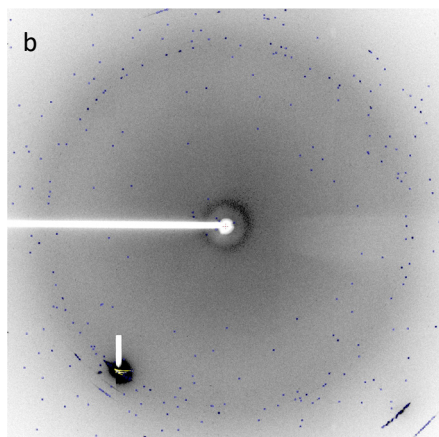
**Figure 27:** Figure shows a pool of nAChR crystal examples generated on LCP using LFC-16 (a,b) and FC-16 (c,d). Crystals showed ambar/green color as expected because of the bounded  $\alpha$ BTx; sharp edges are also noticed in most crystals. All conditions have in common the concentration of precipitant/crystallant agent (greater than 20%); the pH is lower or equal than 6.0. These two aspects correlate with previously reported trends. All crystals were generated in more than a week. Condition in figure (a) shows crystals develop after a 30 day incubation. Green arrows show crystals embedded in the LCP media. The crystallization condition is from Hampton Scientific: Crystal Screen 1 condition 9 (Cs1 9).



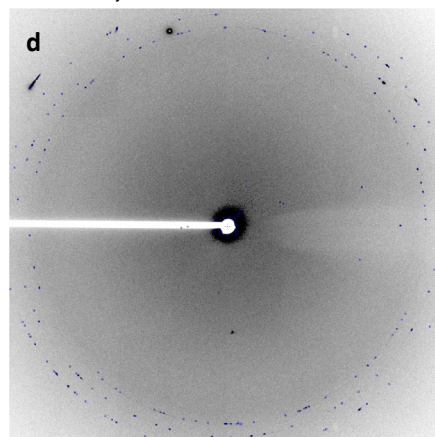
**Precipitant:** 20% (w/v) PEG-3000  
**Buffer:** MES  
**Salt:** 0.2 M MgCl<sub>2</sub>  
**pH:** 6.0  
**Detergent:** LFC-16  
**Concentration:** 4.89 mg/mL  
**Time:** 30 days



**Precipitant:** 30% w/v Polyethylene glycol 4,000  
**Buffer:** 0.2M Ammonium acetate  
**Salt:** 0.1M Sodium citrate tribasic dihydrate  
**pH:** 5.6  
**Conductivity:** 10 mS/cm  
**Detergent:** FC-16  
**Concentration:** 12.27 mg/mL  
**Time:** 10 Days



**Precipitant:** 30% w/v Polyethylene glycol 4,000  
**Buffer:** 0.2M Ammonium acetate  
**Salt:** 0.1M Sodium citrate tribasic dihydrate  
**pH:** 5.6  
**Conductivity:** 10 mS/cm  
**Detergent:** LFC-16  
**Concentration:** 6.09 mg/mL  
**Time:** 9 Days



**Precipitant:** 30% w/v Polyethylene glycol 4,000  
**Buffer:** 0.2M Ammonium acetate  
**Salt:** 0.1M Sodium citrate tribasic dihydrate  
**pH:** 5.6  
**Conductivity:** 10 mS/cm  
**Detergent:** FC-16  
**Concentration:** 8.12 mg/mL  
**Time:** 13 Days

**Figure 28:** Diffraction phase from each crystallization condition presented in Figure 27. None of them showed a significant diffraction pattern. However, small patterns can be observed close to the inner beam stopper, indicating low-resolution X-ray Dispersion.



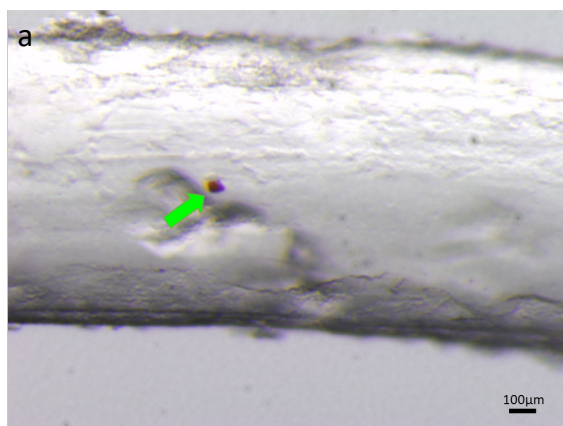
## **8. Lipidic Cubic Phase Crystallization of Detergent Purified nAChR Using Lipid Analog Detergents Applying Electric Potential**

According to our findings, crystallizing the nAChR is dependent on a great variety of elements, including the identity of lipids and how they could support nAChR in a stable and functional conformation, whereas key protein segments are positioned in a precise way to achieve protein nucleation.

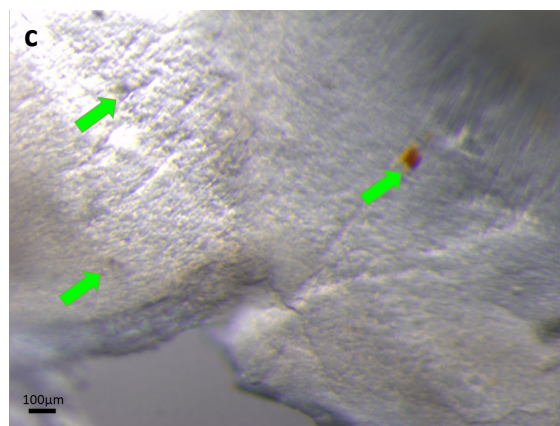
There are a few possible explanations for not obtaining the high-quality crystals necessary for nAChR X-ray structure determination at atomic resolution. First, the nAChR is a highly amphiphilic oligomer, characterized by a vast hydrophobic region that consists of 20 transmembrane segments and two hydrophilic domains: (1) a ligand-binding domain that protrudes extracellularly by ~8 nm and displays an 8 to 9 nm diameter and (2) an intracellular domain that protrudes by ~4.5 nm into the cytoplasm and displays a diameter that narrows from ~4 to 8 nm [9]. Second, the nAChR is an allosteric protein that interconverts spontaneously between at least three alternatives, discrete conformations: resting, active, and desensitized states [10]. Third, the receptor is glycosylated with high-mannose and complex oligosaccharides [11]. All these characteristics create a high level of complexity in nAChR crystallization, in which a lipid-based approach plays a crucial role, and suggest the need of further nAChR stabilization to achieve high-quality crystals in the LCP.

By considering the nAChR characteristics mentioned above, our team designed a new approach that combined the vast knowledge derived from electrophysiology studies with our lipidic approach. The technique is based on the nAChR sensitivity to potentiated environments. It is well known that nAChR currents are influenced by the potential of depolarized membranes. Therefore, the nAChR dependency in potential can be used as an external stimulus that will sustain the nAChR in a fixed conformation allowing the nucleation of well-ordered receptors.

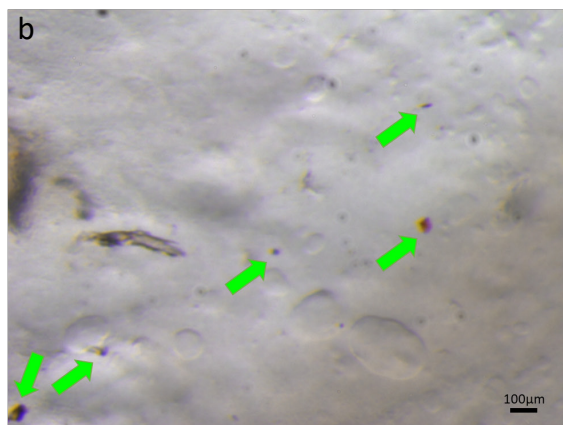
Our results showed that crystallization of under applied potential improved the chances of producing protein crystals from nAChR. nAChR crystallization trials under applied potential yielded an 80% consistency, where 8 out of 10 experiments produced protein crystals using the conditions outlined in (**Figure 29**). In most of the failed experiments, a small leak was noticed through the resin used as a sealant; thus, the isolated environment was cracked allowing ambient humidity to disrupt the experiment. Each experiment yielded more than 10 protein crystals, presenting a significant improvement over previous tests (without applied potential). Protein crystals were confirmed by nanodrop readings at 280 nm, showing that LCP under applied potential is capable of achieving nAChR nucleation. Receptor crystals grown in LCP with -15mV applied potential were approximately 26% larger than those generated in LCP batch. Appearance was as expected; sharp edges were well noticed although sometimes crystal shape was hard to see due to LCP density. The color was Ambar/Green (**Figure 29**), consistent with crystals produced in LCP with no applied potential. The harvested crystals were used for X-ray diffraction at the National Laboratories as described in the materials and method section; however, no diffraction data was generated (**Figure 30**). Perhaps there are additional fine tweaks that the technology needs to overcome to achieve full stability of the nAChRs



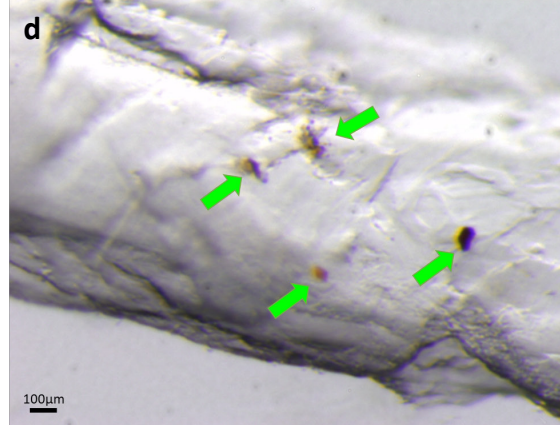
**Precipitant:** 30% w/v Polyethylene glycol 4,000  
**Buffer:** 0.2M Ammonium acetate  
**Salt:** 0.1M Sodium citrate tribasic dihydrate  
**pH:** 5.6  
**Conductivity:** 10 mS/cm  
**Detergent:** LFC-16  
**Concentration:** 4.71 mg/mL  
**Time:** 24 hours



**Precipitant:** 30% w/v Polyethylene glycol 4,000  
**Buffer:** 0.2M Ammonium acetate  
**Salt:** 0.1M Sodium citrate tribasic dihydrate  
**pH:** 5.6  
**Conductivity:** 10 mS/cm  
**Detergent:** FC-16  
**Concentration:** 9.75 mg/mL  
**Time:** 24 hours



**Precipitant:** 30% w/v Polyethylene glycol 4,000  
**Buffer:** 0.2M Ammonium acetate  
**Salt:** 0.1M Sodium citrate tribasic dihydrate  
**pH:** 5.6  
**Conductivity:** 10 mS/cm  
**Detergent:** LFC-16  
**Concentration:** 14.34 mg/mL  
**Time:** 24 hours



**Precipitant:** 30% w/v Polyethylene glycol 4,000  
**Buffer:** 0.2M Ammonium acetate  
**Salt:** 0.1M Sodium citrate tribasic dihydrate  
**pH:** 5.6  
**Conductivity:** 10 mS/cm  
**Detergent:** FC-16  
**Concentration:** 10.44 mg/mL  
**Time:** 24 hours

**Figure 29:** Figure shows a pool of nAChR crystal examples generated on LCP using LFC-16 (a,b) and FC-16 (c,d) and applying -15 mV of voltage potential. Crystals showed ambar/green color as expected because of the bounded  $\alpha$ BTx. Sharp edges are also noticed in most crystals. The crystallization condition is from Hampton Scientific: Crystal Screen 1 condition 9 (Cs1 9). This condition constantly showed nucleation under voltage potential as well as in LCP with no voltage applied. All crystals were generated within 24h. Green arrows show crystals embedded in the LCP media.

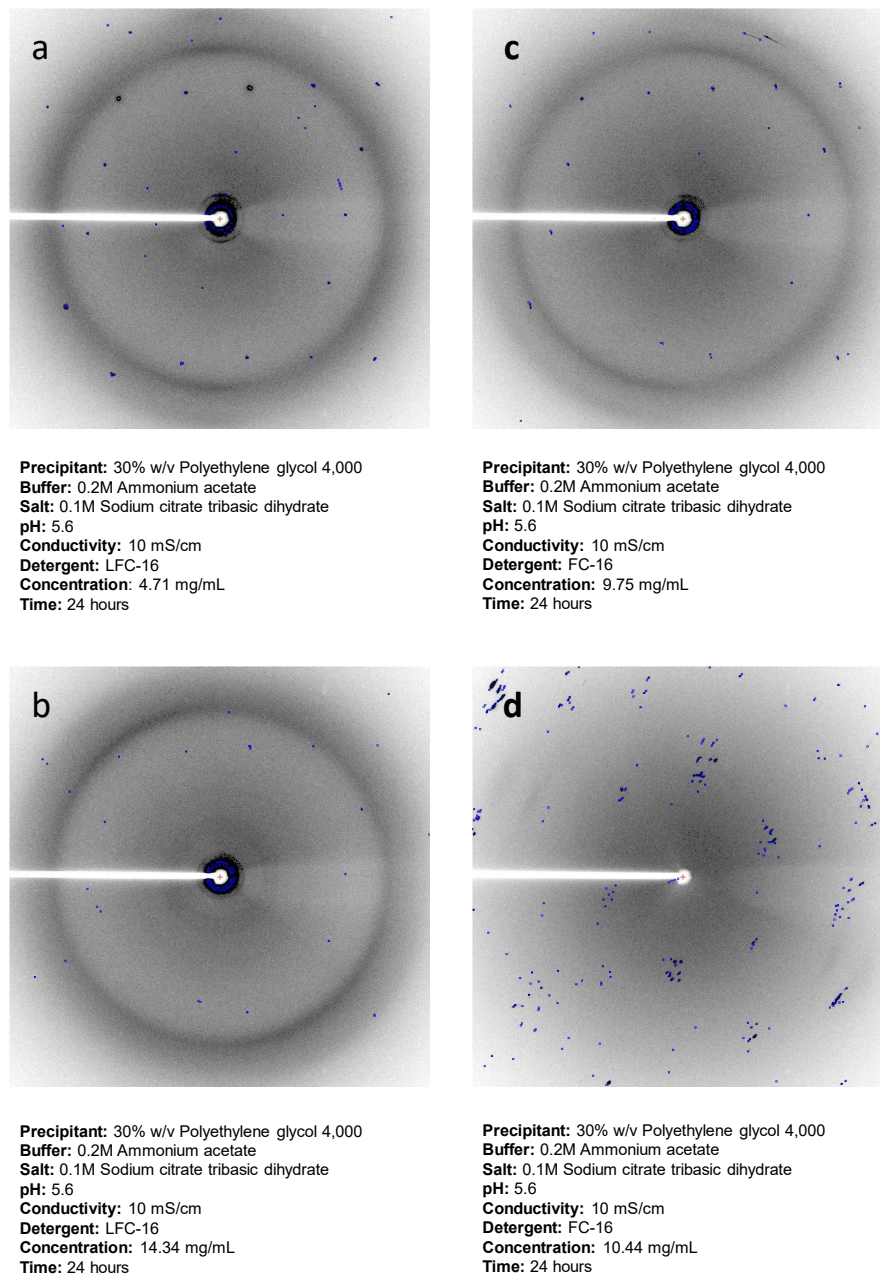


**Figure 30:** Diffraction phase from each crystallization condition presented in Figure 29. None of them showed a significant diffraction pattern. However, small patterns can be observed close to the inner beam stopper, indicating low-resolution X-ray dispersion.

## Results References

1. Asmar-Rovira, G.A. et al. "Biophysical and ion channel functional characterization of the *Torpedo californica* nicotinic acetylcholine receptor in varying detergent–lipid environments" *J. Membr. Biol.* vol. 223 (2008): 13 – 26.
2. Quesada O. et al. "Uncovering the lipidic basis for the preparation of functional nicotinic acetylcholine receptor detergent complexes for structural studies" *Scientific Reports: Nature* vol. 6 (2016): 32766.
3. Nelson, N. et al. "Reconstitution of purified acetylcholine receptors with functional ion channels in planar lipid bilayers" *Proc Natl Acad Sci USA.* vol. 77 (1980): 3057–3061.
4. Montal, M. "Channel properties of the purified acetylcholine receptor from *Torpedo californica* reconstituted in planar lipid bilayer membranes" *Biophys J.* vol. 45, 1 (1984): 165-174.
5. Padilla-Morales, L. F. et al. "Effects of lipid-analog detergent solubilization on the functionality and lipidic cubic phase mobility of the *Torpedo californica* nicotinic acetylcholine receptor" *J. Membr. Biol.* vol. 243 (2011): 47–58.
6. Cherezov, V. et al. "LCP-FRAP assay for prescreening membrane proteins for in meso crystallization" *Cryst. Growth Des.* vol. 8 (2008): 4307–4315.
7. Cherezov, V. et al. "Membrane protein crystallization in lipidic mesophases. A mechanism study using X-ray microdiffraction" *Faraday Discuss* vol. 136 (2007): 195 – 212.
8. Paas, Y. et al. "Electron microscopic evidence for nucleation and growth of 3D acetylcholine receptor microcrystals in structured lipid–detergent matrices" *Proceedings of the National Academy of Sciences.* vol. 100, 20 (2003): 11309-1131

9. Unwin, N. et al. "Nicotinic acetylcholine receptor and the structural basis of fast synaptic transmission" *Philos. Trans. R. Soc. London Ser. B.* vol. 355 (2000): 1813-1829
10. Rosenbusch, J. P. et al. "Stability of membrane proteins: relevance for the selection of appropriate methods for high-resolution structure determinations" *J. Struct. Biol.* vol. 136 (2001): 144 – 157
11. Poulter, L. et al. "Structure, oligosaccharide structures, and posttranslationally modified sites of the nicotinic acetylcholine receptor" *Proc Natl Acad Sci USA.* vol. 86, 17 (1989): 6645-6649.

## CHAPTER 5. Discussion

### 1. Affinity Purification of the nAChR from *T. Californica* Membranes

Affinity Chromatography, which was used for the purification of the nAChR, has been effectively used for decades [1, 2]. Detergent buffers provided the appropriate duality of conditions to support the stability of a membrane protein, hydrophobic interactions with the transmembrane domain and hydrophilic interactions with the intracellular/extracellular domains. This is the main reason why it is so complicated to determine the best conditions for the purification of membrane proteins. It is well known that detergent structure and chemistry in solution can influence residual lipids in membrane proteins during isolation. Thus the stability of such proteins in solution directly correlates with the identity of the detergent used during protein purification [3].

Our purification strategy has reliably shown that using lipid analog detergents is the appropriate strategy to isolate a functional and stable nAChR from *T. californica* crude membranes. SDS-PAGE images clearly showed the appearance of the four subunits that constitute the nAChR from *T. californica*  $\alpha\beta\gamma\delta$  and the subunits are shown in the right proportion  $2\alpha$ ,  $1\beta$ ,  $1\gamma$ , and  $1\delta$ . Purification using long acyl chains phospholipid analog detergents such as FC-16 and LFC-16 has consistently shown higher concentrations of protein in elution samples, from 6.0 mg/mL to 16.0 mg/mL. Meanwhile, shorter acyl chain detergents such FC-12 have shown less concentrated protein elution samples, 3.5 mg/mL to 5.4 mg/mL. These findings indicate that long acyl chain phospholipids analog detergents are more suited for isolation than short acyl chain detergents. In addition, affinity chromatography experiments using cholesterol analog detergents such as CHAPS, CHAPSO and Cholate, showed results like those previously reported by Asmar-Rovira et al. 2008 [1]. Thus, confirming the accuracy of our experimental execution and validating our performance during the purification of nAChR from *T. californica* crude membranes.

In terms of purity and stability, long acyl chain detergents have shown to sustain nAChR stability better, because these detergents have shown less percentage of aggregates and dimers than the short chain counterparts and previously reported cholesterol analogs detergents in Asmar-Rovira et al. 2008 [1]. Moreover, our findings are consistent with further discussed functional and stability data in the LCP. Our data suggest that the appropriate condition to successfully purify the nAChR through affinity chromatography is by employing phospholipid analog detergents as assembled soluble mix micelles capable of solubilizing the nAChR from *T. californica* crude membranes.

## **2. Soluble Stability and Ion Channel Functionality of Detergent Purified nAChR**

Functionality testing using PLB for the affinity-purified *T. californica* nAChR in phospholipid and cholesterol analogs showed no considerable difference in single-channel mean current under the same voltage-clamp conditions, even for members of the same detergent family, as previously reported [1]. Differences in the mean channel current between our previous study published in Asmar-Rovira et al. 2008 [1] and the current work (1.25 pA) are attributed to variability between tissue sources and differences in membrane resistance and capacitance. Membrane capacitance and resistance are highly dependent on the buffer ionic strength and the lipid mixture preparation. The data suggest that both cholesterol-analog and phospholipid-analog detergents were able to sustain functionality in the PLB. The results are consistent with data previously reported by our group in Asmar-Rovira et al. 2008 [1] and others [4,5,6]. Nevertheless, this type of technique doesn't consider the entire population of nAChR purified from the *T. californica* membranes. Perhaps a more holistic approach towards ion channel functionality assessment would give us more information about the total population of receptors.



During the PLB assay, both plastic holder cavities were filled with the same bilayer buffer solution (See method section for a detailed assemble description). However, the final concentration in the front plastic holder was slightly different due to the presence of additional components. This will modify the ion strength/concentration in both chambers, creating membrane cracks alteration associated with an electromotive force that could generate differences between sample preparations. These cracking and alteration to the membrane seals that results from the unbalanced ion strength solutions, could introduce additional background noise and false, yet easy to identify, ion currents on the PLB experiments.

Lipid depletion is an inevitable consequence of the membrane protein solubilization process and could be responsible for aggregation and monomer:dimer ratios that affect ion channel functionality. Overall, results from A-SEC studies suggest that long acyl chain phospholipid analog detergents are better at sustaining the soluble stability of the nAChR. An observation that might be attributed to the capability of the large mixed micelle to accommodate the solubilized nAChR with ease. This, in turn, correlates with the physical property that longer acyl chain phospholipid-analog detergents such as FC-16 and LFC-16 have higher aggregation numbers per formed micelle than short acyl chains phospholipid analog detergents such as FC-12 and cholesterol analog detergents such as CHAPS, CHAPSO and Cholate.

If we consider the nAChR monomer, dimer and aggregate percentages obtained using A-SEC for each of the detergents used in this study and compare them with the total mobile fraction in FRAP assays, a discrepancy in the mobile fraction is apparent. The monomer should display the highest mobility in the LCP matrix; therefore, the mobile fraction values for the cholesterol-analog detergents CHAPS, CHAPSO, Big CHAP, and cholate should be minimal. However, their mobile fraction values of 71%, 81%, 49%, and 87%, respectively, are much higher than expected, with similar results observed for other lipid analog and non-lipid-analog detergents. Furthermore, phospholipid-analog detergents also showed a higher than

expected mobile fraction based on the contribution of the monomers observed in A-SEC assays. In the case of phospholipid-analog detergents, a direct correlation was observed between the amount of monomer detected on A-SEC and the FRAP mobile fraction (**Figure 15** in the Results Section). Bearing in mind that the protein-detergent complex needs to be mixed with the LCP matrix to maximize intermolecular interactions with monoolein, it is not surprising that detergents with hydrophobic regions, consisting mainly of aliphatic chains, can form better stabilizing interactions with the monoolein structure. Such interactions can be the driving force necessary to filter dimers and aggregates of the protein and facilitate their incorporation into the LCP matrix. The cholesterol analog and lipid analog detergents that were chosen for these studies contain moieties in their structure that enable their interaction with the 16-carbon chain of mono-olein. Theoretically, the best interaction should be produced by the LFC-16, which was the detergent that produced an affinity-purified nAChR with the most monomeric species and stable crystals in a 30-day study period (**Figure 23 and 25** in the Results section).

### **3. Macroscopic Ion Channel Functional Assessment of Detergent Solubilized and Affinity Purified nAChR Using Lipid and Non-lipid Analog Detergents.**

Protein functionality assessment has become an essential part of the characterization process; before proceeding with membrane protein crystallization. Several membrane proteins required sequence and post-transcription modifications to achieve the stability necessary for protein nucleation during crystallization trials. In several cases these modifications are substantial; i.e. total depletion of peptide segments to enhance the stability of the 5-HT<sub>3</sub> receptor [7] and the depletion of internal loops on the human  $\alpha$ 4 $\beta$ 2 nicotinic receptor [8], also the insertion of exogenous peptides to increase protein stability as well as the improvement of the hydrophilic:hydrophobic area ratio to increase the possibility of salt bridge formation during crystallogenesis of the G-protein couple Receptor (GPCR) Beta-2

Adrenergic Receptor ( $\beta_2$ AR) [9]. These significant modifications could be key towards protein crystallization but raise questions about how functional these modified receptors are when compared to their native form and how reliable are they as a source of information when crystallized. Therefore, functional characterization during the crystallization process is critical to ensure that the crystallized chimeric protein is representative of the native protein.

Detergent-purification has been known to be affected by the amount and identity of residual lipids in the nAChR, which in turn can affect nAChR functionality after solubilization [3]. Unfortunately, how detergents affect lipid composition/distribution, functionality (ion channel in our case), and the stability of solubilized membrane proteins remains poorly understood regarding the structural biology of membrane proteins in general. For the past 3 decades, the selection of detergents for membrane protein solubilization and/or crystallization has been an empiric experiment. To identify the best detergents for future structural studies on nAChRs, we have developed a strategy that allowed us to assess the function and stability of nAChR detergent complexes simultaneously.

Electrophysiology experiments have been used for decades to assess nAChR ion channel functionality after detergent purification and since the 1980s PLB has been used extensively. However, PLB experiments rely on the assumption that all ion channels isolated from *T. californica* membranes using detergents are equal and that a small portion of the examined proteins is a good representation of the nAChR population in the protein pool. Consequently, a complete functional analysis of the detergent-purified nAChRs is preferred to support the detergent purified nAChR characterization when using lipid analog detergents for further crystallization trials. Previous publications from our laboratory examined the functionality of detergent-solubilized and affinity-purified nAChRs from *T. californica* prior to LCP preparation using PLB [2]. Here, we use two electrodes voltage clamp (TEVC) as a more efficient approach to assessing the functional properties of the *T. californica* nAChR crude membranes and purified nAChR-DCs. This method allows for the acquisition of macroscopic ion channel

currents from nAChRs that incorporate into the plasma membrane after direct injection of nAChR-DC into an oocyte. The injection of oocytes with *T. californica* crude membranes (membranes isolated only by a series of centrifugation and ultracentrifugation coupled with high salt buffer: no detergent present), when exposed to ACh, evoked responses using TEVC. In addition, those responses were sensitive to pre-treatment with  $\alpha$ -BTX (**Figure 8** in the Results Section), suggesting that responses seen in these oocytes are coming from functional nAChRs present in the crude membrane preparation. It is important to mention that we have not been able to perform the same experiments using PLB since synthetic membranes seem to be too unstable to incorporate crude membranes. Perhaps the artificial membranes are not as strong and lack of complex systems as the oocytes to accommodate the crude membranes. In addition, as previously shown by Marsal et al. 1995 [11], the activity of nAChR crude membrane injected into oocytes produces qualitatively similar responses to those generated by the injection of a cocktail of mRNA coding for the nAChR [12 - 22]. These results validate the functional assays of injecting nAChR-DCs into *Xenopus* oocytes. Moreover, once the detailed three-dimensional structure of the nAChR is determined, the approach used herein can be applied during the drug design phase to test novel compounds designed as modulators of the nAChR.

Data strongly suggests that detergent structure, chemical capabilities (i.e., hydrogen bonds, salt bridging, and hydrophobic interactions) and shape used to extract and form complexes with the *T. californica* nAChRs can completely alter receptor functionality. This is aligned with data previously reported by our group on Asmar-Rovira et al. 2008 [1] and Padilla et al. 2011 [2]. When we compare the activation of the nAChRs from crude membranes with nAChRs purified using Cholate, we found there was a significant reduction in the apparent speed at which the channel is able to open (10%–90% rise times =  $4.49 \pm 0.65$  s,  $n = 13$  versus  $1.23 \pm 0.36$  s,  $n=9$  for crude membranes;  $p=0.0008$ ). Similarly, the apparent desensitization rate (estimated from the half-time ( $t_{1/2}$ ) of the macroscopic current time-decay)

displayed a significant reduction for nAChRs purified using Cholate ( $t_{1/2}=11.64\pm 1.65$  s,  $n=13$  versus  $5.59 \pm 1.65$  s,  $n = 9$  for crude membranes;  $p = 0.009$ ).

Unfortunately, injection with 1.5-fold critical micellar concentrations of CHAPS, BigCHAP or CHAPSO reduced oocyte viability, and these detergents could not be tested using this protocol. It is possible that the detergent's structural features are significantly more disruptive than those in Cholate, even though all are considered cholesterol analog detergents. However, we have published PLB data showing a decreased function for both CHAPS and CHAPSO [1,2] and no function for BigCHAP (Asmar-Rovira et al. 2008), implying these detergents are inferior to the phospholipid analog detergents at maintaining the function of *T. californica* nAChRs.

Both FC-14 and FC-16 displayed a noticeable reduction in current amplitude, indicating that they are not able to support proper ion channel function. Furthermore, even though current amplitude is not significantly affected, there is a significant reduction in the apparent rate of activation for nAChRs extracted using FC-12 (10%–90% rise time =  $3.57 \pm 0.52$  s,  $n = 5$  versus  $1.23 \pm 0.36$  s,  $n = 9$  for crude membranes;  $p = 0.007$ ). These results suggest that the ion channel structure in the nAChR-FC-12 DC displays a distorted conformation.

As shown in (**Figure 10** in the Results section), FC-12 displays normal current amplitude with a remarkable reduction in the activation rate; whereas LFC-12 does not support proper channel function. In contrast, LFC-16 was the only detergent that was able to support the function of nAChR with not only the same level of current amplitudes but also the same kinetics when compared to crude membrane preparations. These results emphasize the advantage of using this approach to recognize detergents that retain the native properties of nAChRs.

Data suggest that the longer acyl chain containing detergents in this family (LFC-14 and LFC-16) are able to support channel function better than the shorter side chain detergents. Interestingly, we found that both of these detergents (LFC-14 and LFC-16) maintain the

apparent activation kinetics (10%–90% rise times =  $1.23 \pm 0.36$  s, n = 9;  $2.74 \pm 0.68$  s, n = 4; and  $1.26 \pm 0.21$  s, n=5 for crude membranes, LFC-14, and LFC-16, respectively); and desensitization profile of the *T. californica* nAChR ( $t_{1/2} = 5.59 \pm 1.65$  s, n = 9;  $7.73 \pm 0.72$  s, n = 4; and  $6.11 \pm 0.29$  s, n = 5 for crude membranes, LFC-14, and LFC-16, respectively). The data illustrate the importance of assessing receptor functionality after detergent extraction since minor changes in the structure of the detergent appear to be enough to produce significant effects on the functional behavior of nAChR-DCs (**Figure 12** in the Results Section). Equivalency of detergent solubilization should not be considered as adequate during the crystallization trials after a well performed functional characterization.

Results from both techniques, PLB and TEVC, consistently showed that lipid analog detergents (such as Cholate, FC-12, LFC-14, and LFC-16) are better in sustaining nAChRs ion channel functionality than non-lipid analog detergents (DDM and OG) (**Figure 1-12** in the Result Section). These same techniques demonstrated that non-lipid analog detergents are not able to sustain a favorable environment for nAChR function; which is consistent with previous reports using PLB only that showed these detergents are not able to stabilize nAChRs resulting in the loss of functionality (Asmar-Rovira et al. 2008 and Padilla et al. 2011). Furthermore, the present study shows that not all lipid analog detergents are able to sustain the functional activity of nAChR-DCs equally. Even within phospholipid detergent families, such as foscholine and lysofoscholine, we found that small differences in a detergent structure such as the acyl chain length are critical for the ion channel functionality and can cause remarkable changes in nAChR function. Perhaps detergent length could be associated with a specific interaction with the nAChR. Moreover, the residual amount and identity of lipids could be influenced by the detergent structure.

A possible explanation for the observed differences between the functionality of foscholine and lysofoscholine families is that lipid analog detergents can replace some of the native lipids and interact either transiently or remain bound to the nAChR after reaching the plasma

membrane, as previously suggested by Asmar-Rovira et al. 2008 [1] and outlined in Quesada et al. 2016 [3]. If a detergent remains bound to the nAChR after assembly in the plasma membrane, it is very likely that specific interactions between the detergent and the nAChR might affect specific ion channel properties such as activation and desensitization kinetics that will, in turn, affect the amplitude and decay time of the recorded currents. In addition, residual detergents could have changed the oocyte membrane fluidity, thus affecting the transmembrane domain of the nAChR and as a result influenced the kinetics of the population of the nAChR inserted into the oocyte membrane, as previously described in Baez-Pagan et al. 2016 [22].

#### **4. Mobility Assessment of Detergent Purified nAChR in LCP Using Lipid Analog Detergents**

As mentioned before, a comprehensive characterization of functionality and stability prior to crystallization trials for membranous proteins has become the rule across the laboratories dedicated to membrane protein crystallization. There are countless factors that could influence a successful crystallization process; thus, it is essential to determine the best strategy to follow with a membrane protein crystallization. The use of FRAP in LCP reconstituted proteins, a pre-crystallization assay to select suitable conditions for in meso crystallization of membrane proteins, complemented with PLB and TEVC studies has shown to be a powerful strategy for future nAChR X-ray crystallographic studies. FRAP measurements in LCP, for the nAChR's mobility assessment, were performed using the  $\alpha$ -BTX–Alexa-488 nAChR antagonist to label affinity-purified nAChR in different detergents.

Our FRAP results rule out the possibility that the LCP matrix could not hold the nAChR due to its size, a molecular weight of approximately 290 kDa [23]. Moreover, our results clearly indicated that the LCP matrix could incorporate the nAChR complex because all the samples

assayed showed an adequate mobile fraction. Therefore, it would not be necessary to use a system such as the sponge phase, which is used for the incorporation of large proteins as it provides a larger overall space and better-fitted curvatures for larger proteins.

FRAP curves for the nAChR- $\alpha$ -BTX-Alexa-488 complex in LCP following affinity purification using phospholipid analog detergents (**Figure 14** in the Results section) showed fractional fluorescence recovery ranging 60–87%, with a fast phase of approximately 150 s followed by a slower phase. Data were collected every 0.6 s for the entire experimental period of 500 s. Maximum recoveries were established near the 300 s mark, where FC-16 and LFC-16 were found to have approximately the same value. Interestingly, similar acyl chain lengths demonstrated similar kinetics in the LCP mobility. However, the rate of recovery was different for all lipid-analog detergents assayed, with LFC-16 showing the highest rate of recovery. The diffusion constant obtained for each of the phosphocholine ethers showed a decrease proportional to the length of the acyl carbon chain. This trend suggests possible stabilization of the protein-detergent complexes, as the acyl chain of the detergent increases to the same length of the acyl chain of the mono-olein that composes the LCP matrix. At first glance, this correlation appears to be inappropriate because LFC-16 and FC-16 have the same length in the acyl chain. However, LFC-16 has a sn-1-acylglycerol backbone esterified to a phosphocholine head group; this head group can adopt a different conformation angle in relation to the bilayer plane and has the possibility of establishing ionic interactions with amino acids embedded in the nAChR water-lipid interface. This nAChR interface would not be accessible to other ether analogs, thus increasing nAChR solubility in the LCP matrix. Our FRAP results of nAChR-enriched crude membranes in **Figure 14** in the Results section indicate limited diffusion capacity, which is not surprising since the crude membrane has a significant amount of other integral and membrane-associated proteins that would limit nAChR diffusion.



**Figure 16** in the Results section illustrates the behavior of cholesterol-analog detergents on FRAP measurements using the LCP matrix. The detergents Cholate and CHAPSO have a similar fluorescence recovery rate during the initial 100 s, with slightly different maximum fractional fluorescence values. Big CHAP and CHAPS showed a difference in both the initial rate during the first 100 s and the plateau value of the fractional percentage of fluorescence. The mobile fraction of Big CHAP is approximately half of the mobile fraction of its counterpart cholate, which can be attributed to the polyalcohol functional groups in the head group of Big CHAP. These hydroxyl groups could potentiate hydrogen bonds with other detergent molecules, mono-olein or nAChR amino acids. Such interactions could stabilize nAChR dimers and aggregates and can be responsible for the poor incorporation and slow diffusion of the receptor in the LCP matrix. On the other hand, the negatively charged cholesterol analog cholate showed similar behavior with respect to the FRAP curves and a mobile fraction. Cholate is 85% more efficient at producing nAChR monomer and dimer following affinity column purification [1]. Zwitterionic detergents such as CHAPS and CHAPSO showed mobile fraction values of 71% and 81%, respectively. These values are similar to those obtained for the negatively charged cholate, suggesting that the head-group charge is not a determinant factor in the mobile fraction of the nAChR after affinity column purification with this family of detergents. Interestingly, throughout the cholesterol-analog series, all detergents yielded low amounts of a monomer according to A-SEC results. Despite structural differences between detergents, the mobile fraction is mainly affected by the total lipid composition of the nAChR. As previously reported, the total lipid composition of the affinity-purified nAChR for CHAPS is 45 nmol; for cholate, 47 nmol; and for Big CHAP, 143 nmol [1].

**Figure 19** in the Results section shows two different detergents that contain 8- and 12-carbon aliphatic chains, respectively: OG with a glucopyranoside head group (mobile fraction 76%) and DDM with a maltose head group (mobile fraction 74%). The initial rate of fluorescence recovery during the first 100 s for these detergents is very similar. **Figure 19** in

the Results section, also shows data for LDAO, a 12-alkyl dimethylamine oxide detergent, that yielded a mobile fraction of 83% with a nAChR monomer population of 28% in A-SEC; very similar to that of DDM. Except for OG, which shows a total depletion of the monomer species upon affinity purification in A-SEC, all of these non-lipid-analog detergents have a similar 1:2–1:3 monomer:dimer ratio following purification. In that sense, they present a similar trend to cholesterol-analog detergents, as these showed similar monomer-dimer ratios upon affinity purification. In fact, if we compare the FRAP assays for LFC-16, CHAPS, DDM and OG, they reflect equal diffusion coefficients that are 10 times faster than the other detergents.

These results suggest that despite the aggregation observed in A-SEC and loss of ion channel function in bilayer assays observed for non-lipid-analog detergents, these detergents are capable of diffusion rates on LCP-FRAP that are comparable to some of the rates observed for lipid-analog detergents [1]. The present study provides the first FRAP quantitative measurements for the nAChR in LCP, providing diffusion rates and mobile fractions with different phospholipids- and cholesterol-analog detergents, which can offer guidance for further crystallization trails. Ultimately, decoding the mechanism(s) by which detergents affect the lipid composition, stability and functional state of membrane proteins may lead to the development of novel strategies that would improve the crystallization of membrane proteins.

Our study shows there are remarkable differences in nAChR stability for phospholipid- and cholesterol analog detergents. Phospholipid-analog detergents with 16-carbon chains are more likely to maintain reasonable nAChR function and stability. Results presented herein highlight the importance of determining nAChR function in the LCP matrix since detergent–protein complexes that are nonfunctional in PLB assays yielded highly mobile fractions in LCP-FRAP, and further efforts should be directed toward this goal. Another factor that should be considered is the possibility that the LCP could function as a “filter” for the inclusion of monomeric and exclusion of dimeric protein species into the LCP matrix. These results

provide useful information for the preparation of functionally active nAChR–detergent complexes. An implicit assumption of the results from the detergent-solubilized nAChR with respect to functionality, stability and state of aggregation of the nAChR is that they will be relevant to other important membrane receptor systems, ion channels and membrane proteins.

## **5. LCP Stability Assessment of Detergent Purified nAChR Using Lipid Analog Detergents**

Confocal laser scanning microscopy was used to measure the fluorescence recovery after photobleaching (FRAP) of different preparations of detergent-solubilized nAChR labeled with Alexa  $\alpha$ -BTX in LCP. This approach, introduced by Cherezov et al. 2008 [24], was adapted for its application to the nAChR [2,25] and appears to be a useful technique for the determination of the diffusion coefficient of affinity-purified nAChR using different detergents. As previously mentioned, stability assessment in the LCP has been an essential part of the lipid-based comprehensive approach to crystallize the nAChR from *T. californica*.

In 2011 at least 48 membrane protein structures, from bacteria and mammals, were obtained using LCP technology according to the Protein Data Bank (<http://www.pdb.org>). As of today, near the end of 2018, +200 membrane protein structures are reported to be determined by LCP or other *in meso* technology in the Protein Data Bank. The structures include GPCRs, ion channels, and translocator proteins among several others complex molecules. The success of LCP technology lies on the monoolein amphiphilic properties featuring a polar headgroup and non-polar hydrocarbon chain. However, the LCP should allow the membrane protein to freely diffuse within the three-dimensional cubic phase structure formed by a single connected lipid bilayer [2]. In order to access the stability of the nAChR in LCP, we quantified the diffusion of affinity purified nAChRs solubilized with cholesterol-analog detergents and phospholipid analog detergents for a period of 30 days.

Interestingly, we found that for the cholesterol-analog detergents only CHAPSO and Cholate were able to maintain mobility of a high percentage of receptors during the 30-day testing period. The difference in fractional fluorescence recovery ( $\Delta\text{FFR}$ ) over the 30-day period for CHAPSO was of 0.5 compared to sodium cholate  $\Delta\text{FFR}$  of 0.09. On the other hand, CHAPS and BigCHAP showed substantial instability result; because of a decaying mobile fraction, diffusion coefficients and presents a  $\Delta\text{FFR}$  of 0.32 and 0.22 respectively. It is important to mention that CHAPS was considered an excellent detergent choice for the purification and reconstitution of *T. californica* nAChRs [26]. Moreover, both detergents were shown by our group to reduce the functionality of the nAChR [2]. One possible explanation for the reduced mobility and function was described in Asmar-Rovira et al., 2008 [1], where we found that the amount of residual lipids on purified nAChR is 2-fold greater for a detergent such as BigCHAP versus sodium cholate. Interestingly, we have shown that sodium cholate is able to maintain both mobility and function of the nAChR [27], suggesting that this excess of residual lipids might change the biophysical properties of the LCP resulting in changes to the nAChR molecules. Although Cholate and CHAPSO were able to sustain nAChR stability in more than 70% of the nAChR population, a highly desirable biophysical property when in meso crystallization is used; these detergents produced a non-desirable aggregation state [2], and CHAPSO failed to sustain nAChR functionality. Although Cholate was able to maintain nAChR functionality, previous crystallization trials in our laboratory showed that this detergent crystallizes under acid conditions [1]. Although these cholesterol-analog detergents are highly homologous, they have different functional groups (**Table 1** in the Results section) and consequently different physicochemical characteristics which are likely to provide unique forms of interactions with the protein nAChR and the LCP.

FRAP curves for the nAChR- $\alpha$ BTX-Alexa-488 complex in LCP (**Figure 22** in the Results section) for the FC detergent family showed a maximum fractional fluorescence recovery near 90% with a  $\Delta\text{FFR}$  of less than 0.07, only for the sixteen-saturated carbon chain (FC-16). The

fourteen-carbon FC (FC-14) presented more disperse FRAP curves with a maximum fluorescence recovery of 62% and a  $\Delta\text{FFR}$  of 0.16. The twelve-carbon version of FC (FC-12) showed a more unstable MFs pattern with a dispersed curve ranging from 79% on day 1 to 42% on day 5 and finally increased again to 60% on day 30. This behavior could be explained in terms of the short chain of FC-12 and even FC-14 with a relatively small head-group that enables these detergents to increase the number of molecules that can interact with the hydrophobic surface of the nAChRs transmembrane domain. The alkyl chain of such detergents forms a belt-like arrangement around the hydrophobic nAChR residues and exposes the polar head-group to the aqueous environment. This kind of interaction could promote nAChR stabilization and increase its incorporation into lipid bilayer, but the interaction of the nAChR detergent complex with the LCP integral monoolein molecule could be decreased. This behavior was observed for the FC-12 in terms of the response evoked by ACh on oocytes injected with affinity purified nAChR detergent complex. Increasing the chain length in the FC family decreased or eliminated the activity of the nAChR (**Figure 10** in the Results section). These LCP-FRAP results suggest that small structural differences between different detergents can cause remarkable differences in the stability of the protein-detergent complex (**Figure 22-23** in the Results section). It is important to notice that FC-12 shows varieties in terms of diffusion coefficient between days changing its values from  $10^{-8}$  to  $10^{-9}$ . This behavior can explain the difference between the first day of FRAP in this report compared to Padilla et al. 2011 [2]. The FC-12 detergent is very efficient during the solubilization process and is able to produce a high amount of purified protein. However some proteins tend to aggregate in its presence [28]. These nAChR-FC-12 complex aggregates have been previously confirmed in our laboratory [1]. The FRAP behavior for phospholipid like detergents such as the LFC family is more consistent (**Figure 24-25** in the Results section). Increasing the hydrophobic chain length of LFC detergents linearly improves the fractional fluorescence recovery for the 30-day period assayed, but also reduced the variability between days. LFC-

16 produced a maximum recovery of almost 90% with a  $\Delta\text{FFR}$  of 0.08. The two-carbon difference of LFC-14 attained the maximum fractional fluorescence recovery at 64% with a  $\Delta\text{FFR}$  of 0.06. LFC-12 only presents a maximum recovery at 44% with a  $\Delta\text{FFR}$  of 0.13. The functional assays showed a difference between stability and function regarding the length of the acyl chain (**Figure 24-25** in the Results section). In the LFC family of detergents, we observed that the longer acyl chains sustain the highest levels of functionality, with LFC-14 and LFC-16 displaying macroscopic responses similar to the crude membranes suggesting that the conformation of the channel appears to be almost intact. In contrast, the shorter acyl chain LFC-12 produced a dramatic reduction in nAChR channel function. On the other hand, in the FC family, only the shorter FC-12 was able to sustain unusual ion channel function (lacking fast activation) whereas longer acyl chain containing FC-14 and FC-16 showed a significant reduction in function. If the hydrophobic part of an amphiphilic molecule is the only parameter dictating the physicochemical factors that govern its interaction with a hydrophobic region of another molecule, one might expect that LFC-12 could support the same activity as FC-12; however, that was not the case for this particular detergent. The protein–detergent interaction greatly depends on the amphiphilic nature of the detergent, in other words, the size, electric charge, and polarity of the headgroup as well as the magnitude, flexibility, and shape of the hydrophobic part of the molecule [29,30].

The observed differences between LFCs and FCs detergents could be attributed to the esterified sn-1-acylglycerol as well as the phosphocholine part of the LFCs head-groups. The head-groups of LFCs provide greater stability compared to the head-groups of FCs; it should be noted that LFCs head-groups are more likely to mimic the stabilizing interactions that native-like phosphatidylcholine residues contribute to the nAChR, as previously observed [31]. LCP-FRAP experiments demonstrated that the C12 acyl chain produces the least stable nAChR-DCs for both detergent families; the LFC-12 nAChR-DC (mobile fraction < 0.5) was less stable than the FC12 nAChR-DC (mobile fraction <0.7). Based on these results and

previous observations [31], we suggest that FC12 has a reduced affinity for the nAChR due to the lack of a head-group. Therefore, this detergent could be partially washed from the nAChR-DCs before reaching the plasma membrane. The presence of a head-group in LFC-12 could increase its affinity for the nAChR, leading to more unstable nAChR-DCs with less possibility of removing the C12 acyl chain before reaching the plasma membrane.

Once the nAChR-DCs interact with the membranous like environment, the complexes are able to move freely through the entire network [32,33]. Diffusion across the membranous environment depends on different factors that dictate the mixability of the nAChR-DCs. During mixing the protein-detergent complexes, including the residual native lipids and monoolein, melt and dissolve forming the cubic phase Pn3m monoolein. The Pn3m phase is derived from the proportion of lipid to water mixture. The process of mixing depends on the similarity of the lipid components (detergent-monoolein) and the capacity of the Pn3m to overcome the lipid-protein hydrophobic mismatch [34,35]. Integral proteins are characterized by a specific hydrophobic length along with a natural membrane lipid bilayer thickness [36], that provides a unique environment for stability and functionality. The solubilization of membrane proteins with detergents and reconstitution into other lipid environments can induce an energetically unfavorable hydrophobic mismatch that could affect the native protein conformation and consequently its stability and functional activity. Perhaps the identity of residual lipids could be crucial to sustain the desirable confirmation that would maintain functionality and stability after insertion into the LCP. It is well known that certain lipids and detergents could influence the nAChR functionality. Moreover there are membrane components such as cholesterol, that have shown to modulate ion channel function. It is possible that residual lipids can not only sustain the nAChR conformation that ensures ion channel functionality and stability but could also have a specific binding characteristic that could be considered irreversible. This interpretation is aligned with previous findings by [34,35].

Taking into consideration these requirements, it is not surprising that LFC-16 glycerol phosphocholine head-group moiety confers superior lipid-lipid interactions and mixability with the Pn3m monoolein than FC-12. In addition, different independent studies with membrane proteins such as ion channels, ion pumps, and sugar transporters demonstrated the requirement of acyl chain length to obtain maximum activity [34,37,38,39].

Interestingly, the acyl chain length for optimal functionality of these membrane proteins ranges from 16 to 18 carbon chain. Overall, the present study demonstrates that the nAChR-LFC16 complex is an excellent candidate to be used in LCP crystallization trials and to assess new technologies developed for membrane protein crystallization. Another fundamental aspect that remains to be elucidated is the possibility that the structural basis for the functionality and stability of some of these nAChR-DCs is merely determined by their lipid composition. Recent findings have shown that the lipid environment essential to sustain stability and promote nucleation during crystallization trials of membranous proteins. Such findings support LCP as a tool for membrane protein crystallization as it is based in a lipid-based approach to providing the ideal conditions for membrane protein crystallization.

## **6. Vapor Diffusion Crystallization of Detergent Purified nAChR Using Lipid Analog Detergents**

Several techniques are available for the crystallization of membrane proteins, including the recently developed lipidic cubic phase [40,41], bicelle [42], and vesicle fusion [43] methods. Nevertheless, vapor diffusion is the most common and successful method for membrane protein crystallization. To date, this approach has allowed researchers to determine the crystal structures of several membrane proteins. Even though when compared with a lipid-based matrix the vapor diffusion technique lacks the appropriate stability characteristics, a well performed lipid-based approach such as the use of lipid analog detergents might be ideal for



the crystallization of the nAChR. Examples of successful lipid-based crystallizations are the inner membrane efflux pumps CusA [44], AcrB [45], and MtrD [46], the outer membrane channels CusC [47], MtrE [48] and CmeC [49], as well as the CusBA adaptor-transporter efflux complex [50].

The difference between vapor diffusion crystallization of soluble proteins and membrane proteins is that detergents are essential for membrane protein crystallization using vapor diffusion techniques; detergents sustain membrane protein stability during nucleation. While protein-protein interactions dominate the crystallization of soluble proteins, both detergent-detergent and protein-detergent interactions are additional considerations for the membrane protein crystallographer. Unlike crystallization of water-soluble proteins, choosing the right detergent has been key for the success of our membrane protein crystallization efforts. According to our findings, the detergent selection is the most important factor for obtaining high-quality membrane protein crystals suitable for X-ray diffraction. Thus, emphasis should be on the screening a variety of mild detergents rather than in the optimization of other parameters when crystallizing a new membrane protein.

In a simple crystallization experiment a precipitant solution, containing at least buffer, precipitant, and salt components, is mixed with a protein solution containing the purified protein-detergent complexes; forcing the protein solution into a state of supersaturation. After reaching supersaturation, the protein-detergent complex has two routes: 1) aggregation and 2) nucleation (crystallization). If the crystallization solution is not too harsh and the protein-detergent complex has enough time to make specific interactions with its neighbors, nucleation takes place. In general, a slow introduction of the crystallization solution to the protein-detergent complex facilitates this, resulting in larger crystals with fewer imperfections [50].

During the past 10 years, our laboratory has followed a comprehensive lipid-based approach to understand the nature of nAChR stability [1,2,3]. A vast amount of data and years

of membrane protein crystallization research have contributed to the recent identification of the detergents that sustain the appropriate conditions to generate membrane protein crystals from functional nAChR from *T. californica*. Our data is aligned with previous studies which determine that detergents are essential to sustain membrane protein stability during nucleation when using vapor diffusion as the crystallization technique. In our study, we emphasize the use of detergents that maintain ion channel functionality as well as lower levels of aggregation. Our strategy seeks to ensure that nAChR crystallization will be executed using the nAChR-detergent complex that supports ion channel functionality. Therefore, the outcome of this crystallization experiments would have been a nAChR structure that emerges from the nucleation of functional ion channel receptors.

Moreover, the use of detergents with the capability of sustaining ion channel stability is highly desirable when using vapor diffusion techniques. The nucleation mechanism that generates protein crystals in this technique is one in which a single seed arrangement is formed, and the reticle grows slowly through long periods of time into a protein crystal. Thus, a long-lasting, stable environment is essential for nucleation when using vapor diffusion. Our results demonstrate that it is possible to generate protein nucleation of detergent-purified nAChR when using vapor diffusions crystallization techniques such as Hanging Drop and Sitting Drop. Previously analyzed data support that detergents LFC-16 and FC-16 are more adequate to perform crystallization trials. This is based on their highest levels of monomeric protein as well as the currents observed during the lipid planar bilayer. Even though the macroscopic currents for FC-16 were not comparable with the injection of crude membranes into oocytes, the stability that FC-16 provided during aggregation is highly desirable for this type of crystallization trials. As described by Parker and Newstead 2016, protein endurance during continuously variable crystallization conditions is essential for nucleation.

Only 0.83% of the complete round of trials produced amorphous nucleation of proteins, resulting in non-diffractive crystals; only condition in **Table 2** in the Results section, showed

nucleation. The salt, pH, and crystallant used in these conditions are comparable with the recently determined structures of the nAChR  $\alpha 4\beta 2$  [8], the GuCl [51], and GLIC ion channel [52], ELIC [53], among others using Hanging Drop. Lower pH ( $\leq 6.5$ ) within the crystallization conditions is consistent across the pentameric ion channel receptors structures determined in the last decade. The use of sodium ( $\text{Na}^+$ ) as a positive ion has also been consistent across such structures. Moreover, even though different crystallants or precipitant agents have been used for the determination of recent membrane protein structures, the concentration of crystallant agent has always been relatively high  $\geq 15\%$ . The use of lower pH and sodium ion might be critical to generate nucleation in this type of proteins. Both lower pH and sodium ions could be contributing to protein stabilization by lowering the free energy of the dynamic domains such as the binding sites or the ion channel vestibule before the ion pore, a structure common among these types of receptors [51-54]. This is consistent with the significant amount of water (solvent) found within the vestibule and the ion pore in several determined structures. Nevertheless, a comprehensive study will be required to determine if the contribution of sodium ion and the lower pH are in fact essential. Considering the nAChRs structure, with both a hydrophilic and hydrophobic domains exposed, as well as a significantly large size protein with a large dynamic body in comparison with other globular proteins, nucleation will require a substantial amount of stabilization. Our experiments have confirmed that nucleation can be achieved by Hanging Drop. However, according to our findings, additional stabilization will be required to produce quality diffractive crystals.

## **7. Lipidic Cubic Phase Crystallization of Detergent Purified nAChR Using Lipid Analog Detergents**

As of today, more than +200 records in the Protein Data Bank are associated with *in meso* crystallogensis. This fact provides evidence of booming popularity this method has gained

among crystallographers and biomolecular scientists [55]. The essence of this crystallization method relies on the stability of the host membrane protein provided by the lipid matrix. Thus, the LCP is ideal for the crystallization of membrane proteins, especially complex structures such as the nAChR [56].

The method procedure can be basically described as follows: an isolated biological membrane is treated with detergent, just like our approach using crude membranes from *T. californica*, to solubilize the desired protein. The protein-detergent complex, in a mixed micelle form, is then purified by standard wet-laboratory biochemical methods; we are using affinity purification, one of the most robust and efficient methods to purify any kind of protein. Homogenizing with a monoolein lipid effects a uniform reconstitution of the purified protein into the cubic phase bilayer; this creates a bicontinuous lipid matrix in the sense that both the aqueous and bilayer compartments are continuous in three dimensions (**Figure 1**). Upon reconstitution, the protein ideally retains its native conformation and activity and has complete mobility within the plane of the cubic phase bilayer. A precipitant is added to the mesophase, which triggers a local alteration in mesophase properties that include phase identity, microstructure, long-range order and phase separation. Under conditions leading to crystallization, one of the separated phases is enriched in protein, which supports nucleation and progression to a bulk crystal. This phase has been described as a local lamellar phase that acts as a medium in which nucleation and three-dimensional crystal growth occurs (**Figure 1**).

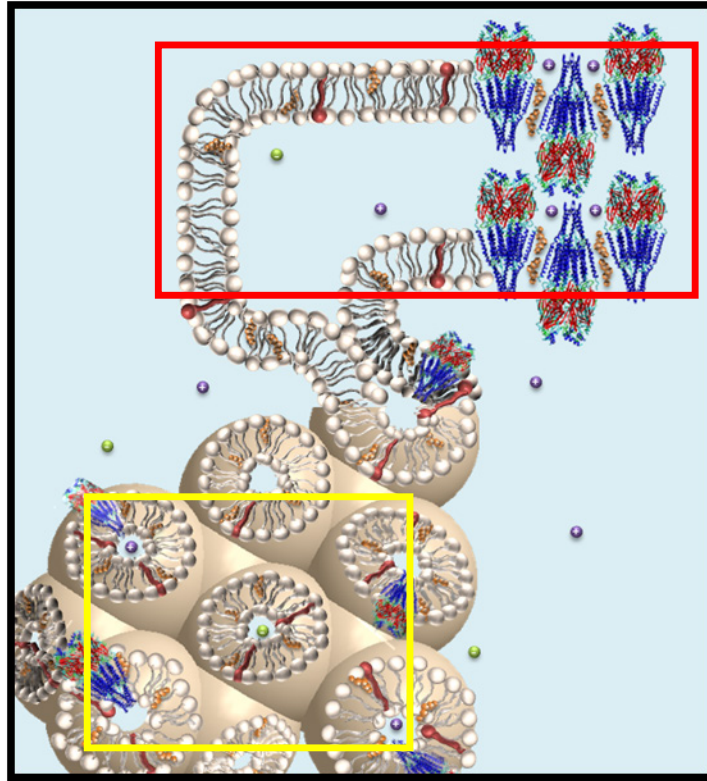


**Figure 1:** A bicontinuous lipid matrix. The main role of the matrix is to retain the stability of reconstituted proteins (yellow box). Upon addition of the crystallization conditions, a local alteration in the mesophase properties is triggered that includes phase identity, microstructure, long-range order and phase separation (red box). This separate phase is enriched in protein and promotes nucleation.

Results showed it is possible to generate low-quality crystals of the *T. californica* nAChR using LCP as an in meso crystallization. Nevertheless, additional stabilization might be required to improve crystal development and quality. Purification using lipid analog detergents has been shown to provide high stability in the LCP, and the LCP bicontinuous lipid matrix has provided stability required to promote nAChR nucleation and subsequent bulk crystal development. The consistency of crystal development was 34%, indicating there are other external factors influencing nAChR dynamics. Incubation with Alexa-488- $\alpha$ BTx contributes to nAChR stabilization by regulating its dynamics, restricting the nAChR into a single inactive conformation as a result of  $\alpha$ BTx antagonist binding. However, there might be other domains not stabilized by  $\alpha$ BTx binding that supersede the stabilization required to achieved uniform nucleation and a subsequent high-quality bulk crystal. Other interventions might be necessary to achieve stabilization of these domains. Modification of the peptide sequence is commonly used to achieve protein stabilization even when using LCP as a crystallization matrix. For example, crystallization of the voltage-gated ion channel KvLm in the LCP required the mutation of a single residue to promote a stationary closed conformation [57]; without this mutation, the ion channel lacked the stabilization necessary for nucleation. Other proteins crystallized in LCP required significant modifications to achieve the protein stabilization necessary for nucleation and bulk crystal formation; the GPCRs Adenosine receptor A<sub>2A</sub> and Adrenergic receptor  $\beta$ <sub>2</sub>AR required significant mutagenesis along the peptide sequence, but more importantly the substitution of an internal loop with an entire exogenous peptide, a lysozyme protein [58,59]. Such modifications in combination with the stabilization provided by the LCP were fundamental for the nucleation of these proteins. It is possible that like these proteins, the nAChR requires additional stabilization mechanisms to ensure that the receptor will a adopt the appropriate conformation and to reduce dynamic movement as much as possible. Perhaps there are alternative non-invasive approaches to reduce protein dynamics and provide the appropriate stabilized conditions to achieve high-resolution crystals. Protein

concentration analysis using nanodrop and fluorescent microscopy through fluorescence obtained from Alexa-488 were used to positively identify protein crystals (**Figure 27** in the Results section)

The nAChR crystals obtained in the LCP range from 5 $\mu$ m to 15 $\mu$ m sizes that are comparable with those seen in the literature as membrane protein crystals generated in LCP have been reported to be under 20 $\mu$ m in size (Cherezov 2009 rastering). The small size of the protein crystals is mostly attributed to the mechanism of nucleation, vapor diffusion techniques allow for high diffusion of proteins, while proteins in the LCP pass through a complex diffusing mechanism involving a change in the lipid phase; thus the supply of proteins is limited to grow a bigger crystal [60]. Because of size, during the diffraction experiments at the Argonne National Laboratory, the use of the raster software was required to identify nAChR protein crystals on the micro crystal mounts. Even though the raster software was able to detect high levels of fluorescence in specific areas around the micro crystal mounts, no significant diffraction patterns were observed; indicating that nAChR crystals developed under the LCP are low quality, lack uniformity and there is no properly defined unit cell. Although crystallization conditions seem to be appropriate, there are still improving grounds in terms of stability. A single conformational state could be required to improve crystal size and quality.

## **8. Lipidic Cubic Phase Crystallization of Detergent Purified nAChR Using Lipid Analog Detergents Applying Electric Potential**

The nAChR is a transmembrane ion channel receptor that facilitates the transport of ions across the cell membrane. The protein has a transmembrane domain (hydrophobic) and extracellular/intracellular domains (hydrophilic). These characteristics make the nAChR and other transmembrane proteins unique when it comes to solubilization and crystallization. For

decades the standard procedure for nAChR purification has required detergents to successfully ensure protein stability while in aqueous solution [1], to perform crystallization experiments subsequently. LCP has recently become the technique of choice for and the production of transmembrane protein structures because it can provide suitable conditions in which transmembrane proteins can engage nucleation while the transmembrane domain remains inserted in a membranous environment. This feature substantially stabilizes the membrane protein, allowing it to endure the nucleation process extended periods. Nevertheless, proteins that are significantly large or highly dynamic could require additional effectors that would increase protein stabilization. Several groups have decided to perform molecular engineering to alternate the protein sequence or eliminate protein loops to reduce protein dynamics. However effective, these procedures could modify the native state of the protein resulting in a non-native conformation that could lead to inappropriate conclusions about the protein mechanistic actions.

Our group has identified a noninvasive strategy to stabilize the nAChR that restricts protein dynamics by applying a very low voltage to the nAChR enriched-LCP media. The rationale behind these strategies is that the nAChR possess domains that are sensitive to voltage. Thus, when a certain voltage is applied, the nAChR favors a specific conformation which minimizes receptor dynamics and constraints all receptors in the LCP media into a single conformation. This characteristic of the nAChR has been known for decades and has been confirmed by experiments that demonstrate how binding of the nAChR to ligands such as Spermine is influenced by voltage. Ligand binding dependency on voltage is due to voltage-dependent conformational changes. When a voltage potential is applied, certain nAChR domains that are sensitive to voltage exposure are capable of regulating protein conformation and allow the protein to favor spacial arrangements that affect ligand binding. When Spermine binds to the nAChRa conformational change that supports nAChR inward rectification is induced in neurons; a study showed that the binding of this ligand is affected by the membrane



depolarization potential. Thus, inward rectification of the nAChR in neuronal membranes is regulated by membrane depolarization potential [61]. In addition, experimental evidence supports that nAChR inward rectification is dependent on the degree of membrane depolarization potential regardless of nAChR expression in neurons or in non-neuronal cells. This observation further supports the ability of nAChRs to adopt specific voltage potential-dependent conformations.

Our group has taken advantage of the nAChR voltage potential dependency to enhance its stabilization during nucleation in the LCP. Results showed that the voltage application increases the probability of obtaining protein crystals by 49% (**Figure 2**). Under LCP conditions (no voltage potential applied) 1 out of 3 experiments achieved nucleation, whereas under voltage potential exposure 8 out 10 experiments produced nucleation. The stabilization provided by nAChR voltage-dependent domains could be promoting crystal formation as it is well understood that protein nucleation during crystallization trials is highly dependent on the homogeneity of protein conformation. Thus, protein nucleation could be promoted by controlling nAChR conformation through nAChR voltage-dependent domain stabilization. Under voltage potential, the nAChR pool could be arranged together with ease because of a homogeneous distribution of conformation. Such behavior is aligned with the application of voltage potential for the crystallization of globular proteins [62].

Nucleation under voltage applied potential seems to be achieved more rapidly. For example, nucleation in LCP took between 3 and 5 days; however, for LCP experiments under voltage well developed crystals were observed in 24 hours. There is a statistically significant decrease in the elapse time to observed nucleation when using voltage potential application, demonstrating that voltage application could, in fact, reduce the time in which nAChR crystals are expected to form in the LCP matrix (**Figure 2**). Nucleation or crystal generation is highly dependent on protein conformation and dynamics. During crystallization, proteins interact between each other in a specific manner; this interaction is highly dependent on conformation.

Thus a heterogeneous mixture of proteins conformations is less likely to form crystals. Perhaps voltage application could be leveling the amount of energy in the system and normalizing the conformation through the voltage-dependent domains within the protein. This type of behavior was observed while performing bilayer electrophysiological experiments. While the nAChR was in the bilayer membrane, the voltage was applied and carbamoyl choline (Carb) to stimulate single channel openings. However, after a reduction of the ion channel activity, the polarity of the voltage potential was a switch to stimulate the nAChR to release the ligands and resume its active state. This characteristic is the result of voltage-dependent domains that respond to the voltage applied potential changing the nAChR and the binding affinity. This behavior is also consistent with the previously mentioned study where Spermine binding was shown to be influenced by voltage potential. Stabilization of the nAChR through voltage potential application might be regulating the nAChR protein pool of conformations and inducing faster nucleation.

During nAChR crystallization trials, differences in crystal size were noticed. nAChR crystals grown in the LCP were smaller in average than those grown under LCP with voltage applied potential (**Figure 2**). As discussed earlier the voltage applied potential might be stabilizing the nAChR conformations allowing crystal formation to occur more rapidly. Is possible that this same effect might be contributing to crystal growth as well. Voltage application during crystallization of globular proteins has shown to promote the development of larger protein crystals [62]. The basis for this behavior is derived from the same principle, voltage-dependent domains will contribute to protein stabilization, and as a result, allow for greater size and quality of crystals. There is, however, another significant characteristic that could be contributing to nAChR crystal size under applied voltage potential. It is known that the LCP, gels and other highly dense medias used to grow protein crystals are substantially restrictive in terms of protein diffusion. The application of voltage potential to the LCP might be increasing the permeability of the media allowing higher levels of nAChR diffusion. The higher

level of nAChR diffusion coupled with the stabilization provided by controlling the nAChR conformation could be key factors contributing to the development of bigger nAChR crystals when the voltage potential is applied.

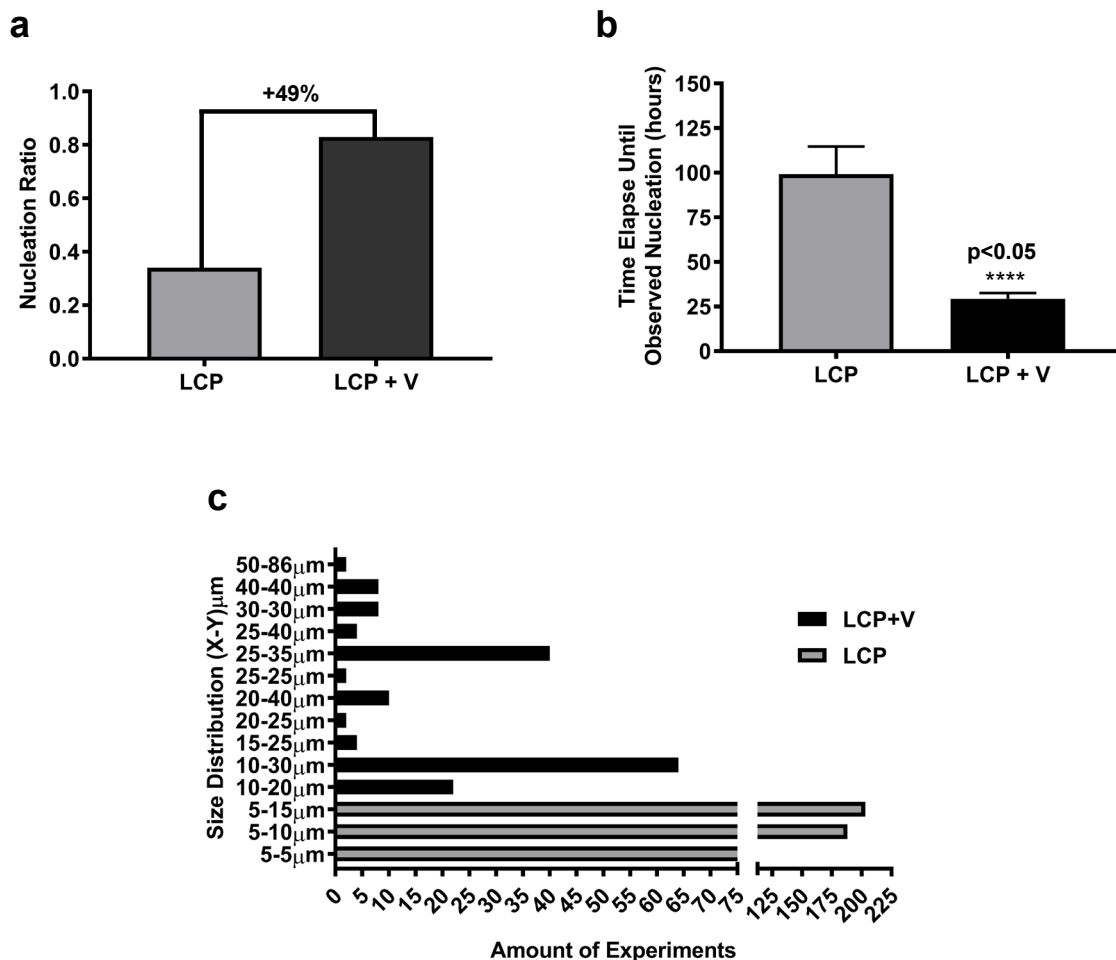


**Figure 2:** LCP and LCP with Voltage potential (LCP + V) crystallization conditions were compared (a). The nucleation ratio for LCP was ~33%, where full crystal development was observed for LCP + voltage potential setup. A 49% increase of crystal development consistency was observed when comparing the two techniques. Time elapse for nucleation was also analyzed (b). Time elapse for nucleation for LCP + V was significantly ( $p < 0.05$ ) lower than the observed nucleation in the LCP in the absence of voltage potential. This indicates that the applied voltage could provide stabilization to promote nucleation. Crystal size was also compared between the two techniques (c); this graph shows the size distribution of crystals developed in LCP and LCP + V. LCP + V seems to generate bigger crystals than LCP.

## Discussion References

1. Asmar-Rovira, G. A. et al. "Biophysical and Ion Channel Functional Characterization of the *Torpedo californica* Nicotinic Acetylcholine Receptor in Varying Detergent–Lipid Environments" *J Membrane Biol* vol. 223, 1 (2008): 13–26.
2. Padilla-Morales, L. F. et al. "Effects of lipid-analog detergent solubilization on the functionality and lipidic cubic phase mobility of the *Torpedo californica* nicotinic acetylcholine receptor" *J Membrane Biol* vol. 243 (2011): 47–58.
3. Quesada, O. et al. "Uncovering the lipidic basis for the preparation of functional nicotinic acetylcholine receptor detergent complexes for structural studies" *Scientific Reports: Nature* vol. 6 (2016): 32766.
4. Schindler, H. et al. "Functional acetylcholine receptor from *Torpedo marmorata* in planar membranes" *Proc Natl Acad Sci USA* vol. 77 (1980): 3052–3056.
5. Nelson, N. et al. "Reconstitution of purified acetylcholine receptors with functional ion channels in planar lipid bilayers" *Proc Natl Acad Sci USA* vol. 77 (1980): 3057–3061.
6. Boheim, G. et al. "Agonist-activated ionic channels in acetylcholine receptor reconstituted into planar lipid bilayers" *Proc Natl Acad Sci USA* vol. 78 (1981): 3586–3590.
7. Hassaine, G. et al. "X-ray structure of the mouse serotonin 5-HT<sub>3</sub> receptor" *Nature* vol. 512, 7514 (2014): 276–281.
8. Morales-Perez, C. L. et al. "X-ray structure of the human  $\alpha 4\beta 2$  nicotinic receptor" *Nature* vol. 538 (2016): 411–415.
9. Cherezov, V. et al. "High-resolution crystal structure of an engineered human beta<sub>2</sub>-adrenergic G protein-coupled receptor" *Science* vol. 318 (2007): 1258-1265

10. Marsal, J. et al. "Incorporation of acetylcholine receptors and Cl-channels in *Xenopus* oocytes injected with Torpedo electroplaque membranes" *Proc. Natl. Acad. Sci. U.S.A.* vol. 92 (1995): 5224–5228.
11. Santiago, J. et al. "Tryptophan scanning mutagenesis in the TM3 domain of the Torpedo californica acetylcholine receptor beta subunit reveals an alpha-helical structure" *Biochemistry* vol. 43 (2004): 10064–10070.
12. Caballero-Rivera, D. et al. "Tryptophan scanning mutagenesis reveals distortions in the helical structure of the  $\delta$ M4 transmembrane domain of the Torpedo californica nicotinic acetylcholine receptor" *Channels* vol. 6 (2012): 111–123.
13. Ortiz-Acevedo, A. A. et al. "Tryptophan scanning mutagenesis of the gammaM4 transmembrane domain of the acetylcholine receptor from Torpedo californica" *J. Biol. Chem.* vol. 279 (2004): 42250–42257.
14. Lasalde, J. A. et al. "Tryptophan substitutions at the lipid-exposed transmembrane segment M4 of Torpedo californica acetylcholine receptor govern channel gating" *Biochemistry* vol. 35 (1996): 14139–14148.
15. Lee, Y. H. et al. "Mutations in the M4 domain of Torpedo californica acetylcholine receptor dramatically alter ion channel function" *Biophys. J.* vol. 66 (1994): 646–653.
16. Ortiz-Miranda, S.I. et al. "Mutations in the M4 domain of the Torpedo californica nicotinic acetylcholine receptor alter channel opening and closing" *J. Membr. Biol.* vol. 158 (1997): 17–30.
17. Santiago, J. et al. "Probing the effects of membrane cholesterol in the Torpedo californica acetylcholine receptor and the novel lipid-exposed mutation alpha C418W in *Xenopus* oocytes" *J. Biol. Chem.* vol. 276 (2001): 46523–46532.
18. Tamamizu, S. et al. "Functional effects of periodic tryptophan substitutions in the alpha M4 transmembrane domain of the Torpedo californica nicotinic acetylcholine receptor" *Biochemistry* vol. 39 (2000): 4666–4673.

19. Caballero-Rivera, D. et al. "Fourier transform coupled tryptophan scanning mutagenesis identifies a bending point on the lipid-exposed  $\delta$ M3 transmembrane domain of the *Torpedo californica* nicotinic acetylcholine receptor" *Channels* vol. 5 (2011): 345–356.
20. Cruz-Martín, J. L. et al. "Tryptophan substitutions at lipid-exposed positions of the gamma M3 transmembrane domain increase the macroscopic ionic current response of the *Torpedo californica* nicotinic acetylcholine receptor" *J. Membr. Biol.* vol. 183 (2001): 61–70.
21. Guzmán, G. R. et al. "Tryptophan scanning mutagenesis in the alphaM3 transmembrane domain of the *Torpedo californica* acetylcholine receptor: functional and structural implications" *Biochemistry* vol. 42 (2003): 12243–12250.
22. Báez-Pagán, C.A. et al. "Heterogeneous Inhibition in Macroscopic Current Responses of Four Nicotinic Acetylcholine Receptor Subtypes by Cholesterol Enrichment" *J Membr Biol.* vol. 249, 4 (2016): 539-549.
23. Unwin, N. Refined structure of the nicotinic acetylcholine receptor at 4Å resolution" *J. Mol. Biol.* vol. 346 (2005): 967–989.
24. Cherezov, V. et al. "LCP-FRAP assay for prescreening membrane proteins for in meso crystallization" *Cryst. Growth Des.* vol. 8 (2008): 4307–4315.
25. Liu, W. et al. "Crystallization of Membrane Proteins in Lipidic Mesophases" *J. Vis. Exp.* vol. 49, 2011: 2501.
26. Schürholz, T. et al. "Functional reconstitution of the nicotinic acetylcholine receptor by CHAPS dialysis depends on the concentrations of salt, lipid, and protein" *Biochemistry* vol. 31 (1992): 5067–5077.
27. Fong, T. M. et al. "Correlation between acetylcholine receptor function and structural properties of membranes" *Biochemistry* vol 25 (1996): 830–840.

28. Matar-Merheb, R. et al. "Structuring detergents for extracting and stabilizing functional membrane proteins" *PLoS One* vol. 6 (2011): 18036.
29. Privé, G. G. et al. "Detergents for the stabilization and crystallization of membrane proteins" *Methods* vol. 41 (2007): 388–397.
30. Seddon, A. M. et al. "Membrane proteins, lipids and detergents: not just a soap opera" *Biochim. Biophys. Acta* vol. 1666 (2004): 105–117.
31. Sunshine, C. et al. "Lipid modulation of nicotinic acetylcholine receptor function: the role of neutral and negatively charged lipids" *Biochim. Biophys. Acta* vol. 1108 (1992): 240–246.
32. Nollert, P. et al. "Molecular mechanism for the crystallization of bacteriorhodopsin in lipidic cubic phases" *FEBS Lett.* vol. 504 (2001): 179–186.
33. Wallace, E. et al. "Monoolein lipid phases as incorporation and enrichment materials for membrane protein Crystallization" *PLoS One* vol. 6 (2011): 24488.
34. Jensen, M. O. et al. "Lipids do influence protein function-the hydrophobic matching hypothesis revisited" *Biochim. Biophys. Acta* vol. 1666 (2004): 205–226.
35. Marsh, D. et al. "Energetics of hydrophobic matching in lipid-protein interactions" *Biophys. J.* vol. 94 (2008): 3996–4013.
36. Tanford, C. "The Hydrophobic Effect: Formation of Micelles and Biological Membranes" *John Wiley & Sons Inc., New York* vol. 1 (1973): 1.
37. Cornelius, F. "Modulation of Na, K-ATPase and Na-ATPase activity by phospholipids and cholesterol. I. Steady-state kinetics" *Biochemistry* vol. 40 (2001): 8842–8851.
38. Dumas, F. "Consequences of hydrophobic mismatch between lipids and melibiose permease on melibiose transport" *Biochemistry* vol. 39 (2000): 4846–4854.
39. Lee, A. G. "How lipids and proteins interact in a membrane: a molecular approach" *Mol. BioSyst.* vol. 1 (2005): 203–212.



40. Landau, E.M. et al. "Lipidic cubic phases: a novel concept for the crystallization of membrane proteins" *Proc Natl Aca. Scie. USA*. vol. 93, 25 (1996):14532–14535.
41. Nollert, P. et al. "Crystallization of membrane proteins in cubo" *Methods in Enzymology*. vol. 343 (2002):183–199.
42. Faham, S. et al. "Bicelle crystallization: a new method for crystallizing membrane proteins yields a monomeric bacteriorhodopsin structure" *Journal of Molecular Biology* vol. 316, 1 (2002): 1 – 6.
43. Takeda, K. et al. "A novel three-dimensional crystal of bacteriorhodopsin obtained by successive fusion of the vesicular assemblies" *Journal of Molecular Biology* vol. 283, 2 (1998): 463–474.
44. Long, F. et al. "Crystal structures of the CusA efflux pump suggest methionine-mediated metal transport" *Nature* vol. 467, 7314 (2010): 484–488.
45. Su, C. et al. "Conformation of the AcrB multidrug efflux pump in mutants of the putative proton relay pathway" *Journal of Bacteriology*. vol. 188, 20 (2006): 7290–7296.
46. Bolla, J. R. et al. "Crystal structure of the *Neisseria gonorrhoeae* MtrD inner membrane multidrug efflux pump" *PLoS ONE* vol. 9, 6 (2014): 97903.
47. Lei, H. et al. "Crystal structures of CusC reveal conformational changes accompanying folding and transmembrane channel formation" *Journal of Molecular Biology* vol. 426, 2 (2014): 403 - 411.
48. Lei, H. et al. "Crystal structure of the open state of the *Neisseria gonorrhoeae* MtrE outer membrane channel" *PLoS ONE* vol. 9 (2014): 97475.
49. Su, C. et al. "Crystal structure of the *Campylobacter jejuni* CmeC outer membrane channel" *Protein Science* vol. 23, 7 (2014): 954–961.
50. Su, C. et al. "Crystal structure of the CusBA heavy-metal efflux complex of *Escherichia coli*" *Nature* vol. 470, 7335 (2011): 558–562.

51. Althoff, T. "X-ray structures of GluCl in apo states reveal a gating mechanism of Cys-loop receptors" *Nature* vol. 512, 7514 (2014): 333–337.
52. Bocquet, N. et al. "X-ray structure of a pentameric ligand-gated ion channel in an apparently open conformation" *Nature* vol. 457, 7225 (2009): 111–114.
53. Hilf, R. J. et al "X-ray structure of a prokaryotic pentameric ligand-gated ion channel" *Nature* vol. 452, 7185 (2008): 375–379.
54. Benvenuti, M. et al. "Crystallization of soluble proteins in vapor diffusion for x-ray crystallography" *Nature Protocols*. vol. 2, 7 (2007): 1633–1651.
55. Berman, H. M. et al. "Announcing the Worldwide Protein Data Bank (2003). *Nature Struct. Biol.* vol. 10 (2003): 1203 – 980.
56. Caffrey, M. et al. "A comprehensive review of the lipid cubic phase or in meso method for crystallizing membrane and soluble proteins and complexes" *Acta Crystallographica Section F, Structural Biology Communications*. Vol. 71 (2015): 3 - 18.
57. Santos, J. S. et al. "Crystal structure of a voltage-gated K<sup>+</sup> channel pore module in a closed state in lipid membranes" *J Biol Chem* vol. 287 (2012): 43063 – 43070.
58. Gutierrez-de-Teran, H. et al. "The role of a sodium ion binding site in the allosteric modulation of the A2A adenosine G Protein-Coupled Receptor" *Structure* vol. 21 (2013): 2175-2185.
59. Cherezov, V. et al. "High-resolution crystal structure of an engineered human beta2-adrenergic G protein-coupled receptor" *Science* vol. 318 (2007): 1258 – 1265.
60. Cherezov, V. et al. "Rastering strategy for screening and centring of microcrystal samples of human membrane proteins with a sub-10 µm size X-ray synchrotron beam" *J. R. Soc. Interface* vol. 6 (2009): S587–S597.

61. García-Colunga, J. et al. "Blockage of muscle and neuronal nicotinic acetylcholine receptors by fluoxetine (Prozac)" *Proc Natl Acad Sci USA*. vol. 94, 5 (1997): 2041 - 2044.
62. Rubin, E. et al. "Crystallization under an External Electric Field: A Case Study of Glucose Isomerase" *Crystals*. vol. 7 (2017): 206.

## **CHAPTER 6. Conclusions and Future Perspectives**

Over the last decades, several research groups have unsuccessfully attempted to obtain a native nAChR X-ray structure at high resolution. Our laboratory has been working with the isolation and solubilization of the nAChR for almost 3 decades now. In our most recent studies, Asmar Rovira et al, 2008 [1], Padilla et al 2011 [2], Padilla et al 2016 [3], and Quesada et al 2016 [4] in collaboration with Dr. Raymond C. Stevens at the Scripps Research Institute (La Jolla, CA), we have shown that during solubilization and affinity purification, detergents may selectively remove a native lipid specie(s) present in the cell membrane that is essential for protein function and/or stability. Moreover, detergents can influence nAChR functionality and stability, a phenomenon driven by the detergent's molecular features.

Detergent-specific delipidation could induce a partial denaturation of the membrane protein hydrophobic domains that could eventually lead to destabilization and premature aggregation [1,2]. Our findings demonstrate that physicochemical properties of detergents, governed by the identity of the hydrophobic tail and head-group, may be critical to lipid exclusion and nAChR stability and functionality. Thus, trends observed in a model membrane protein such as the nAChR could be used to develop correlations in other structurally related membrane proteins. Our study also shows that lipid-analog detergents induce a functional stabilization of the nAChR [2,3,4,5].

This lipid-based analysis of detergent purified nAChR has revealed an innovative perspective towards the preparation of high-quality nAChR crystals. We have performed biophysical characterization studies of the nAChR in the LCP to

comprehend further the dynamics of the nAChR inserted in an engineered lipid environment. Data have demonstrated that the LCP in combination with the lipid-based approach could lead to nAChR nucleation and crystal formation [2,3,5]. This approach is technically significant because it can concurrently and systematically assess the lipid composition, ion channel function, and stability (i.e., state of aggregation, LCP mobility and diffusion in a short and long-term perspective considering crystallization process of membrane proteins) of detergent purified nAChR. Our study is innovative because it uses LCP-FRAP to estimate the nAChR mobile fraction and diffusion coefficient that in turn correlate with receptor stability and/or aggregation; as well as novel crystallization strategies involving voltage applied potential in the LCP [2,3,4,5]. We are confident our research approach will become the standard for crystallization trials of complex membrane proteins.

Our study specifically shows there are remarkable differences in nAChR stability for phospholipid- and cholesterol analog detergents. Phospholipid-analog detergents with 16 carbon chains are more likely to sustain reasonable nAChR function and stability [2,3]. Our results highlight the importance of determining nAChR function in the LCP matrix because detergent–nAChR complexes that are nonfunctional in PLB assays yielded high mobile fractions in LCP-FRAP; and further efforts should be directed toward this goal. Another factor to be considered is the possibility that the LCP could function as a “filter” for the inclusion of monomeric and exclusion of dimeric protein species into the LCP matrix. Our data provided important insights for the preparation of functionally active nAChR–detergent complexes [1,2,3]. An implicit assumption of the results from the detergent-solubilized nAChR with respect to

functionality, stability, and state of aggregation of the nAChR is that they will be relevant to other important membrane receptor systems, ion channels and membrane proteins.

Overall, the present study not only demonstrates that the nAChR-LFC-16 complex is an excellent candidate to be used in LCP crystallization trails, but also to assess new technologies developed for membrane protein crystallization. Another fundamental aspect that remains to be elucidated is the possibility that the structural basis for the ion channel functionality and stability of detergent purified nAChRs is merely determined by their lipid composition. Although, recent findings by Quesada et al. 2016 provided the foundations necessary to decide on the best conditions that will provide appropriate lipids and lipid proportion that will favor nAChRs stability and functionality. Moreover, our team has designed a novel approach towards membrane protein crystallization in lipidic matrixes, using the application of voltage potential to increase protein stability by applying, to our advantage, the voltage dependence of nAChR conformational states. Decades of generated data support the voltage potential approach to enhance nAChRs stabilization. Meanwhile our team is the first to apply for the crystallization of the nAChR. Data in this study shows that voltage application could, in fact, support faster crystal development as well as improved nAChRs nucleation in the LCP and as a result yield bigger crystals. However, the mechanism by which this occurs remains poorly understood. Future experiments should be focused on elucidating the mechanism by which voltage application to the LCP improves nAChRs crystal development and size. Perhaps, long-term LCP

confocal imaging coupled with LCP-FRAP could provide useful information on nAChR's dynamics in the LCP under voltage potential.

The primary outcome of this dissertation has been the patent application: “High-throughput crystallographic screening device and method for membrane proteins,” Application number: 62/356,266 (<http://nachrs.org/intellectual-property/>), in which membrane proteins can be crystallized through the application of a controlled voltage potential to increase protein stability.

## Conclusions and Future Perspectives References

1. Asmar-Rovira, G.A. et al. "Biophysical and ion channel functional characterization of the *Torpedo californica* nicotinic acetylcholine receptor in varying detergent–lipid environments" *J. Membr. Biol.* vol. 223 (2008): 13 – 26.
2. Padilla-Morales, L. F. et al. "Effects of lipid-analog detergent solubilization on the functionality and lipidic cubic phase mobility of the *Torpedo californica* nicotinic acetylcholine receptor" *J Membrane Biol* vol. 243 (2011): 47 – 58.
3. Padilla-Morales, L. F. et al. "Assessment of the functionality and stability of detergent purified nAChR from *Torpedo* using lipidic matrixes and macroscopic electrophysiology" *Biochim Biophys Acta.* vol. 1858, 1 (2016): 47 - 56.
4. Quesada, O. et al. "Uncovering the lipidic basis for the preparation of functional nicotinic acetylcholine receptor detergent complexes for structural studies" *Scientific Reports: Nature* vol. 6 (2016): 32766.
5. Padilla-Morales, L.F. et al. "Functionality and stability data of detergent purified nAChR from *Torpedo* using lipidic matrixes and macroscopic electrophysiology" *Data in Brief* vol. 6 (2016): 433 – 437.